

**Heptadentate, octadentate or even nonadentate? Denticity in the
unexpected formation of an all-carbon donor atom ligand in
Rh^{III}(Cp*)(anthracenyl-NHC) complexes**

Betty Y. T. Lee,^a Andrew D. Phillips,^b Muhammad Hanif,^a Kelvin K. H. Tong,^a Tilo
Söhnel,^a Christian G. Hartinger^{a,*}

^a School of Chemical Sciences, University of Auckland, Private Bag 92019, Auckland
1142, New Zealand.

^b School of Chemistry, Science South, University College Dublin, Belfield, Dublin 4,
Ireland.

* School of Chemical Sciences, University of Auckland, Private Bag 92019, Auckland
1142, New Zealand. <http://hartinger.auckland.ac.nz/>

E-mail: c.hartinger@auckland.ac.nz; Fax: (+64) 9 373 7599 ext 87422

Table of Contents

Experimental part

X-ray crystallography data and data collection parameters

NMR and mass spectra used in the characterization of compounds

Reactivity studies by MS and NMR spectroscopy

Details on the theoretical calculations

Experimental

Materials and methods

All reactions were carried out under nitrogen atmosphere using standard Schlenk techniques. Chemicals obtained from commercial suppliers were used as received and were of analytical grade. Acetonitrile and dichloromethane were purchased from J.T. Baker, ethylacetate was from Macron, potassium carbonate and n-hexane from ECP, 9-chloromethylathracene, methylimidazole, methylbenzimidazole and benzimidazole from AK Scientific, anthracene, 1,2,3,4,5-pentamethylcyclopentadiene and silver hexafluorophosphate from Sigma-Aldrich, silver oxide from Oakwood, methyl iodide from Merck, and $\text{RhCl}_3 \cdot 3\text{H}_2\text{O}$ (99%) from Precious Metals Online. The dimer $[\text{Rh}(\text{Cp}^*)\text{Cl}_2]_2$ was synthesized by adapting literature procedures.^{1,2} Methanol (Macron, AR), dimethylformamide (J.T. Baker, AR) and tetrahydrofuran (J.T. Baker, AR) were dried over activated molecular sieves (3 Å) in a round bottom flask for two days prior use. $[\text{Dichlorido}(\eta^5\text{-1,3-dimethylbenzimidazol-2-ylidene})(\eta^5\text{-pentamethylcyclopentadienyl})\text{rhodium(III)}]$ **7** was synthesized following literature procedure.³

^1H and $^{13}\text{C}\{^1\text{H}\}$ and 2D (COSY, HSQC, HMBC) NMR spectra were recorded on a Bruker Avance AVIII 400 MHz NMR spectrometer at ambient temperature at 400.13 MHz (^1H) or 100.61 MHz ($^{13}\text{C}\{^1\text{H}\}$) or 161.87 MHz ($^{31}\text{P}\{^1\text{H}\}$). Chemical shifts are reported *versus* SiMe_4 and were determined by reference to the residual solvent peaks. High resolution mass spectra were recorded on a Bruker micrOTOF-QII mass spectrometer in positive electrospray ionization (ESI) mode. Elemental analyses were conducted on a Vario EL cube (Elementar Analysensysteme GmbH, Hanau, Germany).

X-ray diffraction measurements of single crystals of **1a**, **3a**, **4a**, **5a** and **6a** were performed on a Rigaku Oxford Diffraction XtaLAB-Synergy-S single-crystal diffractometer with a PILATUS 200K hybrid pixel array detector using Cu K α radiation ($\lambda = 1.54184$ Å; Table S1). The data were processed with the SHELX2018/3 and Olex2 1.3 software packages.⁴⁻⁶ All non-hydrogen atoms were refined anisotropically. Hydrogen atoms were inserted at calculated positions and refined with a riding model or without restrictions. Mercury 2020.1 was used to visualize the molecular structure.

Table S1. X-ray diffraction measurement parameters for **1a**, **3a**, **4a**, **5a** and **6a**.

	1a	3a	4a	5a	6a
CCDC	2016954	2016955	2016956	2016957	2016958
Formula	C ₂₉ H ₃₁ Cl ₂ N ₂ Rh	C ₂₉ H ₃₀ ClN ₂ Rh	C ₃₃ H ₃₂ ClN ₂ Rh	C ₂₉ H ₃₀ N ₂ Rh · PF ₆	C ₃₃ H ₃₂ N ₂ Rh·PF ₆ ·CHCl ₃
Molecular weight (g mol ⁻¹)	581.37	544.91	594.96	654.43	823.85
Crystal size (mm)	0.20 × 0.14 × 0.10	0.10 × 0.10 × 0.10	0.26 × 0.22 × 0.20	0.20 × 0.20 × 0.20	0.26 × 0.10 × 0.05
Temperature (K)	100.0(1)	100.0(1)	109(1)	100.0(2)	100.0(6)
Crystal system	monoclinic	monoclinic	monoclinic	monoclinic	monoclinic
Space group	<i>P</i> 2 ₁ / <i>n</i>	<i>P</i> 2 ₁ / <i>c</i>	<i>P</i> 2 ₁ / <i>c</i>	<i>P</i> 2 ₁ / <i>c</i>	<i>P</i> 2/ <i>n</i>
<i>a</i> (Å)	15.1187(2)	12.9512(2)	11.5695(2)	11.7446(2)	8.6147(2)
<i>b</i> (Å)	11.2931(1)	11.7816(2)	12.9043(2)	15.2722(2)	19.0747(3)
<i>c</i> (Å)	15.5926(2)	15.7480(2)	18.2119(2)	14.2161(2)	19.9284(3)
β (°)	106.356(1)	95.209(1)	106.991(1)	95.002(1)	97.505(2)
Volume (Å ³)	2554.49(5)	2393.00(6)	2600.29(7)	2540.17(7)	3246.64(10)
Z	4	4	4	4	4
Calculated Density (mg/mm ³)	1.512	1.512	1.520	1.711	1.685
Absorption coefficient (mm ⁻¹)	7.478	6.939	6.441	6.636	7.554
F(000)	1192	1120	1224	1328	1664
Theta range (°)	11.830 to 135.476	11.284 to 148.64	12.262 to 135.48	11.599 to 135.462	11.696 to 135.408
Index ranges	-18 ≤ <i>h</i> ≤ 18, -13 ≤ <i>k</i> ≤ 12, -14 ≤ <i>l</i> ≤ 18	-16 ≤ <i>h</i> ≤ 15, -14 ≤ <i>k</i> ≤ 14, -18 ≤ <i>l</i> ≤ 19	-13 ≤ <i>h</i> ≤ 13, -14 ≤ <i>k</i> ≤ 15, -17 ≤ <i>l</i> ≤ 21	-14 ≤ <i>h</i> ≤ 13, -18 ≤ <i>k</i> ≤ 17, -17 ≤ <i>l</i> ≤ 13	-10 ≤ <i>h</i> ≤ 10, -22 ≤ <i>k</i> ≤ 22, -23 ≤ <i>l</i> ≤ 21
Reflections collected	24649	24230	19557	19679	32558
Independent reflections	4606 [R _{int} = 0.0457]	4694 [R _{int} = 0.0308]	4693 [R _{int} = 0.0303]	4576 [R _{int} = 0.0335]	5886 [R _{int} = 0.0570]
Data/restraints/parameters	4606 / 0 / 313	4694 / 0 / 303	4693 / 0 / 339	4576 / 0 / 357	5886 / 51 / 509
Final R indices [<i>I</i> > 2σ(<i>I</i>)]	R ₁ = 0.0297, wR ₂ = 0.0697	R ₁ = 0.0224 wR ₂ = 0.0521	R ₁ = 0.0219 wR ₂ = 0.0545	R ₁ = 0.0227 wR ₂ = 0.0565	R ₁ = 0.0537 wR ₂ = 0.1244
R indices (all data)	R ₁ = 0.0323, wR ₂ = 0.0707	R ₁ = 0.0250 wR ₂ = 0.0531	R ₁ = 0.0230 wR ₂ = 0.0551	R ₁ = 0.0241 wR ₂ = 0.0573	R ₁ = 0.0574 wR ₂ = 0.1264
Goodness-of-fit on F ²	1.072	1.043	1.029	1.044	1.182

Table S2. Selected bond lengths for complexes **1a**, **3a**, **4a**, **5a**, and **6a** as determined by X-ray diffraction analysis.

Bond	Bond length / Å				
	1a	3a	4a	5a	6a
C8a'–C9'	1.407(5)	1.503(3)	1.503(3)	1.486(3)	1.471(6)
C9'–C9a'	1.421(5)	1.508(3)	1.508(3)	1.465(3)	1.481(6)
C4a'–C9a'	1.442(5)	1.409(3)	1.406(3)	1.430(3)	1.406(7)
C4a'–C10'	1.392(5)	1.498(3)	1.495(3)	1.505(3)	1.498(7)
C10'–C10a'	1.396(5)	1.497(3)	1.498(3)	1.508(3)	1.503(7)
C8a'–C10a'	1.439(5)	1.410(3)	1.407(3)	1.401(3)	1.432(6)

Table S3. ESI-MS data for compounds **1a**, **3a**, **4a**, **5a** and **6a**, and the adducts of **5a** with 1,3-dimethylbenzimidazole (**3a^{dmbz}**), pta (**3a^{pta}**) and *tert*-butylisonitrile (**3a^{BIN}**) analyzed in positive mode.

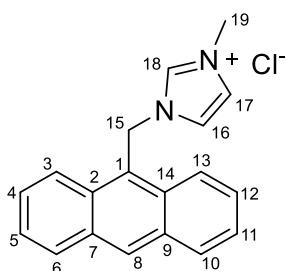
Compound	<i>m/z</i>	<i>m/z</i> _{calculated}	Peak assignment
1a	509.1442	509.1459	[M – 2Cl – H] ⁺
3a	509.1457	509.1459	[M – Cl] ⁺
3a^{dmbz}	655.2277	655.2303	[3a – Cl + dmbz] ⁺
3a^{pta}	666.2215	666.2227	[3a – Cl + pta] ⁺
3a^{BIN}	592.2171	592.2199	[3a – Cl + BIN] ⁺
4a	595.1349	595.1387	[M + H] ⁺
5a	509.1450	509.1459	[M – PF ₆] ⁺
6a	559.1614	559.1615	[M – PF ₆] ⁺

Synthesis

General procedure for the synthesis of 1 and 2

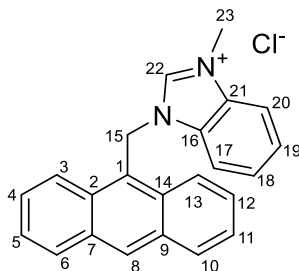
A mixture of 9-chloromethylantracene (1 eq.) and methyl(benz)imidazole (1 eq.) in 5 mL acetonitrile was refluxed under nitrogen in darkness for 2 d, following a literature procedure.⁷ Ethylacetate (40–60 mL) was added to the reaction mixture and a pale yellow precipitate formed immediately. The precipitate was filtered, washed with ethylacetate and dried under vacuum to afford **1** and **2**.

Synthesis of 1-(anthracen-9-ylmethyl)-3-methylimidazolium chloride, **1**



Pro-carbene **1** was prepared by following the general procedure using 9-chloromethylantracene (250 mg, 1.1 mmol) and methylimidazole (87.9 μ L, 1.1 mmol). Yield: 313 mg (92%). ^1H NMR (400.13 MHz, DMSO- d_6): δ (ppm) = 3.74 (s, 3H, H19), 6.48 (s, 2H, H15), 7.60–7.73 (m, 6H, H4/5/11/12/16/17), 8.23 (d, 3J = 8 Hz, 2H, H3/6/10/13), 8.47 (d, 3J = 9 Hz, 2H, H3/6/10/13), 8.85 (s, 1H, H8), 8.91 (s, 1H, H18). $^{13}\text{C}\{^1\text{H}\}$ NMR (100.61 MHz, DMSO- d_6): δ (ppm) = 35.8 (CH₃, C19), 44.8 (CH₂, C15), 122.5 (CH, C16/17), 123.5 (CH, C3/6/10/13), 123.6 (C, C1), 123.7 (CH, C16/17), 125.6 (CH, C4/5/11/12), 127.8 (CH, C4/5/11/12), 129.4 (CH, C3/6/10/13), 130.1 (CH, C8), 130.6 (C, C2/7/9/14), 131.1 (C, C2/7/9/14), 136.1 (CH, C18).

Synthesis of 1-(anthracen-9-ylmethyl)-3-methylbenzimidazolium chloride, **2**



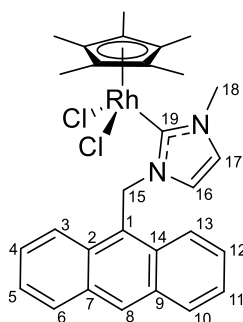
Pro-carbene **2** was prepared by following the general procedure using 9-chloromethylantracene (500 mg, 2.2 mmol) and methylbenzimidazole (290 mg,

2.2 mmol). Yield: 433 mg (55%). ^1H NMR (400.13 MHz, $\text{DMSO}-d_6$): δ (ppm) = 3.89 (s, 3H, H23), 6.72 (s, 2H, H15), 7.60-7.67 (m, 4H, H4,5,11,12), 7.76-7.84 (m, 2H, H18,19), 8.02 (d, $^3J = 8$ Hz, 1H, H17/20), 8.26-8.28 (m, 2H, H3/6/10/13), 8.35-8.39 (m, 3H, H3/6/10/13/17/20), 8.92 (s, 2H, H8,22). $^{13}\text{C}\{^1\text{H}\}$ NMR (100.61 MHz, $\text{DMSO}-d_6$): δ (ppm) = 33.2 (CH_3 , C23), 43.2 (CH_2 , C15), 113.7 (CH , C17/20), 114.1 (CH , C17/20), 122.1 (C , C1), 123.5 (CH , C3/6/10/13), 125.6 (CH , C4/5/11/12), 126.7 (CH , C18/19), 126.8 (CH , C18/19), 127.8 (CH , C4/5/11/12), 129.4 (CH , C3/6/10/13), 130.4 (CH , C8), 131.0 (C , C2/7/9/14), 131.2 (C , C2/7/9/14), 131.6 (C , C16/21), 132.1 (C , C16/21), 141.5 (CH , C22).

General procedure for the synthesis of NHC-Rh^{III}(Cp) complexes*

1-(Anthracen-9-ylmethyl)-3-methyl(benz)imidazolium chloride was dissolved, silver oxide was added to the solution and the mixture was refluxed for 4 h under nitrogen in darkness. A solution of $[\text{Rh}(\text{Cp}^*)\text{Cl}_2]_2$ **a** in dichloromethane (5 mL) was added to the reaction mixture which was refluxed for 18 h. The resulting suspension was filtered through celite, the filtrate was collected and the solvent was evaporated under reduced pressure. The residue was dissolved in a minimal volume of dichloromethane (1 mL) and *n*-hexane was added to the solution, which led to immediate formation of an orange precipitate. The precipitate was filtered, washed with *n*-hexane and dried under vacuum to afford the desired complexes.

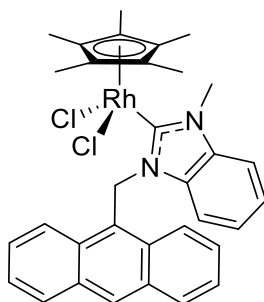
Synthesis of [dichlorido{1-(anthracen-9-ylmethyl)-3-methylimidazole-2-ylidene}(η^5 -pentamethylcyclopentadienyl)rhodium(III)], **1a**



Compound **1a** was prepared by following the general procedure using 1-(anthracen-9-ylmethyl)-3-methylimidazolium chloride **1** (50 mg, 0.16 mmol, 2 eq.) in tetrahydrofuran (5 mL), dimethylformamide (3 mL), dichloromethane (5 mL) and methanol (0.2 mL), silver oxide (18 mg, 0.08 mmol, 1 eq.) and $[\text{Rh}(\text{Cp}^*)\text{Cl}_2]_2$ (50 mg,

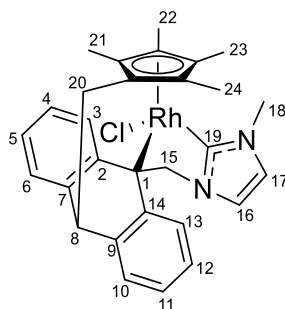
0.08 mmol, 1 eq.). Yield: 31 mg (33%). Single crystals suitable for X-ray diffraction analysis were grown from CH₂Cl₂/diethyl ether. ¹H NMR (400.13 MHz, CDCl₃): δ (ppm) = 1.79 (s, 15H, Cp*), 4.09 (s, 3H, H18), 5.67 (brs, 1H, H15), 6.09 (d, ³J = 2 Hz, 1H, H16), 6.68 (d, ³J = 2 Hz, 1H, H17), 7.47-7.57 (m, 4H, H3/4/5/6/10/11/12/13), 7.77 (brs, 1H, H15), 8.04-8.16 (m, 3H, H3/4/5/6/10/11/12/13), 8.56 (s, 1H, H3/4/5/6/10/11/12/13), 8.72 (brs, 1H, H8). ¹³C{¹H} NMR (100.61 MHz, CDCl₃): δ (ppm) = 9.8 (CH₃, Cp*), 39.4 (CH, C18), 47.3 (CH₂, C15), 96.3 (C, Cp*), 122.0 (CH, C16), 122.9 (CH, C17), 125.2 (C, C2/7/9/14), 129.3 (CH, C3/4/5/6/10/11/12/13), 168.6 (d, ¹J = 56 Hz, C_{NHC}-Rh). MS (ESI⁺): *m/z* 509.1442 [M – 2Cl – H]⁺ (*m*_{calc} = 509.1459). Elemental analysis calculated for C₂₉H₃₁Cl₂N₂Rh·0.75CH₂Cl₂·0.1C₆H₁₄: C 55.76, H 5.23, N 4.29%. Found: C 55.68, H 5.33, N 3.89%.

Synthesis of [dichlorido{1-(anthracen-9-ylmethyl)-3-methylbenzimidazole-2-ylidene}(η⁵-pentamethylcyclopentadienyl)rhodium(III)], **2a**



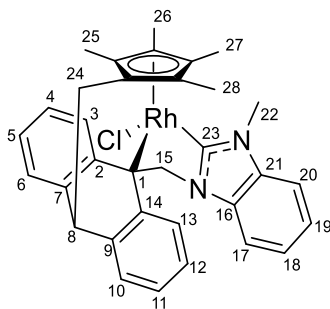
Compound **2a** was prepared by following the general procedure using 1-(anthracen-9-ylmethyl)-3-methylbenzimidazolium chloride **2** (37 mg, 0.10 mmol, 2 eq.) in tetrahydrofuran (5 mL), dimethylformamide (3 mL), dichloromethane (5 mL) and methanol (0.2 mL), silver oxide (12 mg, 0.05 mmol, 1 eq.) and [Rh(Cp*)Cl₂]₂ (32 mg, 0.05 mmol, 1 eq.). The precipitate formed was a mixture of **2a** and **4a** as confirmed by ¹H NMR spectroscopy (Figure S2). **2a** was not isolated from the precipitate mixture.

Synthesis of [chlorido{1-methyl-3-({10-[(η^5 -2,3,4,5-tetramethylcyclopentadienyl)methyl]-9,10-dihydroanthracene-9-yl- κ C)methyl}imidazole-2-ylidene}rhodium(III)], **3a**



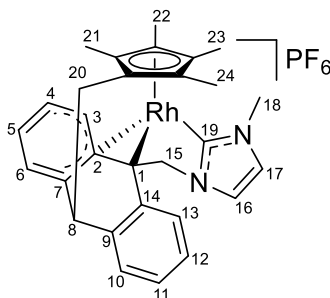
1-(Anthracen-9-ylmethyl)-3-methylimidazolium chloride **1** (50 mg, 0.16 mmol, 2 eq.) was dissolved in tetrahydrofuran (5 mL), dimethylformamide (3 mL), dichloromethane (5 mL) and methanol (0.2 mL), silver oxide (18 mg, 0.08 mmol, 1 eq.) was added to the solution and the mixture was refluxed for 4 h under nitrogen in darkness. A solution of [Rh(Cp*)Cl₂]₂ (50 mg, 0.08 mmol, 1 eq.) in dichloromethane (5 mL) was added to the reaction mixture which was refluxed for 18 h. The resulting suspension was filtered through celite, the filtrate was collected and the solvent was removed under vacuum. A minimal volume of dichloromethane (1 mL) was used to dissolve the residue. Addition of *n*-hexane to the solution led to the immediate formation of an orange precipitate. The precipitate was filtered and the filtrate was collected and allowed to stand at room temperature for 2 d to form red crystals of **3a**. Yield: 3 mg (3%). ¹H NMR (400.13 MHz, CDCl₃): δ (ppm) = -0.28 (s, 3H, H21/22/23/24), 0.39 (s, 3H, H21/22/23/24), 1.58 (s, 3H, H21/22/23/24), 1.86 (s, 3H, H21/22/23/24), 1.97 (d, ²J = 12 Hz, 1H, H20), 2.25 (d, ²J = 12 Hz, 1H, H20), 3.85 (s, 3H, H18), 4.19 (d, ²J = 11 Hz, 1H, H15), 5.15 (t, ³J = 4 Hz, 1H, H8), 5.47 (d, ²J = 11 Hz, 1H, H15), 6.54 (d, ³J = 7 Hz, 1H, H16/17), 6.89-7.05 (m, 4H, H3/4/5/6/10/11/12/13), 7.13-7.25 (m, 4H, H3/4/5/6/10/11/12/13), 7.77 (d, ³J = 7 Hz, 1H, H16/17). MS (ESI⁺): *m/z* 509.1457 [M – Cl]⁺ (*m*_{calc} = 509.1459). Elemental analysis calculated for C₂₉H₃₀ClN₂Rh·CH₂Cl₂: C 57.21, H 5.12, N 4.45%. Found: C 57.30, H 5.12, N 4.18%.

Synthesis of [chlorido{1-methyl-3-({10-[(η^5 -2,3,4,5-tetramethylcyclopentadienyl)methyl]-9,10-dihydroanthracene-9-yl- κ C)methyl}benzimidazole-2-ylidene}rhodium(III)], **4a**



1-(Anthracen-9-ylmethyl)-3-methylbenzimidazolium chloride **2** (37 mg, 0.10 mmol, 2 eq.) in dichloromethane (5 mL) and methanol (0.2 mL), and silver oxide (12 mg, 0.05 mmol, 1 eq.) was added to the reaction mixture which was refluxed for 4 h under nitrogen in darkness. A solution of $[\text{Rh}(\text{Cp}^*)\text{Cl}_2]_2$ (32 mg, 0.05 mmol, 1 eq.) in dichloromethane (5 mL) was added to the reaction mixture and refluxed for 18 h. The resulting suspension was filtered through celite, the filtrate was collected and the solvent was evaporated under reduced pressure. The residue was dissolved in minimal volume of dichloromethane (1 mL) and *n*-hexane was added to the solution and an orange precipitate formed. The precipitate was filtered and the filtrate was stored at room temperature in a sealed flask for crystallization which yielded crystals of **4a** after 2 d. Yield: 3 mg (5%). ^1H NMR (400.13 MHz, CDCl_3): δ (ppm) = -0.28 (s, 3H, H25/26/27/28), 0.47 (s, 3H, H25/26/27/28), 1.64 (s, 3H, H25/26/27/28), 1.92 (s, 3H, H25/26/27/28), 2.03 (dd, $^2J = 12$ Hz, 1H, H24), 2.33 (dd, $^2J = 12$ Hz, 1H, H24), 4.06 (s, 3H, H22), 4.50 (d, $^2J = 11$ Hz, 1H, H15), 5.20 (t, $^3J = 4$ Hz, 1H, H8), 5.46 (d, $^2J = 11$ Hz, 1H, H15), 6.54 (d, $^3J = 8$ Hz, 1H, H3/6/10/13/17/20), 6.82 (t, $^3J = 8$ Hz, 1H, H4/5/11/12/18/19), 6.95 (t, $^3J = 7$ Hz, 1H, H4/5/11/12/18/19), 7.07 (t, $^3J = 7$ Hz, 1H, H4/5/11/12/18/19), 7.16-7.22 (m, 2H, H3/4/5/6/10/11/12/13/17/18/19/20), 7.29-7.41 (m, 4H, H3/4/5/6/10/11/12/13/17/18/19/20), 7.52-7.54 (m, 1H, H3/4/5/6/10/11/12/13/17/18/19/20), 7.83 (d, $^3J = 8$ Hz, 1H, H3/6/10/13/17/20). MS (ESI $^+$): m/z 595.1379 $[\text{M} + \text{H}]^+$ ($m_{\text{calc}} = 595.1387$).

Synthesis of [{1-methyl-3-({10-[(η^5 -2,3,4,5-tetramethylcyclopentadienyl)methyl]-9,10-dihydroanthracene-9-yl- κ C)methyl}imidazole-2-ylidene}rhodium(III)], **5a**



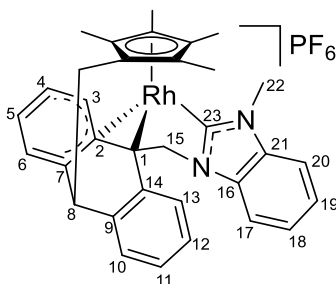
Procedure 1. **1a** (10 mg, 0.02 mmol, 1 eq.) was dissolved in dichloromethane (5 mL), silver oxide (4 mg, 0.02 mmol, 1 eq.) was added to the solution and the mixture was refluxed for 24 h under nitrogen in darkness. AgPF₆ (4 mg, 0.02 mmol, 1 eq.) was added to the solution and the mixture was refluxed for 24 h under nitrogen in darkness. The resulting suspension was filtered through celite, the blue filtrate was collected and the solvent was evaporated. A minimal volume of dichloromethane was added to dissolve the residue. *n*-Hexane was added to the solution and a blue precipitate formed immediately. The precipitate was filtered, washed with *n*-hexane and dried under vacuum to afford the complex **5a**. Yield: 4 mg (36%).

Procedure 2. 1-(Anthracen-9-ylmethyl)-3-methylimidazolium chloride **1** (49 mg, 0.16 mmol, 2 eq.) was dissolved in tetrahydrofuran (5 mL), dimethylformamide (3 mL), dichloromethane (5 mL) and methanol (0.2 mL), silver hexafluorophosphate (40 mg, 0.16 mmol, 2 eq.) was added to the solution and the mixture was refluxed for 4 h under nitrogen in darkness. Silver oxide (28 mg, 0.12 mmol, 1.5 eq.) was added to the reaction mixture and refluxed for 16 h. A solution of [Rh(Cp*)Cl₂]₂ (50 mg, 0.08 mmol, 1 eq.) in dichloromethane (5 mL) was added to the reaction mixture which was refluxed for 18 h. The resulting suspension was filtered through celite, the blue filtrate was collected and the solvent was evaporated. A minimal volume of dichloromethane was added to dissolve the residue. *n*-Hexane was added to the solution and blue precipitate formed immediately. The precipitate was filtered, washed with *n*-hexane and dried under vacuum to afford the complex **5a**. Yield: 45 mg (43%). Single crystals suitable for X-ray diffraction analysis were grown from CH₂Cl₂/diethyl ether.

¹H NMR (400.13 MHz, CDCl₃): δ (ppm) = 0.39 (s, 6H, H21/22/23/24), 1.88 (s, 6H, H21/22/23/24), 2.19 (d, ³J = 4 Hz, 2H, H20), 4.05 (s, 3H, H18), 4.38 (s, 2H, H15), 4.74 (t, ³J = 4 Hz, 1H, H8), 6.36 (d, ³J = 8 Hz, 2H, H16/17), 7.19-7.24 (m, 4H, H4/5/11/12),

7.35 (d, $^3J = 7$ Hz, 2H, H10,13), 7.59 (dt, $^3J = 7$ Hz, 2H, H3,6). $^{13}\text{C}\{^1\text{H}\}$ NMR (100.61 MHz, CDCl_3): δ (ppm) = 5.8 (CH_3 , C21/22/23/24), 11.4 (CH_3 , C21/22/23/24), 29.1 (CH_2 , C20), 38.2 (CH, C18), 45.3 (CH, C8), 52.7 (CH, C15), 65.6 (Rh-C), 85.1 (Rh-C), 98.0 (C, Cp^*), 98.1 (C, Cp^*), 102.0 (C, Cp^*), 102.1 (C, Cp^*), 116.7 (C, C2/7/9/14), 117.8 (CH, C16/17), 119.3 (CH, C5), 125.3 (CH, C4), 127.7 (CH, C11,12), 128.3 (CH, C3,6), 129.8 (CH, C10,13), 136.9 (C, C2/7/9/14), 172.9 (d, $^1J = 56$ Hz, $\text{C}_{\text{NHC-Rh}}$). MS (ESI $^+$): m/z 509.1450 $[\text{M} - \text{PF}_6]^+$ ($m_{\text{calc}} = 509.1459$). Elemental analysis calculated for $\text{C}_{29}\text{H}_{30}\text{N}_2\text{RhPF}_6 \cdot 0.5 \text{CH}_2\text{Cl}_2$: C 50.84, H 4.48, N 4.02%. Found: C 50.55, H 4.74, N 3.99%.

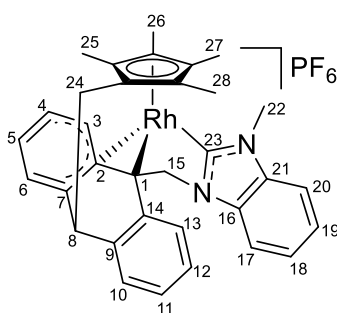
Synthesis of [$\{1\text{-methyl-3-}(\{10\text{-}[(\eta^5\text{-2,3,4,5-tetramethylcyclopentadienyl)methyl]-9,10\text{-dihydroanthracene-9-yl-}\kappa\text{C}\}\text{methyl})\text{benzimidazole-2-ylidene}\}\text{rhodium(III)}\}$], **6a**



Procedure 1. 1-(Anthracen-9-ylmethyl)-3-methylbenzimidazolium chloride **2** (30 mg, 0.08 mmol, 2 eq.) was dissolved in dichloromethane (5 mL) and methanol (0.2 mL), silver oxide (9 mg, 0.04 mmol, 1 eq.) was added to the reaction mixture and the mixture was refluxed for 4 h under nitrogen in darkness. A solution of $[\text{Rh}(\text{Cp}^*)\text{Cl}_2]_2$ (25 mg, 0.04 mmol, 1 eq.) in dichloromethane (5 mL) was added to the reaction mixture which was refluxed for 18 h. Another equivalent of silver oxide (9 mg, 0.04 mmol, 1 eq.) was added to the reaction mixture which was continued to be refluxed for 18 h. Silver hexafluorophosphate (10 mg, 0.08 mmol, 2 eq.) was added to the solution and the mixture was refluxed for 24 h under nitrogen in darkness. The resulting suspension was filtered through celite, the blue filtrate was collected and the solvent was evaporated. A minimal volume of dichloromethane was added to dissolve the residue. *n*-Hexane was added to the solution and a blue precipitate formed immediately. The precipitate was filtered, washed with *n*-hexane and dried under vacuum to afford **6a**. Yield: 20 mg (34%).

Procedure 2. 1-(Anthracen-9-ylmethyl)-3-methylbenzimidazolium chloride **2** (50 mg, 0.14 mmol, 2 eq.) was dissolved in dichloromethane (5 mL) and methanol (0.2 mL),

silver hexafluorophosphate (35 mg, 0.14 mmol, 2 eq.) was added to the solution and the mixture was refluxed for 4 h under nitrogen in darkness. Silver oxide (24 mg, 0.10 mmol, 1.5 eq.) was added to the reaction mixture which was refluxed for 16 h. A solution of $[\text{Rh}(\text{Cp}^*)\text{Cl}_2]_2$ (43 mg, 0.07 mmol, 1 eq.) in dichloromethane (5 mL) was added to the reaction mixture which was continued to be refluxed for 18 h. The resulting suspension was filtered through celite, the blue filtrate was collected and the solvent was evaporated. A minimal volume of dichloromethane was added to dissolve the residue. *n*-Hexane was added to the solution and a blue precipitate formed immediately. The precipitate was filtered, washed with *n*-hexane and dried under vacuum to afford complex **6a**. Yield: 42 mg (43%). Single crystals suitable for X-ray diffraction analysis were grown from $\text{CH}_2\text{Cl}_2/\text{diethyl ether}$.



^1H NMR (400.13 MHz, CDCl_3): δ (ppm) = 0.43 (s, 6H, H25/26/27/28), 1.96 (s, 6H, H25/26/27/28), 2.25 (d, $^3J = 4$ Hz, 2H, H24), 4.28 (s, 3H, H22), 4.51 (s, 2H, H15), 4.81 (t, $^3J = 4$ Hz, 1H, H8), 6.43 (d, $^3J = 8$ Hz, 2H, H17,20), 7.21-7.24 (m, 2H, H18,19), 7.38-7.46 (m, 5H, H4,5,11,12, 10/13), 7.59-7.67 (m, 3H, H3,6, 10/13). $^{13}\text{C}\{^1\text{H}\}$ NMR (100.61 MHz, CDCl_3): δ (ppm) = 5.8 (CH_3 , C25/26/27/28), 11.4 (CH_3 , C25/26/27/28), 29.2 (CH_2 , C24), 35.3 (CH, C22), 45.2 (CH, C8), 50.2 (CH, C15), 99.2 (C-Cp*), 110.6 (CH, C10/13), 111.4 (CH, C10/13), 117.4 (CH, C17/20), 124.2 (CH, C4/5), 124.3 (CH, C4/5), 127.7 (CH, C18,19), 128.8 (CH, C3,6), 130.1 (CH, C11,12), 132.3 (CH, C1/2/14), 135.8 (CH, C16,21), 137.2 (C, C1/2/14). MS (ESI $^+$): m/z 559.1614 $[\text{M} - \text{PF}_6]^+$ ($m_{\text{calc}} = 559.1615$). Elemental analysis calculated for $\text{C}_{33}\text{H}_{32}\text{N}_2\text{RhPF}_6 \cdot 0.5 \text{H}_2\text{O} \cdot 0.2\text{C}_6\text{H}_{14}$: C 56.21, H 4.94, N 3.83%. Found: C 55.9, H 5.28, N 3.76%.

Reactions of [dichlorido(1,3-dimethylbenzimidazol-2-ylidene)(η^5 -pentamethylcyclopentadienyl)rhodium(III)] (7**)**

Table S4. Reaction conditions investigated involving [dichlorido(1,3-dimethylbenzimidazol-2-ylidene)(η^5 -pentamethylcyclopentadienyl)rhodium(III)] **7** and various compounds used in the syntheses of **1a**, **3a** and **5a**.

Reaction	K ₂ CO ₃	Anthracene	AgPF ₆	Ag ₂ O	1
1	•				
2		•	•		
3		•		•	
4	•	•		•	
5					•
6	•				•
7	•			•	•
8			•	•	•

*Reaction 1. Reaction of **7** with potassium carbonate*

A mixture of **7** (10 mg, 0.02 mmol, 1 eq.) and potassium carbonate (6 mg, 0.04 mmol, 2 eq.) in 10 mL DCM was refluxed under nitrogen in darkness for 16 h. The reaction was monitored by ¹H NMR spectroscopy. No reaction occurred during this time.

*Reaction 2. Reaction of **7** with anthracene and AgPF₆*

A mixture of **7** (10 mg, 0.02 mmol, 1 eq.), anthracene (4 mg, 0.02 mmol, 1 eq.) and AgPF₆ (11 mg, 0.04 mmol, 2 eq.) in 10 mL DCM was refluxed under nitrogen in darkness for 16 h. The reaction was monitored by ¹H NMR spectroscopy. No reaction occurred during this time.

*Reaction 3. Reaction of **7** with anthracene and silver oxide*

A mixture of **7** (10 mg, 0.02 mmol, 1 eq.), anthracene (4 mg, 0.02 mmol, 1 eq.) and Ag₂O (10 mg, 0.04 mmol, 2 eq.) in 8 mL DCM was refluxed under nitrogen in darkness

for 16 h. The reaction was monitored by ^1H NMR spectroscopy. No reaction occurred during this time.

Reaction 4. Reaction of 7 with potassium carbonate, anthracene and silver oxide

A mixture of **7** (10 mg, 0.02 mmol, 1 eq.), potassium carbonate (6 mg, 0.04 mmol, 2 eq.) and anthracene (4 mg, 0.02 mmol, 1 eq.) in 10 mL DCM was refluxed under nitrogen in darkness for 16 h. A ^1H NMR spectrum of the reaction mixture was recorded. Then Ag_2O (10 mg, 0.04 mmol, 2 eq.) was added to the reaction mixture which was then refluxed under nitrogen in darkness for another 16 h. The reaction was monitored by ^1H NMR spectroscopy. No reaction occurred during this time.

Reaction 5. Reaction of 7 with 1

A mixture of **7** (10 mg, 0.02 mmol, 1 eq.) and **1** (7 mg, 0.02 mmol, 1 eq.) in 10 mL DCM and MeOH (0.2 mL) was refluxed under nitrogen in darkness for 16 h. The reaction was monitored by ^1H NMR spectroscopy. No reaction occurred during this time.

Reaction 6. Reaction of 7 with 1 and potassium carbonate

A mixture of **7** (10 mg, 0.02 mmol, 1 eq.), potassium carbonate (6 mg, 0.04 mmol, 2 eq.) and **1** (7 mg, 0.02 mmol, 1 eq.) in 10 mL DCM and MeOH (0.2 mL) was refluxed under nitrogen in darkness for 16 h. The reaction was monitored by ^1H NMR spectroscopy. No reaction occurred during this time.

Reaction 7. Reaction of 7 with 1, potassium carbonate and silver oxide

A mixture of **7** (10 mg, 0.02 mmol, 1 eq.), potassium carbonate (6 mg, 0.04 mmol, 2 eq.), Ag_2O (20 mg, 0.08 mmol, 4 eq.) and **1** (7 mg, 0.02 mmol, 1 eq.) in DCM (10 mL) and MeOH (0.2 mL) was refluxed under nitrogen in darkness for 16 h. The reaction was monitored by ^1H NMR spectroscopy (Figure S3). Complex **7** reacted with **1** leading to the formation of **3a**^{dmbz}.

Reaction 8. Reaction of 7 with 1, silver oxide and AgPF_6

A mixture of Ag_2O (8 mg, 0.03 mmol, 1 eq.) and **1** (10 mg, 0.03 mmol, 1 eq.) in DCM (10 mL) and MeOH (0.2 mL) was refluxed under nitrogen in darkness for 6 h. A solution of **7** (15 mg, 0.03 mmol, 1 eq.) in DCM (2 mL) was added to the reaction mixture which

was refluxed under nitrogen in darkness for 64 h. ^1H NMR and ESI-mass spectra of the orange reaction mixture were recorded (Figures S3 and S4). After addition of AgPF_6 (8 mg, 0.0303 mmol, 1 eq.) to the orange reaction mixture, the color of the solution changed immediately to blue. The mixture was refluxed under nitrogen in darkness for 16 h. ^1H NMR and ESI-mass spectra of the blue reaction mixture were recorded (Figures S3 and S5). Complex **7** reacted with **1** leading to the formation of **3a**^{dmbz} as confirmed by ESI-MS (Figure S5) where a peak at m/z 655.2277 was assigned to $[\mathbf{3a} - \text{Cl} + \text{dmbz}]^+$ ($m_{\text{calc}} = 655.2303$). In addition, the cleavage of 1,3-dimethylbenzimidazole-2-ylidene ligand from the Rh center was observed as indicated by peaks at m/z 147.0873 ($[\text{dmbz} + \text{H}]^+$, $m_{\text{calc}} = 147.0917$) and m/z 509.1451 ($[\mathbf{3a} - \text{Cl}]^+$ and $[\mathbf{5a} - \text{PF}_6]^+$, $m_{\text{calc}} = 509.1615$) (Figure S5).

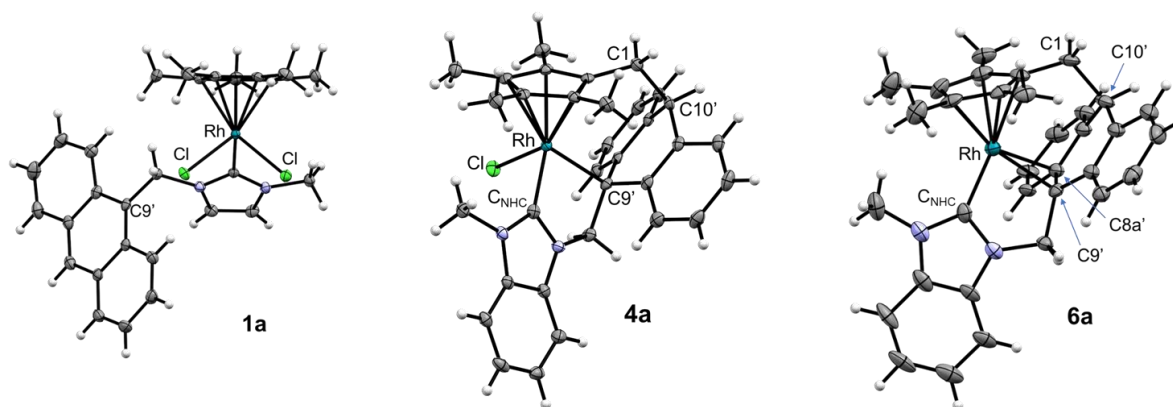
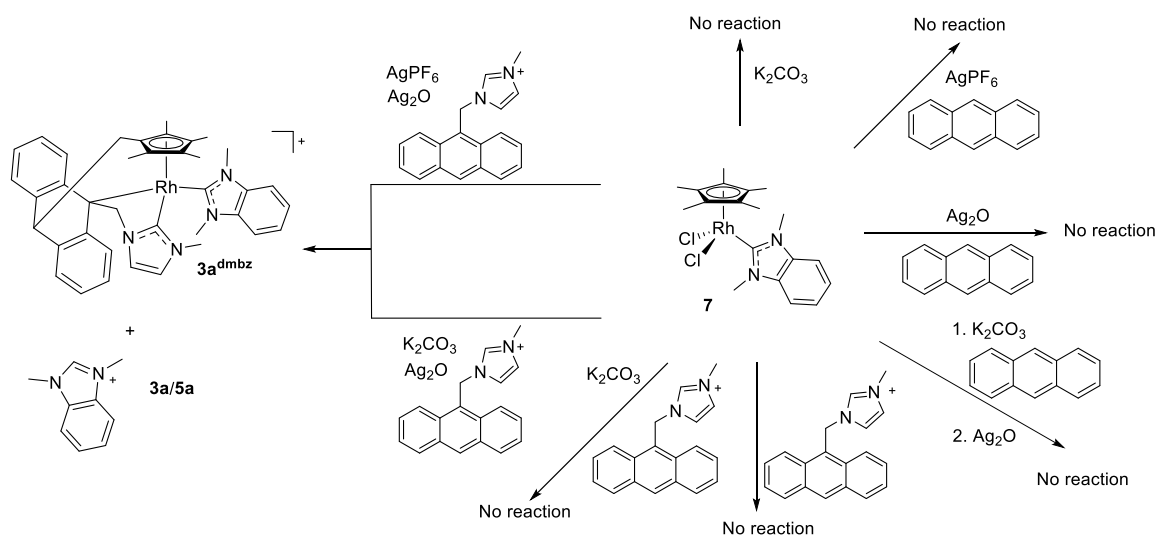


Figure S1. Molecular structures of **1a**, **4a** and **6a** drawn at 50% probability level. Any counterions or co-crystallized solvent molecules have been omitted for clarity.



Scheme S1. Reactions of [dichlorido(1,3-dimethylbenzimidazol-2-ylidene)(η^5 -pentamethylcyclopentadienyl)rhodium(III)] **7** under different conditions with various compounds.

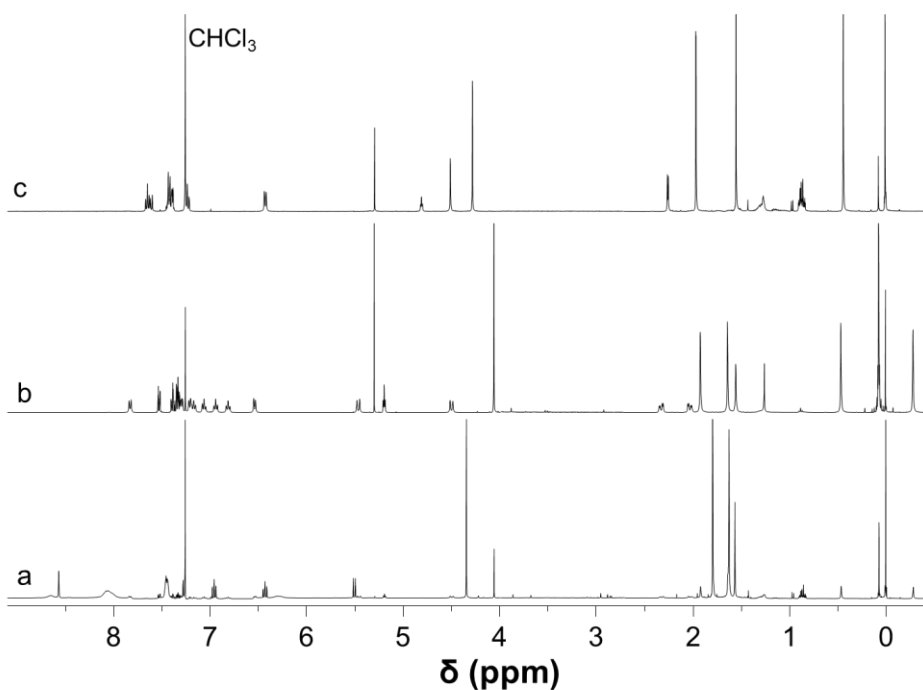


Figure S2. ^1H NMR spectra of (a) a mixture of **2a** and **4a**, (b) **4a** and (c) benzimidazolium Rh complex **6a** in CDCl_3 .

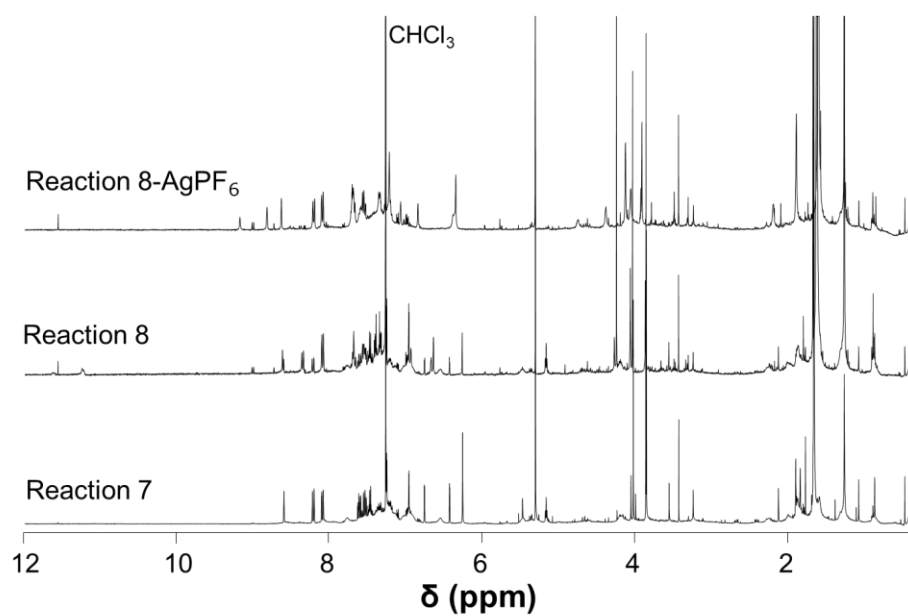


Figure S3. ^1H NMR spectra in CDCl_3 of reactions 7 and 8, before and after AgPF_6 (8-AgPF₆) was added.

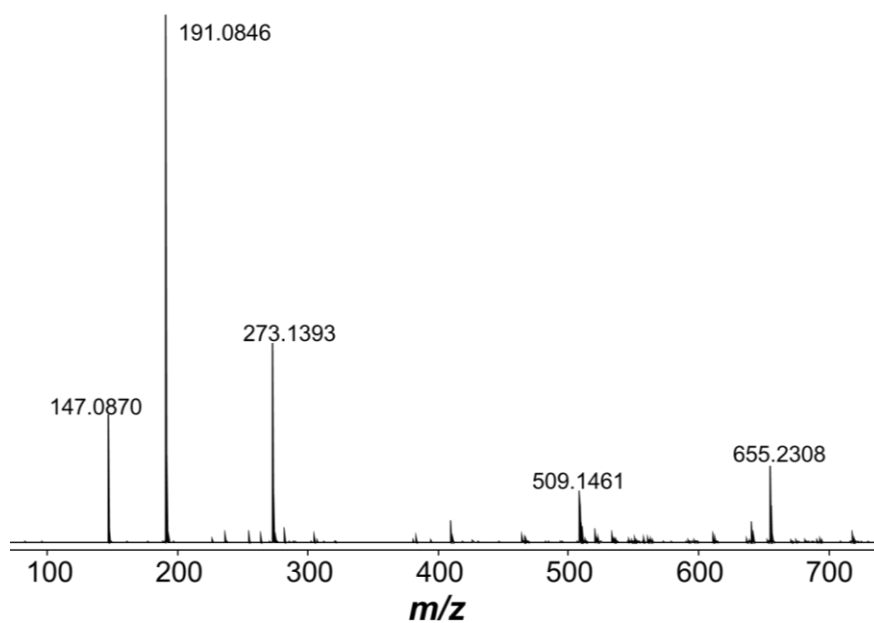


Figure S4. ESI-mass spectrum of reaction 8 before AgPF_6 was added.

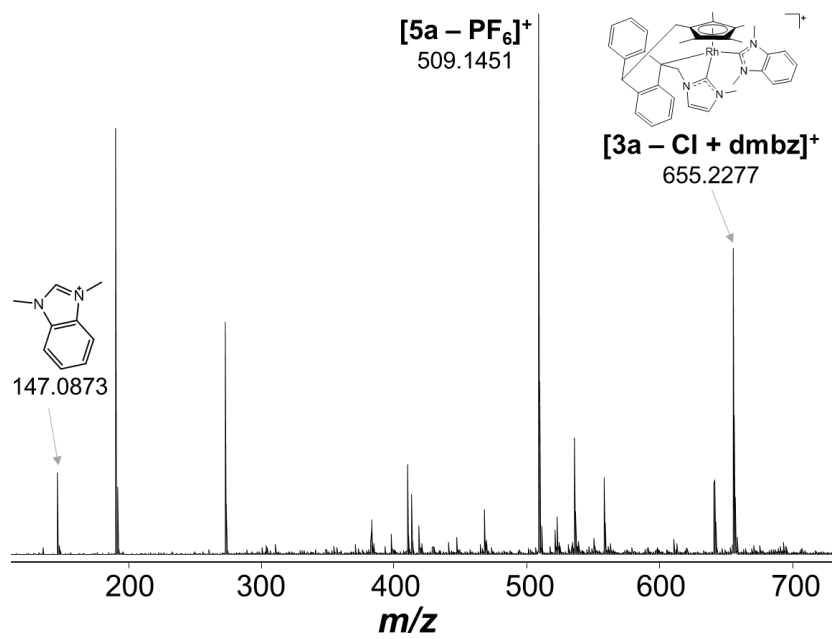


Figure S5. ESI-mass spectrum of reaction 8 after AgPF_6 was added.

Computational Details

Geometry optimizations, frequency analyses, IRC, Mayer bond indexes, CM5 charges and energies were calculated with density functional theory using the Gaussian 16 suite of programs, revision c01 running on ICHEC supercomputer cluster Kay (2 × 20 core 2.4 GHz Intel Gold Skylake 6148 processors). The three-parameter hybrid gradient-corrected functional (ω B97xD) was employed for all calculations as developed by Gordon-Head *et al.*, and incorporates a modified version of Becke's exchange functional (B97),⁸ with the non-local correlation of Perdew-Wang. This functional contains a small degree of HF exchange for short range exact exchange.⁹ Moreover, this particular functional features a long range empirical function to account for dispersion effects.

The reaction pathways were constructed from geometry-optimized structures representing energy minima or saddle points (transition states) using the ω B97xD level of theory, which has an established reputation for producing highly accurate structural parameters for organometallic complexes.⁹⁻¹² This method incorporates a modified version of Grimme's D2 algorithm for calculating damped long range dispersion corrections, which are beneficial in providing realistic energies for complexes where strong internal interactions between substituents are present.^{13,14} Calculated gas-phase energies were corrected through the application of an approximated solvent potential using the SMD protocol.¹⁵ Synthetically, a mixture of solvents was used, but for computational purposes the corrections were based on the most polar solvent, *i.e.*, methanol.

For each step of the geometry optimizations, self-consistent iterations were performed until a convergence criterion of 10^{-8} was obtained. A double zeta Gaussian-type basis set of Petersson was used and augmented with an additional set of d-orbitals for C, N and Cl and an additional p-orbital for hydrogen (6-31G(d,p)).¹⁶ The rhodium center was modelled with the Stoll and Preuss SDDAll basis set of double zeta quality, substituting the core electron wave-functions with an effective pseudopotential.¹⁷ Optimized structures were verified to be stationary minima as indicated by the absence of imaginary frequencies or transition states as indicated by a single imaginary frequency. All transition states were verified to be connected to the appropriate minima by performing intrinsic reaction coordinate (IRC) analyses using the geometry and frequency analysis of the transition state as the starting point. Population analysis was performed using CM5 which employs the charge fitting methodology (Charge Model

5) as developed by Truhlar and Cramer *et al.*¹⁸ Post-quantum analysis including charge decomposition analysis was performed using the AO-MIX suite of programs.¹⁹ QTAIM analyses²⁰ were performed using the MULTIWFN program. Where appropriate, the density gradient was analyzed for non-covalent interactions using the NCI algorithm as outlined by Contreras-García, Yang and Johnson²¹ and implemented through the MULTIWFN program.²² Moreover, combined visualization of covalent and non-covalent interactions was performed using Density Overlap Regions Indicator algorithm (DORI) as developed by de Silva and Corminboeuf,²³ and implemented using MULTIWFN.²² Ball and stick diagrams were drawn using the Chemray program.²⁴ NCI and DORI plots were generated using VMD,²⁵ molecular orbital pictures were drawn using the iQmol program.

Geometry Comparison and Benchmarking (Computational versus Experimental Models)

To benchmark the chosen level of theory and basis set, optimization of **A**, **J**, and **L**, representing the three experimentally obtained structures **1a**, **3a**, and **5a**, showed excellent agreement between computational and experimental data with RMS values <1% for **A** and **L** (Figure S6, Scheme S2). The higher RMS value for **J** is related to greater rotation of the NHC ligand towards the plane of the η^5 -C₅Me₄R ligand (Cl–Rh–C11–N: -108.40°, 67.74°) in the solid-state structure than in the DFT model (-86.34°, 80.74°), which further twists the core of the substituted anthracene group.

Complex **J** displayed the largest discrepancy with the solid-state structure (**3a**) mainly due to a rotation of the NHC ligand (about the Rh–C_{NHC} bond) which has a knock-on effect of displacing the connected anthracene and Cp* moieties. These differences are hypothesized to be the result of packing effects where (Rh)Cl is engaged in a short intermolecular interaction (2.680 Å) with H18B which belongs to the methylene group that bridges the NHC and anthracene moieties.

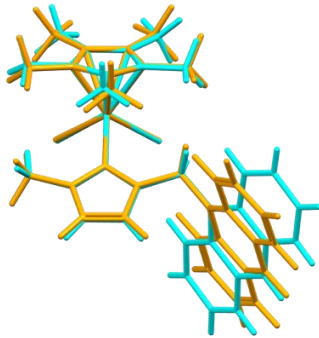
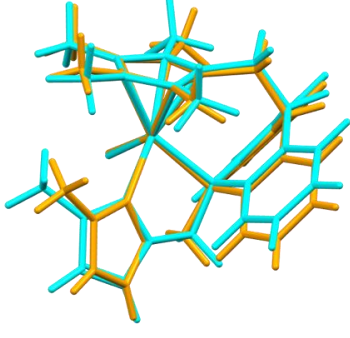
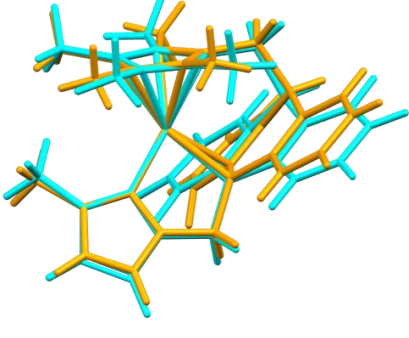
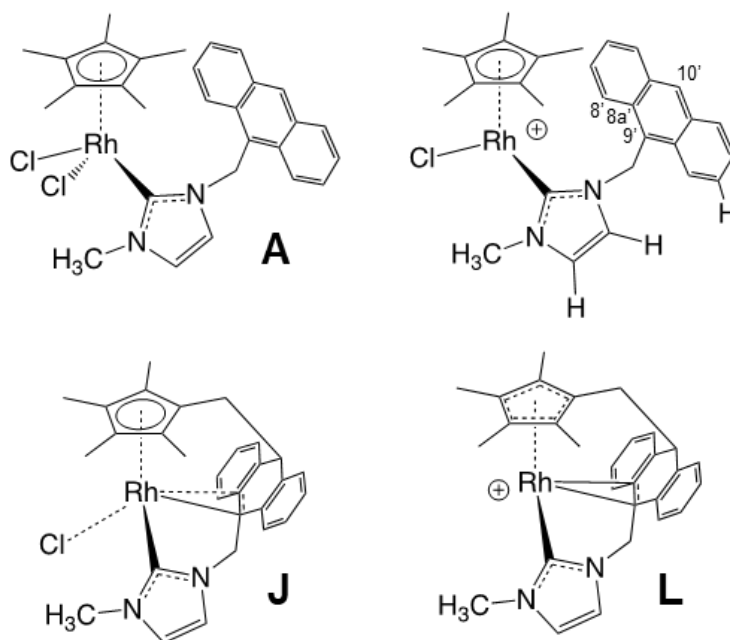
A_{syn} (1a)	J (3a)	L (5a)
		
Orange – experimental	Orange – experimental -116.29° DFT = -114.94°	Orange – experimental
Cyan - DFT	Cyan - DFT	Cyan - DFT
RMS = 0.00603 (0.6%)	RMS = 0.0909 (9.1%)	RMS = 0.00347 (0.35%)

Figure S6. Tube representation of the crystallographically obtained solid-state structures of **1a**, **3a**, and **5a** (orange) with DFT calculated gas-phase models (cyan). The root mean (RMS) square differences for selected core bond lengths, bond angles and torsional angle is given. Any counterions were omitted for clarity.

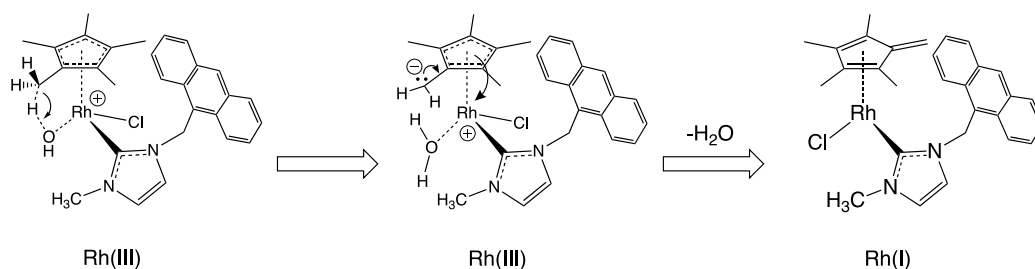


Scheme S2. Representative model structures of complexes obtained by X-ray diffraction analysis with the relevant numbering scheme to the computational investigation.

Reaction pathway investigations for the conversion of **1a** to **3a**

Starting with structure **A** (Scheme S2), it was necessary to optimize **A_{syn}** whereby the substituted methylene-9-anthracene was positioned with a *syn* conformation with respect to the Ru–C_{NHC} bond in order to facilitate the upcoming cycloaddition process. In contrast, the solid-state structure of **1a** showed that the 9'-anthracene substituent is in an *anti*-position. The energy difference between **A_{anti}** and **A_{syn}** is minor at -4.26 kcal mol⁻¹ with no notable changes in the metal associated bond lengths.

For the conversion **1a**→**3a**, we envisaged that the resulting cyclic motif is due to an intramolecular C–C bond being formed from a [4+2] cycloaddition between the 9',10' positions of anthracene and an external ene functionality of an *in situ* generated η^4 -tetramethylfulvene derived from a deprotonated methyl group associated with the Cp* ligand. It is well established that anthracene and related extended polycyclic aromatics undergo photochemically-mediated cycloadditions with a vast array of π -bonded substrates, including alkenes and alkynes.²⁶ Although the alkyl C-H bonds do not generally undergo deprotonation, in this case generation of an exo-ene functionality is reasonable as the transformation of the metal coordinated anionic η^5 -pentamethylcyclopentadienyl ligand into a neutral η^4 -tetramethylfulvene is electronically favorable. This type of coordinated-ligand conversion has been reported to be promoted by a variety of reagents including O₂,^{27,28} bases,²⁹ and through hydride abstraction with Ph₃C[B(C₆F₅)₄].³⁰ For the described process, experimentally a base (Ag₂O) is present and, therefore, the formation of OH⁻ and its role as a base in the calculated reaction pathway is justifiable.³¹ However, deprotonation of the Cp* methyl group has to be accompanied by an electron pair transfer, which conveniently results in reduction of Rh(III) to Rh(I). Our initial approach to directly deprotonate **A_{syn}** with hydroxide, unassisted by the Rh center, was unsuccessful. Therefore, we hypothesized that this particular step proceeded within the metal coordination sphere (Scheme S3). This suggests *a priori* that one Cl⁻ ligand is replaced by OH⁻ resulting in complex **D**, after the weak association between Cl⁻ and complex **C** is broken (**C**→**D**). A scan of **A_{syn}** involving Cl⁻ removal from the Rh center revealed a barrierless pathway with no transition state but is accompanied by an increase in energy of +11.21 kcal mol⁻¹ (**A**→**B**).³²



Scheme S3. Intermediates in the conversion of **1a** to a Rh^I(η^4 -tetramethylfulvene) derivative.

One of the key steps in the conversion of **1a** to **3a** is the removal of a proton from the Cp* ligand in order to facilitate the formation of the external ene which can undergo cycloaddition with the 9',10' positions of the anthracene component. Transfer *via* external formation of hydride can be ruled out from the reaction conditions. Extraction *via* a proton can only result in electron transfer and reduction of the Rh center. Since the synthetic reaction involves the highly basic reagent Ag₂O, we reasoned that OH⁻ is a likely and suitable nucleophile with the formation of water. A variety of alternative pathways were tried but ultimately failed. This included deprotonation on top of the Cp* ligand outside the metal coordination, but without first removal of Cl from **A_{syn}**, this was energetically unfeasible. An attempt was made to deprotonate the methyl group of Cp* on the top side of structure **C**. This resulted in model complexes whereby a doubly bridged OH⁻ ion is positioned between hydrogen atoms belonging to two methyl groups and no deprotonation is observed. Another attempt resulted in a nucleophilic attack on the Cp* ring. The addition of OH⁻ to **A_{syn}** (with 2 Cl ligands) proved unfavorable and resulted in loss of the neutral NHC ligand. The only viable pathway was the replacement of one Cl by OH, then deprotonation of a methyl group while the OH⁻ remained partially bonded to Rh center (**E_{Ts}**, Scheme S3). The IRC analysis of **E_{Ts}** showed the expulsion of water and not a rebounded coordination to the Rh center. This is explained by the post reduction of Rh, whereby Rh(I) being more electron rich and less Lewis-acidic, does not favor additional coordination by water. In fact, two purposeful attempts to optimize a structure with Rh-OH₂ motif were not successful and the water molecule maintained only a hydrogen bonding interaction with the organometallic complex.

It is conceivable that other methyl groups of the Cp* are deprotonated leading to the exo-ene bond on sides away from the anthracene moiety, but these pathways were not investigated. Only the pathway where the exo-ene bond ended in close proximity to the anthracene moiety was modelled in detail.

An IRC analysis³³ of the PES using **E_{TS}** as the starting point revealed that proton and electron transfer originated from the formally anionic deprotonated Cp* ligand. Formally the deprotonation resulted in an anionic methylene group which quickly transformed into an exo-ene when the pair of electrons transfers from the Cp* to the Rh center. A scan involving the displacement of the hydroxido ligand from the Rh center in **D** revealed the location of the transition state **E_{TS}** ($\nu_{\text{img}} = -1351 \text{ cm}^{-1}$) on the PES (Figure S7) corresponding to methyl deprotonation of the Cp* ligand with $E_a = 20.17 \text{ kcal mol}^{-1}$ (**D**→**E_{TS}**). Water formation is concurrent with Rh–O bond cleavage affording a coordinately unsaturated metal center.^{34,35} The relaxed PES scan (**D**→**E_{TS}**) also revealed the necessary two-electron transfer step from the η^4 -tetramethylfulvene to the Rh center. A CM5-derived charge analysis at various points of the PES scan revealed a gradual reduction of the Rh(III) center in **D** to Rh(I) in **E_{TS}** to a minimum value in the post **E_{TS}** complex (prior **F**), which coincides with the complete transfer of H^+ to OH^- (Figure S8). Ogo *et al.* suggested that the O_2 promoted transformation of the Cp* ligand into η^4 -tetramethylfulvene in $[\text{RuCl}\{\kappa^2\text{-NMe(H)CH}_2\text{CH}_2\text{N(H)Me(Cp}^*)\}\}\text{BPh}_4$ involved one of three possible mechanisms for the electron transfer between the metal and deprotonated Cp* ligand; hydride transfer (HT), hydrogen atom transfer (HAT) or proton-coupled electron transfer (PCET).³⁶ In our case, the concurrent removal of the proton by hydroxide and metal reduction strongly suggests a concurrent PCET mechanism, whereby proton transfer is coupled with electron transfer. Complex **F** features the resulting water molecule which is hydrogen-bonded with the NHC and anthracene ligands. Dissociation of H_2O from **F** leading to **G** is energetically higher by only $+4.45 \text{ kcal mol}^{-1}$.

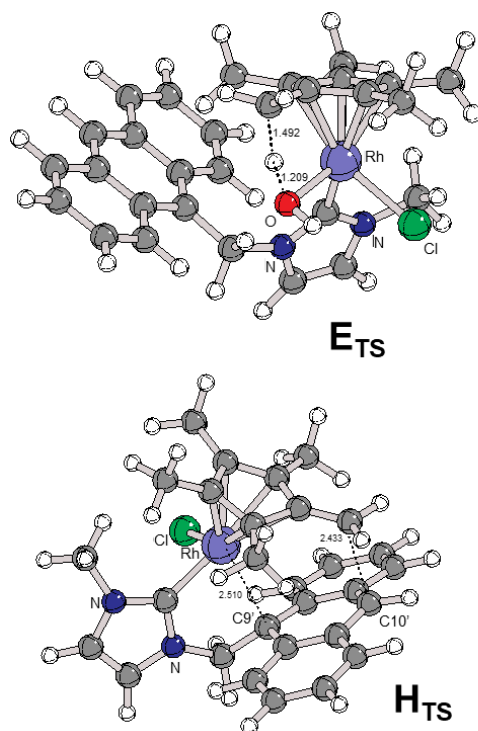


Figure S7. Geometries of the two key transition states **E_{TS}** (proton extraction/reduction) and **H_{TS}** (metallocycloaddition) for the conversion of **A_{syn}** (**1a**) into **I** (**3a**). All distances are in units of Å.

Figure S8 shows the progression of MBI values for the bonds that demonstrate the greatest amount of change associated with PES surrounding the transition state **E_{TS}**. Moreover, the reduction in charge at the Rh center is also shown. Importantly, the graph shows that the proton transfer process occurs simultaneously with a rapid change in charge (reduction of Rh from a formal +3 to +1 oxidation state) while the exo-ene π -bond is fully formed. However, at **E_{TS}**, the Rh charge value is midway between the two oxidation state extremes. The transition state **E_{TS}** features equal strength bonds for the transferred proton, C6–H9 and O65–H9. Moreover, the Rh–O65 bond, which at the beginning of forming the transition state is moderately strong, rapidly decreases and eventually breaks as the IRC coordinate passes through **E_{TS}**, and the metal-coordinated hydroxide is converted into free water.

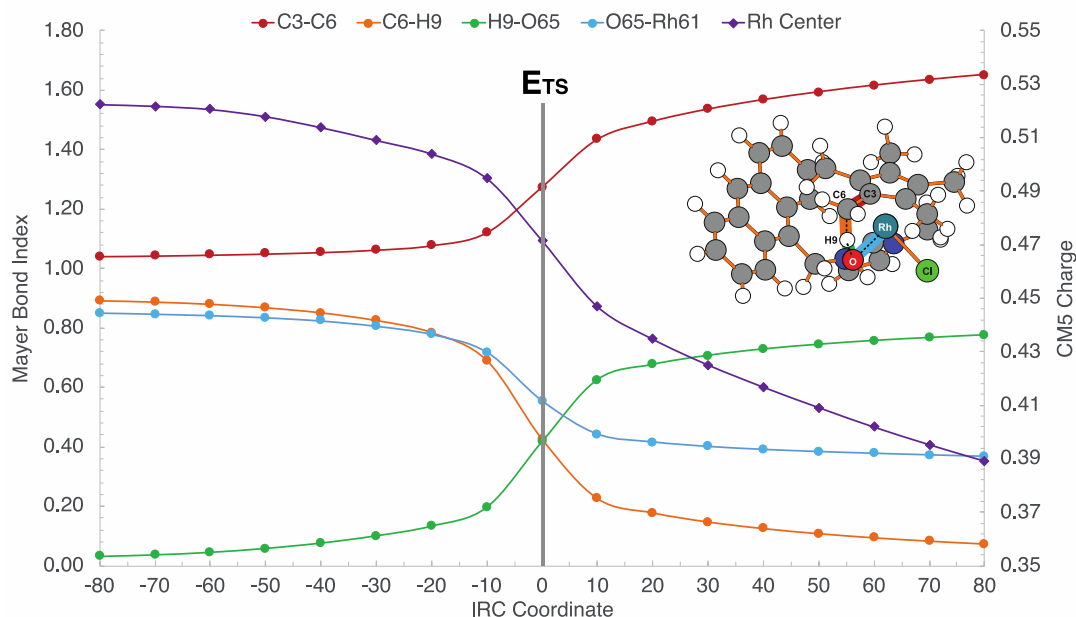
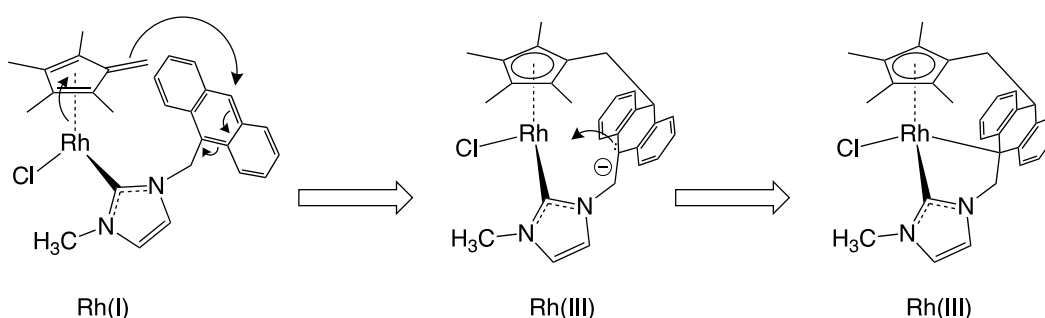


Figure S8. Evolution of the changes in the MBI values for the bonds associated with the proton transfer (H9) for the IRC coordinate around the transition state E_{Ts} , during the steps $D \rightarrow E_{Ts} \rightarrow F$. C3-C6 represents the exo-ene bond. The change in atomic population for the Rh center during the proton transfer are shown as calculated using Truhlar and Cramer class IV charge fitting method CM5.¹⁸

An interesting observation during $E_{Ts} \rightarrow F$ is the simultaneous rotation of the η^4 -tetramethylfulvene ligand, whereby the exo-ene is aligned with the 9',10' positions of the anthracene substituent, which shortens the distance between the two ligands and enables the cycloaddition to proceed as represented by H_{Ts} (Figure S7). The driving force for the rotation is hypothesized to be partial relief of steric hindrance between the fulvene and NHC ligands, as the exo-ene bond is folded upwards, away from the central of plane of the fulvene. Rotation about the Rh–C_{NHC} bond in **G** is more facile due to a more open metal coordination environment. Examination of **G** reveals that the exo-ene bond does not coordinate to the metal center as observed in a number of other complexes featuring $\eta^2:\eta^4$ -tetramethylfulvene ligands where the external ene bond is strongly bent inwards towards the metal center. Examples include $[Ru(COD)(\eta^2:\eta^4\text{-tetramethylfulvene})]$,³⁷ $[RuCl(\kappa^2\text{-NMe(H)CH}_2\text{CH}_2\text{N(H)Me})(\eta^2:\eta^4\text{-tetramethylfulvene})]BPh_4$,³⁶ and $[Ir(CH_3)_2(NHC)(\eta^2:\eta^4\text{-tetramethylfulvene})]BAr^F_4$, where NHC is 1,3-*N,N*-dimethylimidazol-2-ylidene.³⁰

Further Details Regarding the Cycloaddition between Tetramethylfulvene and Anthracene Ligands. As discussed, two principal bonds are formed; a C–C bond between the terminal carbon of the exo-ene bond and the 10 position of anthracene, while a Rh–C bond is created with the 9-position of anthracene. The source of electrons for the Rh–C bond originates from the anthracene, while the Rh center transfers electrons to rearomatize the Cp* ligand resulting in oxidation of the Rh to the formally +3 state (Scheme S4).



Scheme S4. Key steps in the mechanism outlining the formal movement of electrons and Rh–C and C–C bond formation.

The Rh(fulvene)–9',10'-anthracene cycloaddition step involves two bond formations, *i.e.*, coupling between C10' and the exo-ene C1 of the fulvene ligand in addition to Rh–C9' (Scheme S4). Before the cycloaddition step (**G**→**H_{TS}**), an NCI analysis of **G** revealed a coordinately-unsaturated Rh center with no covalent interaction between Rh and C9' (Figure S9). Examination of the PES before and after **H_{TS}** by intrinsic coordinate analysis (IRC) showed that the Rh–C9' bond formed first and, as it strengthens, simultaneously a bond is formed between the exo-ene (C1) and the anthracene C10'. Mayer bond indices (MBI) analysis revealed that as the exo-ene approaches the anthracene component, the Rh and C9' centers combine to afford stronger covalent character than the C1'–C10' bond at **H_{TS}**. The cycloaddition process features a low energy barrier (**G**→**H_{TS}**, $E_a = +14.49 \text{ kcal mol}^{-1}$) with a substantial decrease in energy after crossing the transition state (**H_{TS}**→**I**, $E = -34.47 \text{ kcal mol}^{-1}$) indicating a unidirectional non-reversible reaction. The process is completed by the restoration of a substituted aromatic η^5 -cyclopentadienyl ligand. The intramolecular Rh–C9'/C1–C10' coupling process is rationalized by an overlap of the HOMO (fulvene-based) with the unoccupied LUMO (anthracene-based), while the origin of the metal–anthracene Rh–C9' bond appears to be a charge transfer from an occupied MO on

anthracene (HOMO-1) to an empty d-orbital on Rh (LUMO+1; Figure S10). A CM5 charge analysis of **I** (Figure S10) indicated oxidation of Rh to +3. Employing MBI analysis indicated some degree of ring strain as Rh–C9' is weaker (0.597) than the Rh–C_{NHC} (C11) σ -bond (0.710) (Figure S11).

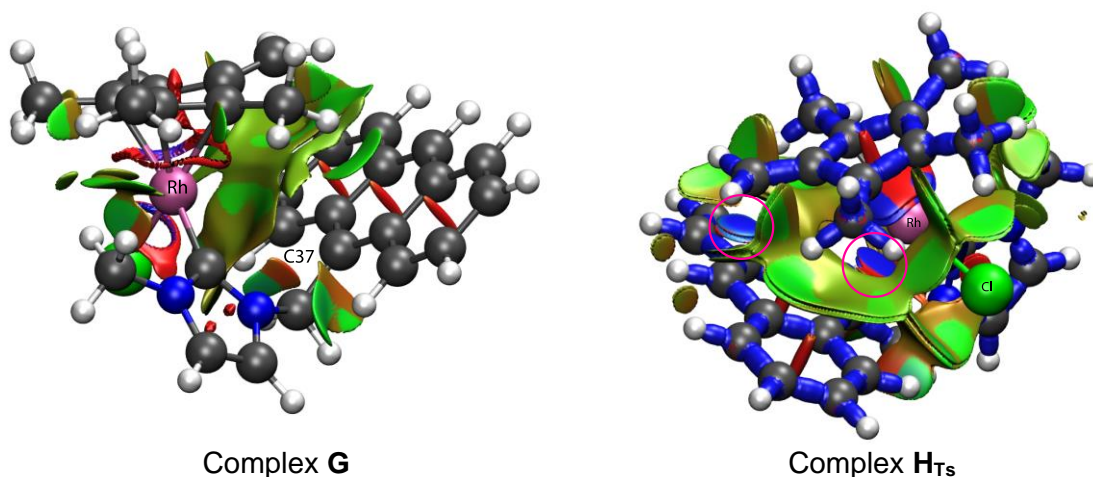


Figure S9. Left: NCI analysis of complex **G** revealing only non-covalent, van der Waals interactions (green) in the region of space between the Rh/exo-ene and anthracene moieties, confirming no Rh–C bonding. The plot is based on $s(\rho)$ plotted with $s = 0.8$ and $-0.1 < \rho < 0.1$ a.u. Right: DORI analysis of the transition state **H_{Ts}** confirming the development of new C–C and Rh–C covalent bonds as indicated within the red circles. Blue regions indicate covalent interactions while green regions represent non-covalent van der Waals interactions. The surfaces are plotted with a color-coded scheme based on $\text{sgn}(\lambda_2)/\rho(r)$ with a range of -0.02 au (red) to 0.02 a.u. (blue).

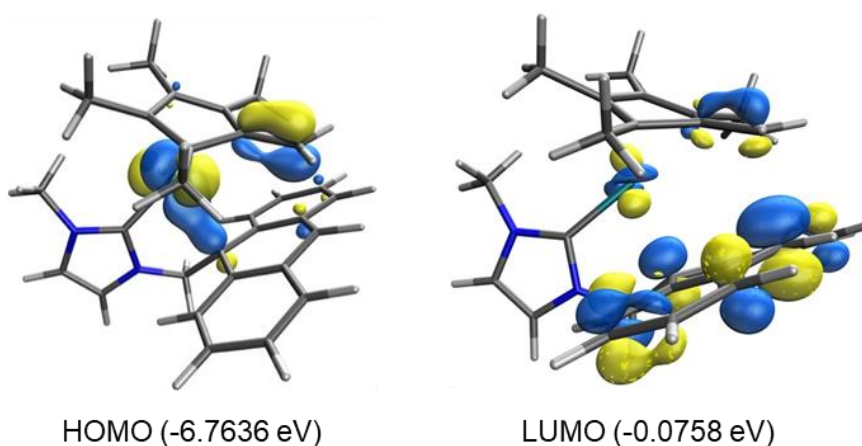


Figure S10. DFT calculated MOs (HOMO and LUMO) with complex **G** before the cycloaddition process. MOs are drawn with an isovalue of 0.05 a.u.

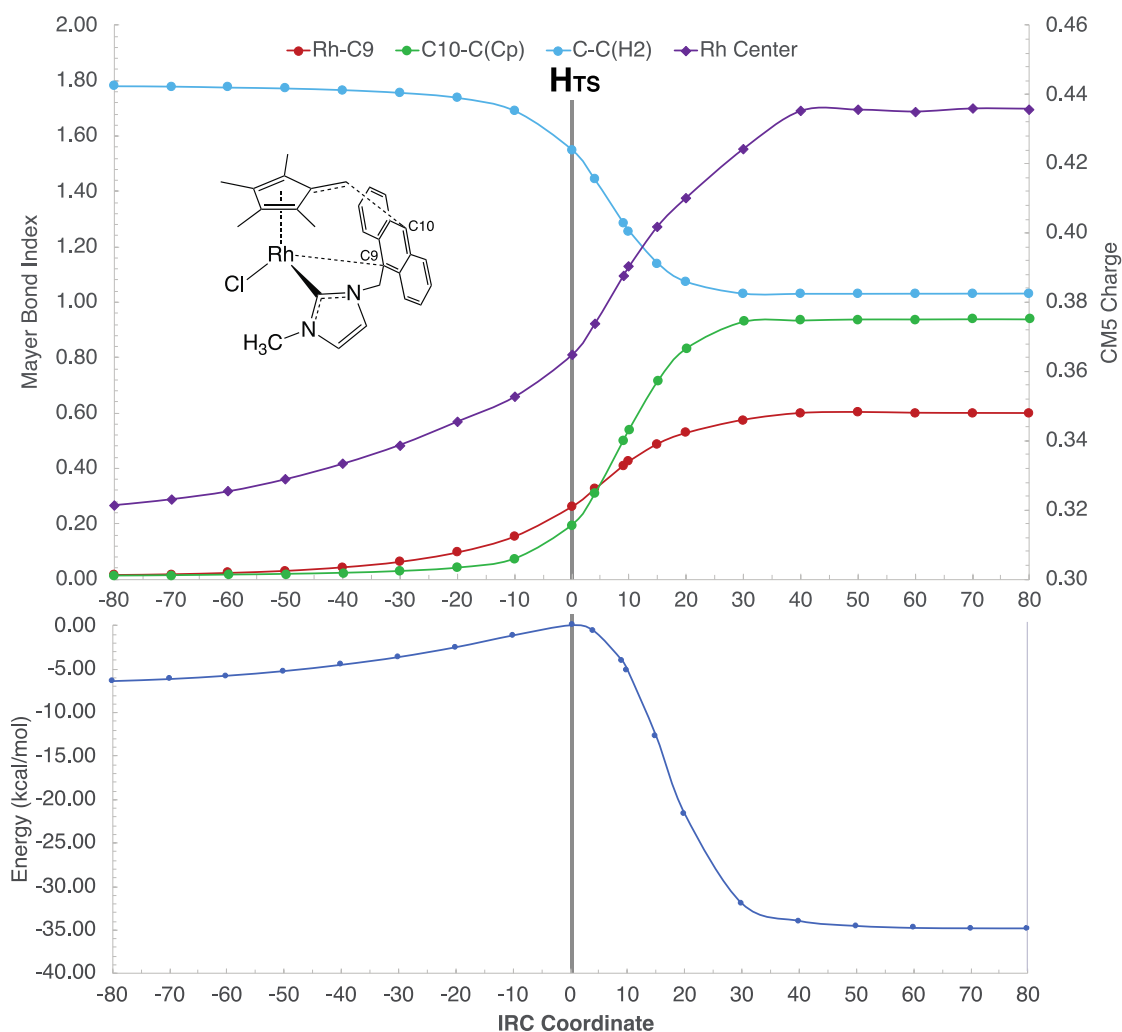


Figure S11. Top: Evolution of the changes in the MBI values for the bonds associated with the cycloaddition process for the IRC coordinate around the transition state H_{Ts} , during the steps $G \rightarrow H_{Ts} \rightarrow I$. The changes in atomic population for the Rh center during the proton transfer are shown as calculated using Truhlar and Cramer class IV charge fitting method CM5.¹⁸ Bottom: Enthalpy changes (gas phase) in units of kJ mol^{-1} versus IRC coordinate.

Before the coupling process, as represented by the transition state H_{Ts} , complex **G** featuring a tetramethylfulvene ligand and a Rh(I) center showed no covalent bonding between the metal and the anthracene moiety as demonstrated through an NCI analysis (Figure S9, left). This calculation confirmed the low oxidation state of the metal and its associated reduced Lewis acidity. To follow the important changes during the coupling process, both MBI and CM5 charge analyses were performed at various steps of the IRC coordinate around H_{Ts} (Figure S11). The analysis revealed that the Rh–C bond was well developed at the transition state, while there was only weak

covalent bonding between the terminal exo-ene C center and C10' of the anthracene. A NCI plot of **H_{TS}** revealed the development of covalent bonding between Rh and C1 and C9',C10'. At **H_{TS}**, the π -bond of the exo-ene functional group was not sufficiently weakened, hence the C–C bond is only weakly developed. Interestingly, at **H_{TS}**, the charge of Rh is a midway point through the oxidation process with parallel Rh–C bond formation. The subsequent formation of the C–C bond post **H_{TS}** suggests that this is dominant the driving force of the cycloaddition addition step. This indicates that the Cp* re-aromatization process, resulting from electron transfer from the Rh center, helps to initiate the cycloaddition process by feeding electrons into the exo-ene group.

*Reaction pathway investigations for the conversion of **3a** to **5a***

The second reaction yielding the cationic complex **L** (**5a**) is synthetically promoted by an extraction of the remaining chlorido ligand from **I** (**3a**) by employing a silver salt. Computationally, this process was simulated by evoking a relaxed PES scan whereby the Rh–Cl distance is gradually lengthened beyond the sum of the combined covalent radii for Rh and Cl (2.34 Å). At a Rh...Cl distance of 3.717 Å, analysis of the RMS gradient indicated a transition state (**J_{TS}**) which was confirmed through optimization and frequency analysis (-33.7 cm⁻¹). Continuation of **J_{TS}**→**K** results in a local minimum energy structure featuring a Rh...Cl distance of 3.811 Å where the Cl⁻ counterion is easily dissociated as indicated by almost neglectable energy descent of -0.28 kcal mol⁻¹. An NCI analysis of **K** revealed that the chloride anion forms only H-bonding interactions with hydrogens associated with methyl groups of the η^5 -cyclopentadienyl and NHC ligands (Figure S12). The complete PES pathway for the conversion of **I** (**3a**) into **L** (**5**) is shown in Scheme 2.

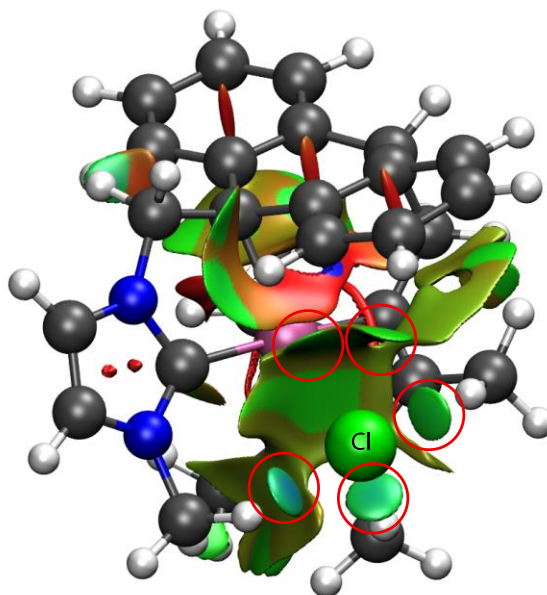
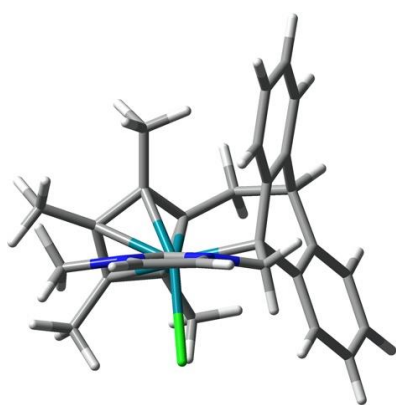
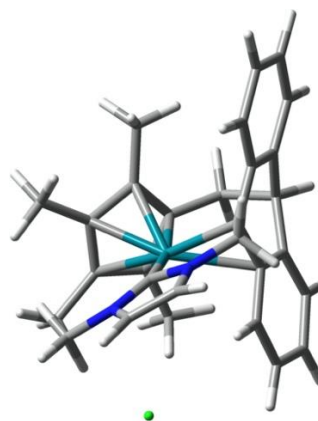


Figure S12. NCI analysis of complex **K** revealing only non-covalent, van der Waals interactions (green) in the region of space between the Rh and Cl centers. The chloride forms only H-bonds with the surrounding ligands as indicated by red circles.

An interesting observation is the rotation of the NHC ligand about the Rh–C_{NHC} bond during the breakage of the Rh–Cl bond (**I**→**J**_{TS}), which from the connectivity of NHC to the anthracene component has the knock-on effect of twisting the anthracene such that it is significantly tilted (Figure S13). Consequently, the C8a' and C8' centers of the anthracene are brought to a shorter distance to the Rh center (2.374 Å). This distance is close to the sum of the covalent radii for Rh and C(sp²) (2.18 Å). A transition state structure (**M**_{TS}) was located on the PES whereby the ring plane of the anthracene is tilted away from the Rh center (Rh···C8a' 2.874 Å) and is +8.69 kcal mol⁻¹ higher in energy than **L**. Therefore, due to the coordinatively unsaturated metal environment within **L** (**5a**) and the short metal distance with a ring of the anthracene, the nature of the interaction between Rh and the anthracene component was investigated using topological analyses based on the computationally-derived electron density (ED) and a MO-based approach.



Structure **I** Rh–Cl distance: 2.431 Å



Structure **K** Rh...Cl distance: 3.671 Å

Figure S13. Before and after Rh–Cl bond dissociation (i.e., **I**→**J**→**K**), showing the twisting of the NHC ligand and the connected anthracene.

The MBI analysis, based on the integration of AO overlap,³⁸ indicated two potential interactions; Rh...C8a' and Rh...C8' (2.016, 0.202), and both are significantly weaker (less than half) than the Rh–C9' (0.578) or Rh–C_{NHC} (0.695) bonds. Analysis of the electron density (ED) employing QTAIM methodology²⁰ failed to locate a BCP between Rh and C8a' or C8'. However, there is an increasing number of literature examples indicating that metal-ligand BCPs are lost in the vicinity of the metal center. This is frequently reported for metallocyclic structures where two critical points^{39,40} (here a BCP and a RCP) are degenerate and have collapsed onto one another affording a situation termed a catastrophe point.⁴¹ Further scrutiny of the ED topology associated with **L**, using the non-covalent interaction (NCI) analysis,²¹ highlighted a hole in the reduced density gradient (RDG) isosurface between C8'/C8a' and Rh (Figure 3, top), suggesting the presence of covalent bonding. Moreover, a density overlap regions indicator (DORI) analysis was performed which defines a molecular scalar and differentiates covalent and non-covalent interactions on the basis of $\Theta(\mathbf{r}) = (\nabla \mathbf{k}^2(\mathbf{r}))^2 / (\mathbf{k}^2(\mathbf{r}))^3$, where $\mathbf{k}(\mathbf{r}) = \nabla \rho(\mathbf{r}) / \rho(\mathbf{r})$.²³ The DORI analysis suggests a weak covalent interaction in the region defined by Rh, C8' and C8a' (Figure 3, bottom). For comparison, both NCI and DORI analyses on the transition state complex **M**_{Ts} indicate only steric interactions with no covalent bonding between C8'/8a' and Rh (Figure S14). Thus, the *in silico* ED analysis supports the experimental observations and suggests the presence of an octadentate (κ^8) ligand coordinating to the Rh center, which

possibly approaches nonadenticity (κ^9), although the auxiliary Rh \cdots C8' interaction was extremely weak in nature.

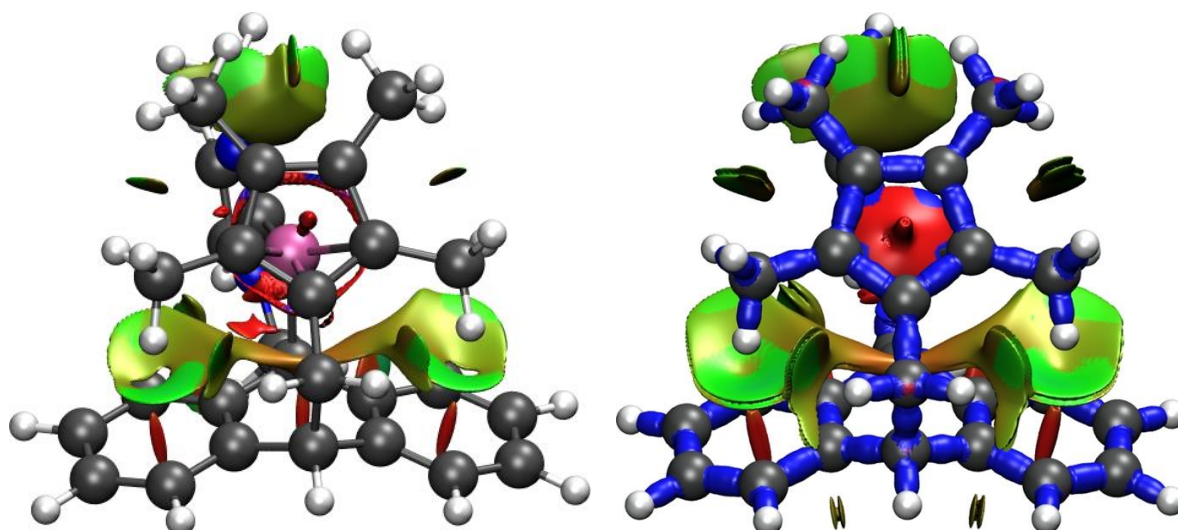


Figure S14. Left: NCI analysis of transition state M_{Ts} revealing only non-covalent, van der Waals interactions (green) in the region of space between the Rh/exo-ene and anthracene moieties, confirming no Rh–C bonding with the ring carbons. The plot is based on $s(\rho)$ plotted with $s = 0.8$ and $-0.1 < \rho < 0.1$ a.u. Right: DORI analysis of the transition state M_{Ts} confirming no covalent bonds with the C8'/C8a ring carbons of the anthracene component. Blue regions indicate covalent interactions while green regions represent non-covalent van der Waals interactions. The surfaces are plotted with a color-coded scheme based on $\text{sgn}(\lambda_2)/\rho(r)$ with a range of -0.02 au (red) to 0.02 a.u. (blue).

MO fragmentation analysis of **L** revealed multiple MOs (Figure S15) where a π -type MO centered on C8' and C8a' of the anthracene moiety weakly overlaps with d orbitals of Rh. However, the weakness of the Rh–C8a' bond is in part due to the presence of an antibonding interaction within HOMO-3 (Figure S15). MBI analysis indicates that the aromatic character of the ring C8' and C8a' positions is unperturbed by the presence of a metal interaction, further supporting the extremely weak bonds formed between the π -type MOs of the anthracene and the Rh center. A complete list of MOs involving Rh and C8'/C8a' is shown in Figure S16.

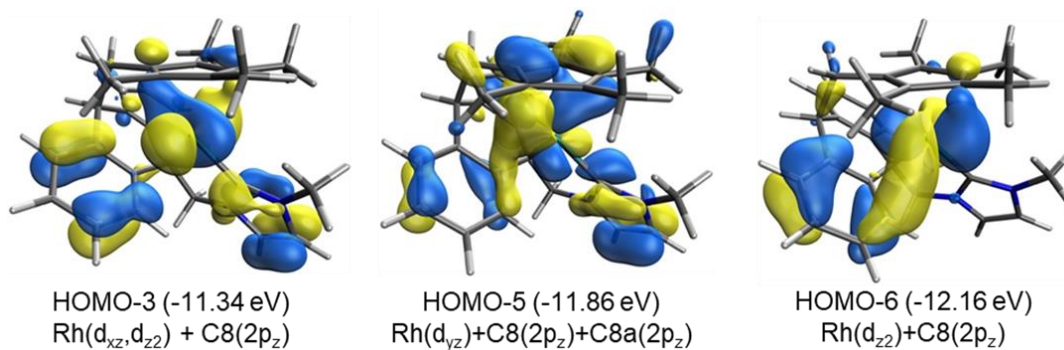


Figure S15. Three representative MOs associated with complex **L** (**5a**) demonstrating antibonding (HOMO-3) and bonding (HOMO-5, HOMO-6) character between the d orbitals of Rh and C8'/C8a' centers of the anthracene moiety. MOs are drawn with an isovalue of 0.100 a.u. The highest contributing AOs are also shown.

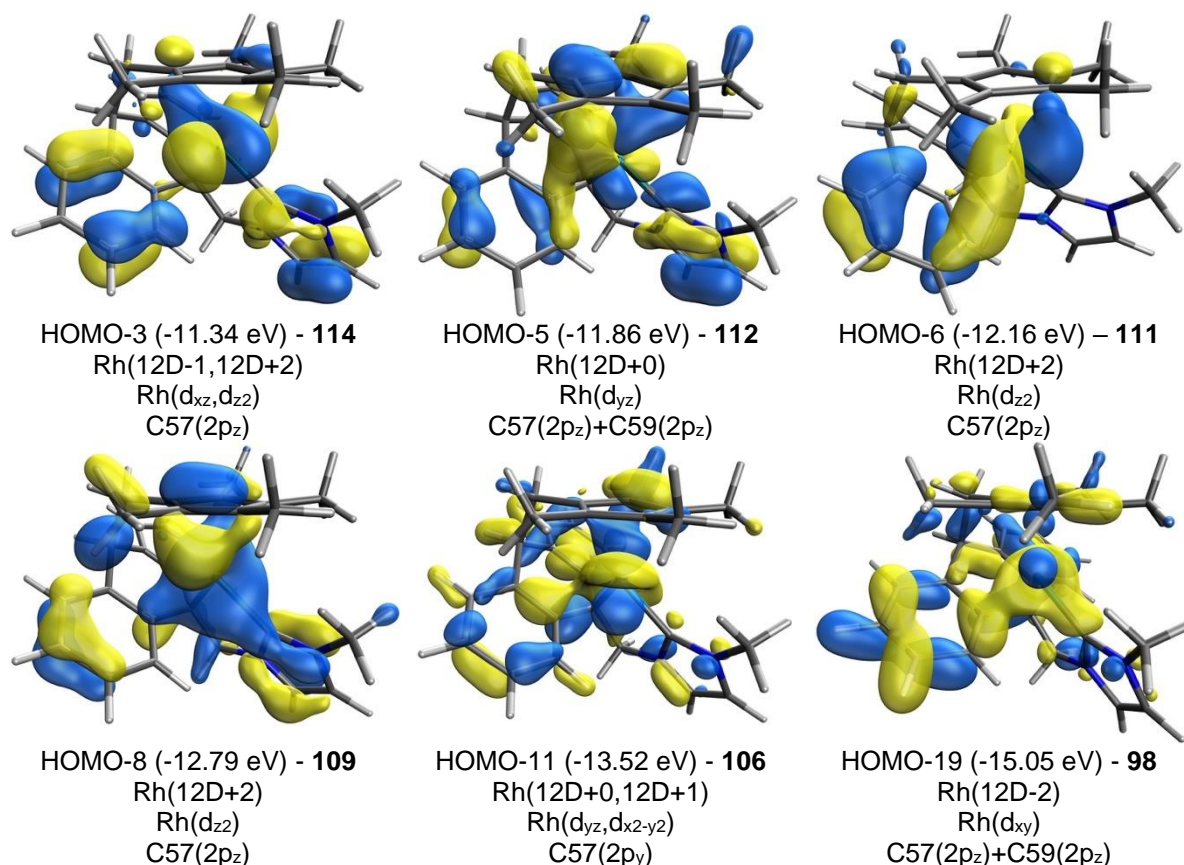


Figure S16. All MOs demonstrating bonding character between the d-orbitals of Rh and C8'/C8a' centers of the anthracene moiety. MOs are drawn with an isovalue of 0.100 a.u.

In the absence of a solid structure of **3a^{BIN}**, compound **N** was modelled to probe the interaction between **L** and external donors, whereby the smaller MeNC was coordinated to the Rh center in place of BIN. The structures of both cations, uncoordinated **L** and MeNC-coordinated **N** are shown in Figure S17. Considerable stability is demonstrated by an enthalpy drop of -34.88 kcal mol⁻¹ when MeNC coordinates to **L**. A comparison of the MBI values between **L** and **N** (Table S5) shows a very strong bond between Rh and C_{CNMe} of the isonitrile, while the metal–C_{NHC} bond strengthens fractionally, but Rh–C9' in comparison is significantly stronger in the adduct **N**. Importantly, is no longer present. Moreover, this was confirmed by a DORI analysis (Figure S18) which indicates that in the space defined by the Rh, C9, C8a and C8a' atoms, no covalent bonding is present, but dispersion forces. Moreover, the coordinated isonitrile forms only dispersion interactions with the anthracene component.

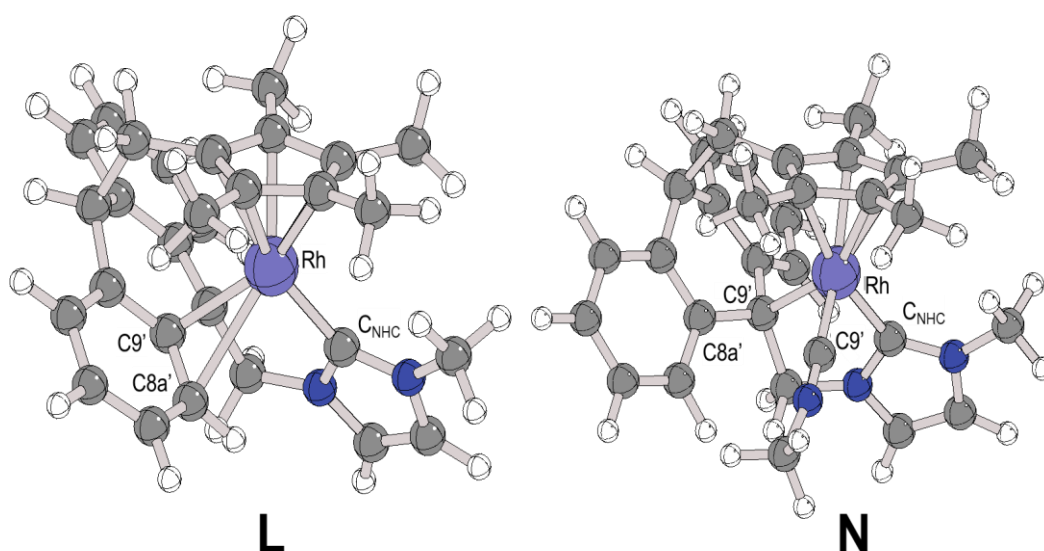


Figure S17. Geometry/energy-optimized structures of the uncoordinated complex **L** and the MeNC-coordinated adduct **N**. The smaller MeNC was used in place of the synthetically employed BIN.

Table S5. MBI values for selected bonds in the uncoordinated complex **L** and the MeNC-coordinated complex **N**.

Bond	Complex	
	L	N
Rh–C _{NHC}	0.694	0.705
Rh–C9	0.578	0.622
Rh–C8a'	0.216	0.000
Rh–C(NMe)	-	0.860

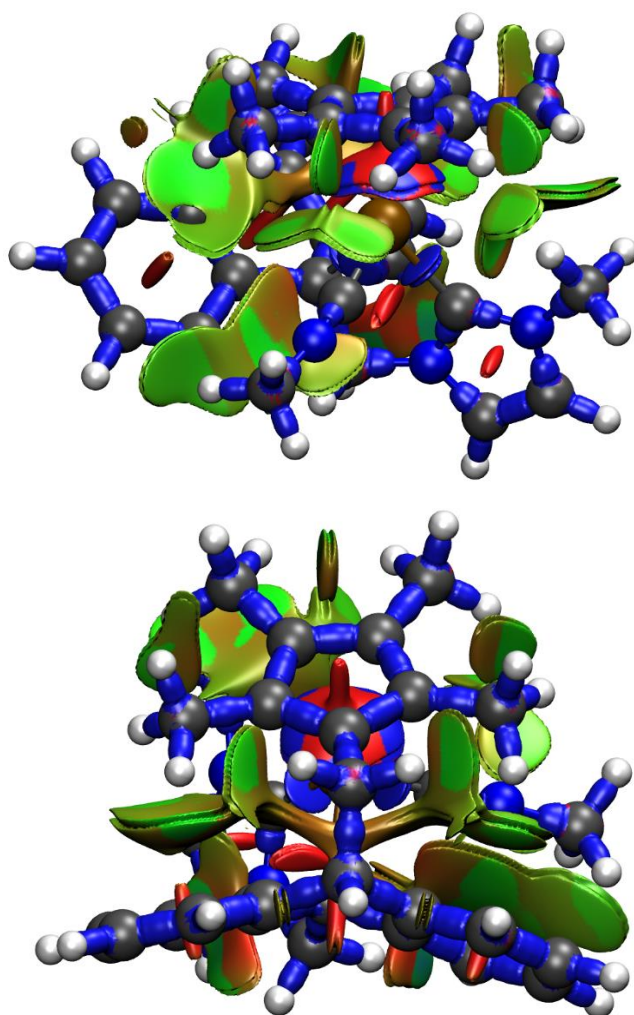
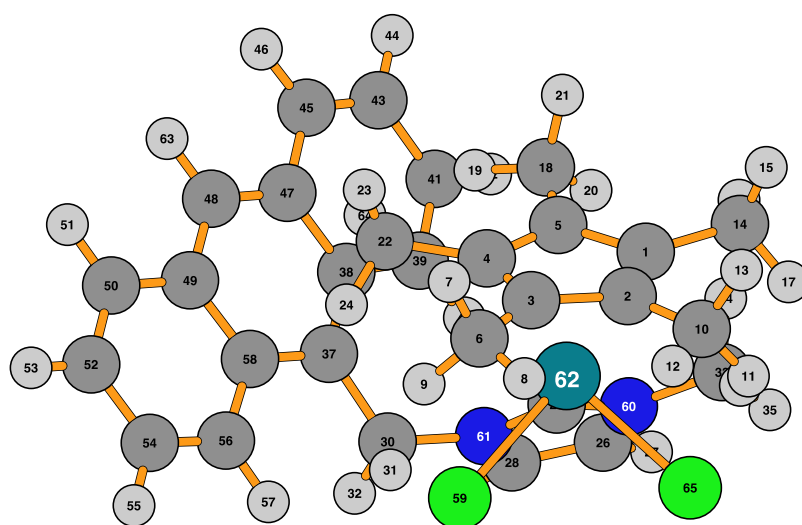


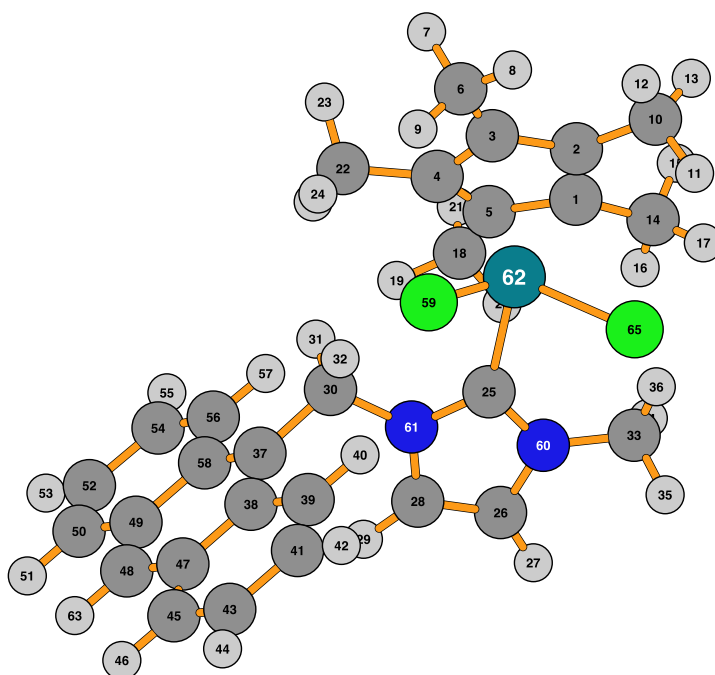
Figure S18. Two different orientations of the DORI graphical analysis of the MeNC adduct **N** confirming no covalent bonds with the C8' and C8a ring carbons of the anthracene component. Blue regions indicate covalent interactions while green regions represent non-covalent van der Waals interactions. The surfaces are plotted with a color-coded scheme based on $\text{sgn}(\lambda_2)/\rho(r)$ with a range of -0.02 au (red) to 0.02 a.u. (blue).

Coordinates for Complex A



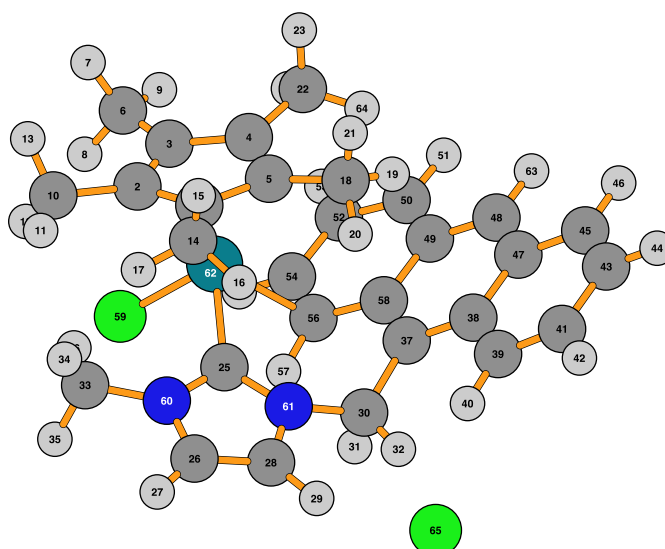
C	-2.47551400	-0.10259200	1.84925100	H	-2.55945300	-3.31008000	0.26367500
C	-2.80832600	1.29583500	1.63582600	H	-3.35335800	-3.49722500	-1.31932200
C	-1.60653100	2.01380300	1.49404600	H	-3.45388900	-1.93756800	-0.48609800
C	-0.49761200	1.08138800	1.62498600	C	2.32150000	-0.36972000	-0.89273000
C	-1.04631400	-0.21094600	1.90407400	C	2.59709200	-1.42471200	0.00795600
C	-1.43666600	3.48104000	1.27595300	C	1.98717400	-2.72683500	-0.03798800
H	-1.05341400	3.94944100	2.18937500	H	1.29920500	-2.97728500	-0.82760300
H	-2.37990300	3.95851800	1.00805200	C	2.26125500	-3.68955100	0.88741100
H	-0.73097800	3.66237000	0.46184000	H	1.77942700	-4.65899100	0.80410900
C	-4.20456700	1.82396700	1.59586000	C	3.16721100	-3.44732200	1.95621100
H	-4.79309200	1.27630700	0.85451900	H	3.36008300	-4.22087500	2.69239700
H	-4.22535100	2.87974400	1.32348400	C	3.79988100	-2.24587400	2.02844000
H	-4.67436000	1.70929700	2.57895500	H	4.51441200	-2.04124500	2.82094800
C	-3.47978300	-1.14736200	2.21758600	C	3.56007200	-1.21712000	1.06150100
H	-3.85942500	-0.95950200	3.22851600	C	4.25992500	-0.01836600	1.14168600
H	-3.04327500	-2.14770300	2.20615700	C	4.05592900	1.00081500	0.21653300
H	-4.33028900	-1.12786300	1.53080200	C	4.79567800	2.22080100	0.30674100
C	-0.28569600	-1.44525600	2.27194900	H	5.53276300	2.31568600	1.09924100
H	0.76862200	-1.36051400	2.01038100	C	4.58241200	3.23663600	-0.57340700
H	-0.68190200	-2.32814300	1.76505300	H	5.14639000	4.16068600	-0.49754500
H	-0.35805800	-1.61249200	3.35223000	C	3.60832200	3.08416300	-1.59756000
C	0.93258700	1.50657500	1.67677500	H	3.43341900	3.89708400	-2.29472300
H	1.11457300	2.09029200	2.58662900	C	2.88271700	1.93483800	-1.71414400
H	1.17956100	2.13216300	0.81562600	H	2.14483400	1.88047700	-2.50282400
C	-0.94496500	-1.19709400	-1.15025600	C	3.06912500	0.83327500	-0.81105100
C	-0.97024000	-3.16126700	-2.27744800	Cl	-0.84738500	2.02867400	-1.71617600
H	-1.37006100	-4.11140700	-2.59148500	N	-1.61182000	-2.36641200	-1.35032300
C	0.14195600	-2.49723200	-2.65198800	N	0.16636600	-1.32163500	-1.92724000
H	0.92669100	-2.75619100	-3.34377700	Rh	-1.66862900	0.42512800	-0.09524800
C	1.28221900	-0.38942500	-2.00855100	H	4.98510600	0.12225600	1.93952600
H	0.81655200	0.59412400	-2.06466100	H	1.60917000	0.65221700	1.68176600
H	1.77458000	-0.57956600	-2.96818600	Cl	-3.69678800	0.25951700	-1.39373300
C	-2.81987700	-2.80258700	-0.66906400				

Coordinates for Complex **A_{syn}**



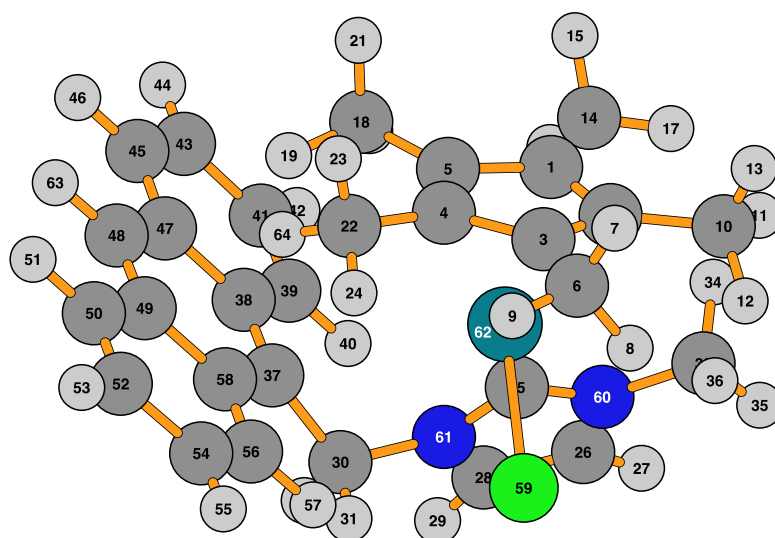
C	-2.28575000	-0.08675400	1.71468900	H	-2.70172700	-3.52306800	0.07189100
C	-2.78428400	1.26852800	1.54032300	H	-3.32294400	-3.52479200	-1.59979100
C	-1.70161300	2.09457200	1.18965200	H	-3.47113800	-2.05351200	-0.62831700
C	-0.49496000	1.27793400	1.16570800	C	2.32578800	-0.55726600	-2.81003000
C	-0.85773200	-0.05055000	1.55189400	C	2.10580800	-0.25904200	-4.17079800
C	-1.71468500	3.55824800	0.89119200	C	0.86275400	0.26808600	-4.65287200
H	-1.16333900	4.10641300	1.66303900	H	0.05026500	0.47277900	-3.96325000
H	-2.73191000	3.94929000	0.84850600	C	0.68525700	0.53535400	-5.97854700
H	-1.24414200	3.74595700	-0.07827900	H	-0.26403000	0.93708700	-6.31754900
C	-4.21919200	1.65077300	1.69893400	C	1.72645200	0.30202800	-6.92101200
H	-4.83784100	1.08363200	0.99663300	H	1.56087900	0.52630600	-7.96999800
H	-4.37542000	2.71180700	1.50120900	C	2.92286500	-0.19805700	-6.50489000
H	-4.55302100	1.43497800	2.71942900	H	3.72691200	-0.38096400	-7.21234400
C	-3.11760300	-1.22618400	2.21182400	C	3.14999300	-0.49957800	-5.12564400
H	-3.33778200	-1.10291100	3.27839500	C	4.36630000	-1.02521900	-4.69292300
H	-2.60607600	-2.18240400	2.08348800	C	4.58702200	-1.35226700	-3.35678200
H	-4.06682600	-1.27005000	1.67146600	C	5.83025000	-1.91927100	-2.93266400
C	0.07585400	-1.19974700	1.77763200	H	6.60825900	-2.06426000	-3.67705800
H	0.98832900	-1.09424900	1.18684500	C	6.03533500	-2.27692500	-1.63525400
H	-0.38869800	-2.14892600	1.50061700	H	6.98107300	-2.70921100	-1.32519800
H	0.35994800	-1.25325900	2.83372500	C	4.99659700	-2.09170500	-0.67942900
C	0.87480400	1.84259600	0.95636100	H	5.15857100	-2.39669600	0.34975800
H	1.09821200	2.58048000	1.73444200	C	3.80301000	-1.54154500	-1.04210100
H	0.93707800	2.34309900	-0.01439300	H	3.02960000	-1.43354900	-0.28975900
C	-1.03022500	-1.21315200	-1.24326800	C	3.54445900	-1.13094900	-2.39295400
C	-0.64829500	-3.34224300	-1.89030100	Cl	-1.23556600	1.92417700	-2.13800500
H	-0.89013200	-4.37910200	-2.05781600	N	-1.55116100	-2.46484000	-1.32139400
C	0.46568900	-2.63502200	-2.16814200	N	0.21893200	-1.33647300	-1.76678400
H	1.39529400	-2.92433700	-2.62809800	Rh	-1.82602100	0.42886200	-0.33392800
C	1.23403500	-0.27184800	-1.80978500	H	5.15860600	-1.19625000	-5.41811100
H	1.64839800	-0.16252600	-0.80820100	H	1.64584800	1.07065300	1.00270000
H	0.71431700	0.65997600	-2.03511300	Cl	-3.97168700	0.11220100	-1.36718500
C	-2.84293300	-2.91885100	-0.82902100				

Coordinates for Complex B



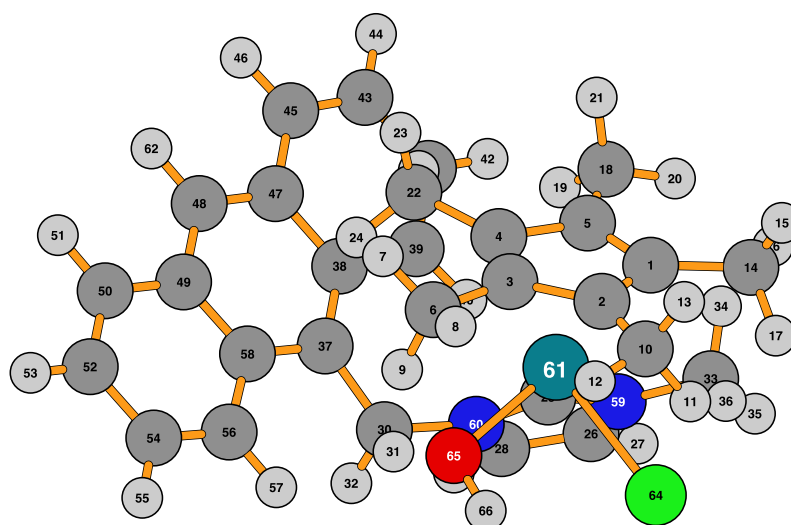
C	-1.68500300	-0.12552100	1.42916100	H	-3.99064700	-0.94496200	-1.24318500
C	-2.31225500	1.14563100	1.17721400	H	-3.64504700	-0.56037900	-2.94234800
C	-1.37743500	2.18960500	1.55661200	H	-3.11958900	0.56427000	-1.68644100
C	-0.20250900	1.56550100	2.01647100	C	2.34456400	-1.09416800	-0.55721200
C	-0.35103000	0.12656700	1.87399000	C	3.09879100	-1.92866100	0.29889700
C	-1.68106700	3.65201200	1.50458000	C	3.01838900	-3.35770600	0.25526100
H	-2.41263600	3.91895300	2.27490500	H	2.39899700	-3.87049600	-0.48319100
H	-2.09203700	3.91717500	0.52647400	C	3.75194100	-4.11920600	1.11875400
H	-0.78231400	4.24968200	1.66611800	H	3.67606100	-5.19970900	1.05353500
C	-3.73737800	1.41681700	0.82081800	C	4.61878100	-3.52671900	2.07845500
H	-4.27335100	0.50797200	0.54858300	H	5.19342700	-4.15925600	2.74787600
H	-3.79870800	2.12630800	-0.00868500	C	4.73216300	-2.17105600	2.14884500
H	-4.24208400	1.86061900	1.68578400	H	5.39401500	-1.70162900	2.87137900
C	-2.31092700	-1.48099700	1.34579400	C	3.97942500	-1.33170000	1.27057600
H	-2.57090600	-1.81662700	2.35529100	C	4.08592800	0.05670500	1.34547300
H	-1.62597600	-2.21308500	0.91260900	C	3.31939600	0.88517500	0.52721300
H	-3.22293800	-1.47341700	0.74891200	C	3.41167100	2.30777400	0.61580500
C	0.59979000	-0.91519200	2.36611700	H	4.13230900	2.73015400	1.31177900
H	1.62886000	-0.55596200	2.36144300	C	2.60528200	3.12694200	-0.12162400
H	0.56394200	-1.81288700	1.74592000	H	2.67645000	4.20525600	-0.02817000
H	0.34219700	-1.19992200	3.39262900	C	1.68356800	2.56036100	-1.03593500
C	0.94786900	2.24520800	2.67554600	H	1.06105200	3.19984700	-1.65105400
H	0.70162500	2.38283400	3.73459700	C	1.59944800	1.19027200	-1.20526600
H	1.15051600	3.22516700	2.24269100	H	1.07661600	0.82495800	-2.08321500
C	-0.81359400	-0.71536900	-1.37253800	C	2.41969700	0.29848600	-0.42041700
C	-1.84453900	-2.45607500	-2.36896200	Cl	-1.47730900	2.39811300	-1.85972000
H	-2.67504600	-2.99504500	-2.79499300	N	-1.99301600	-1.18122800	-1.85025300
C	-0.54721600	-2.79328800	-2.23446200	N	0.07871800	-1.71194300	-1.62784800
H	0.03100200	-3.69126600	-2.48800700	Rh	-0.63004900	0.93308800	-0.14643100
C	1.55862200	-1.66656700	-1.71008200	H	4.77279800	0.50135300	2.06224600
H	1.80027100	-1.09739900	-2.61296700	H	1.85734300	1.64881600	2.61638800
H	1.85753700	-2.70017800	-1.92160000	Cl	1.73710300	-5.08203000	-2.38608400
C	-3.26554700	-0.48618400	-1.92139200				

Coordinates for Complex C



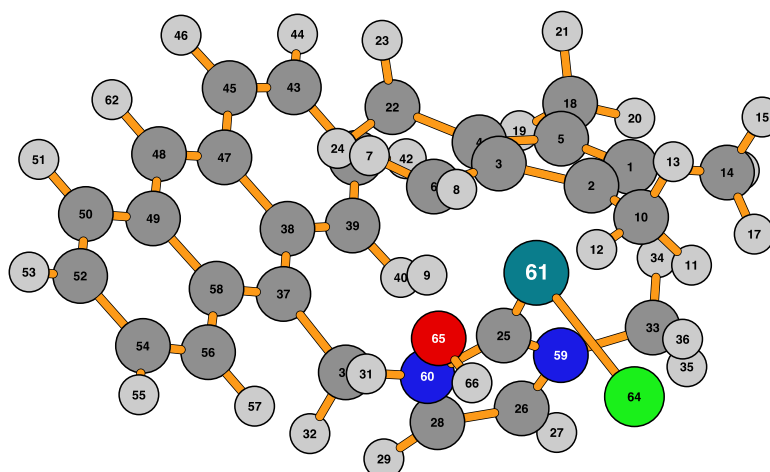
C	-1.69930600	-0.11493000	1.88429700	C	-3.41455100	-1.54861100	-1.16566100
C	-2.48185700	1.00484900	1.40156200	H	-3.60747100	-1.94013200	-0.16591100
C	-1.63380100	2.18581000	1.37659200	H	-4.08393200	-2.03738400	-1.87317400
C	-0.33854700	1.77965700	1.74708500	H	-3.59812100	-0.47486600	-1.19484400
C	-0.37013300	0.34504600	2.04933800	C	2.20854000	-0.78805600	-0.75711400
C	-2.08848100	3.55598300	0.99251700	C	2.55411800	-1.88628500	0.06360200
H	-2.66650800	3.99995300	1.80932200	C	2.01222000	-3.20043100	-0.11578400
H	-2.71592500	3.52525600	0.09907600	H	1.30967000	-3.39310400	-0.91534500
H	-1.24140300	4.20779000	0.77770000	C	2.35340400	-4.23024700	0.71394200
C	-3.95166900	1.03923800	1.15107500	H	1.92331700	-5.21368200	0.55345500
H	-4.38195000	0.04144900	1.06754700	C	3.27336600	-4.03791700	1.78061600
H	-4.18238300	1.60264100	0.24392700	H	3.53153700	-4.87018400	2.42632500
H	-4.43973800	1.54771700	1.98999900	C	3.83457200	-2.81152000	1.97244400
C	-2.18262200	-1.48739800	2.23609100	H	4.55056500	-2.64849800	2.77258900
H	-2.07861200	-1.64443500	3.31417400	C	3.49961200	-1.70895300	1.12766100
H	-1.59949300	-2.25909500	1.72803800	C	4.08282000	-0.45767800	1.32446900
H	-3.23556800	-1.62333000	1.98656700	C	3.73871200	0.63984200	0.54003600
C	0.75590000	-0.45753000	2.60142300	C	4.34712600	1.91589200	0.77117900
H	1.72194200	-0.05357000	2.30171600	H	5.08436300	1.99600400	1.56459300
H	0.70593500	-1.49796600	2.27416000	C	4.01774600	2.99798500	0.01438100
H	0.70642600	-0.43938400	3.69634100	H	4.48827500	3.95912500	0.19136200
C	0.87237100	2.64438000	1.83086900	C	3.04615300	2.86416700	-1.01718400
H	0.92406500	3.09772500	2.82685300	H	2.77289700	3.73112500	-1.60979400
H	0.84386300	3.44343200	1.08894800	C	2.45046500	1.66485900	-1.27507000
C	-0.96882000	-1.06576300	-1.20830300	H	1.69855000	1.63017700	-2.05244400
C	-1.68367100	-2.78707200	-2.47331800	C	2.76941000	0.48813800	-0.51476900
H	-2.39747500	-3.48331300	-2.88242300	Cl	-1.09059300	1.81959800	-1.99487700
C	-0.35912500	-2.64563000	-2.68820200	N	-2.04137200	-1.80875100	-1.56548000
H	0.31558300	-3.19403900	-3.32571900	N	0.06551100	-1.58850300	-1.90181500
C	1.41939900	-1.02581800	-2.02731000	Rh	-0.96040600	0.62120800	-0.02641800
H	1.32448200	-0.11380300	-2.61266900	H	4.82324400	-0.33576700	2.11116100
H	1.97244100	-1.73947600	-2.64487800	H	1.78651500	2.07225800	1.67152900

Coordinates for Complex D



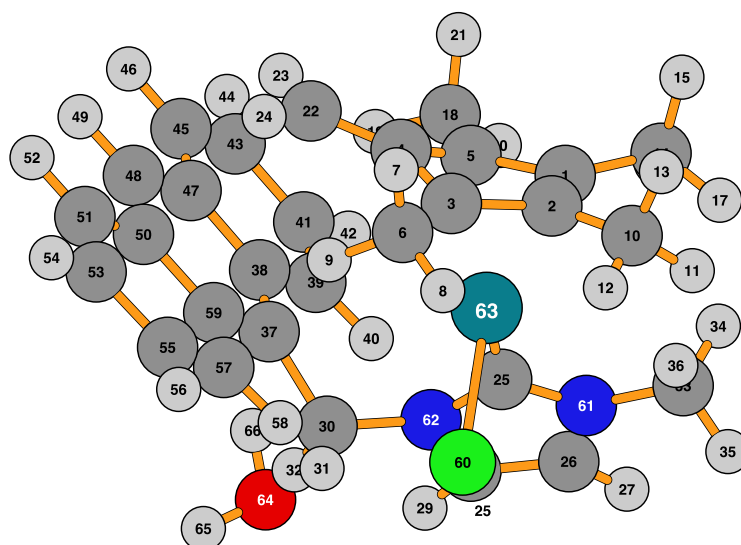
C	-2.78859100	-0.05051000	1.79628400	H	-2.58564500	-3.28188100	0.26940900
C	-2.71849800	1.38969000	1.56547500	H	-3.20298300	-3.64691900	-1.35961400
C	-1.36121600	1.77384800	1.61252800	H	-3.42973800	-2.01799400	-0.68578100
C	-0.56058600	0.58758300	1.81232700	C	2.34557400	-0.19934100	-0.90995300
C	-1.46518900	-0.52802200	1.98460500	C	2.73448400	-1.20971700	-0.00094000
C	-0.78660300	3.12686600	1.35164400	C	2.10929300	-2.50121400	0.11522700
H	0.05335100	3.32600200	2.02288500	H	1.31210600	-2.78345400	-0.55058300
H	-1.53218100	3.91277900	1.48660600	C	2.49188000	-3.41179600	1.05606500
H	-0.43116500	3.15173500	0.31216000	H	1.98438500	-4.37070500	1.10295100
C	-3.91042800	2.26716200	1.35098100	C	3.54561000	-3.13154900	1.96884700
H	-4.56347000	1.83935300	0.58534300	H	3.83382200	-3.86894700	2.71095800
H	-3.61144900	3.26012900	1.01098100	C	4.18637600	-1.93544700	1.89042600
H	-4.48109400	2.37488000	2.28013800	H	4.99914900	-1.69569200	2.57051200
C	-4.07196900	-0.81080300	1.91017600	C	3.81111600	-0.94814300	0.92335000
H	-4.59808700	-0.53350600	2.83018700	C	4.47786100	0.27038100	0.89701400
H	-3.90205500	-1.88937800	1.93171900	C	4.11556400	1.27262400	0.00211600
H	-4.72372000	-0.58398000	1.06136100	C	4.80694000	2.52405500	-0.00777100
C	-1.03489600	-1.90890500	2.37317500	H	5.63046200	2.65983200	0.68785700
H	-0.18522200	-2.24417400	1.77250700	C	4.44335500	3.51936700	-0.86192300
H	-1.84629500	-2.63077900	2.26157000	H	4.97246700	4.46699700	-0.86257600
H	-0.72406100	-1.91909300	3.42358600	C	3.35251300	3.31685500	-1.75084500
C	0.90272500	0.59224000	2.11818700	H	3.04949400	4.11911600	-2.41603900
H	1.07092900	1.00025900	3.12233400	C	2.67215700	2.13459900	-1.77246100
H	1.45782900	1.20622600	1.40584000	H	1.83070500	2.04202400	-2.44510600
C	-0.88616000	-1.26279400	-1.11841200	C	3.02653500	1.04708200	-0.90273500
C	-0.79125400	-3.23368700	-2.22290100	N	-1.50090600	-2.45643500	-1.32785500
H	-1.13487700	-4.20575800	-2.53680200	N	0.24073900	-1.33360000	-1.87059200
C	0.30137900	-2.52109700	-2.57321600	Rh	-1.64231900	0.30203800	-0.04574600
H	1.12128100	-2.75221000	-3.23332700	H	5.29317300	0.44646000	1.59452400
C	1.24367000	-0.28336100	-1.95704800	H	1.31852500	-0.41531200	2.09111600
H	0.64482600	0.63817600	-1.91152000	Cl	-3.54133300	0.31486600	-1.56110100
H	1.69581800	-0.36194100	-2.95183600	O	-0.77849200	1.63123100	-1.34496000
C	-2.75836000	-2.87531800	-0.72963800	H	-1.48021700	1.77941100	-1.98958800

Coordinates for Complex E_{Ts}



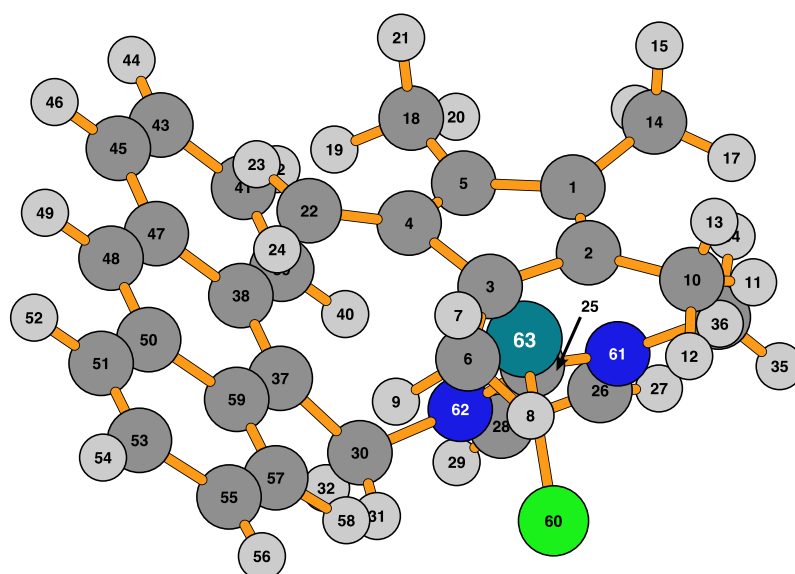
C	-2.83579000	-0.02591900	1.84617100	H	-2.48813400	-3.28083800	0.30417800
C	-2.69090300	1.38512400	1.57664200	H	-3.02985600	-3.83641900	-1.29723900
C	-1.30414600	1.74980400	1.70170800	H	-3.40044200	-2.17366400	-0.76805800
C	-0.57707600	0.49308000	1.87872000	C	2.33598800	-0.14968900	-0.92895100
C	-1.52739400	-0.57327000	2.05239400	C	2.72136100	-1.16425700	-0.02367100
C	-0.70995000	2.97508600	1.29246200	C	2.09951100	-2.45853300	0.08813900
H	0.32048300	3.13492600	1.60434900	H	1.31773400	-2.75120500	-0.59060000
H	-1.33357500	3.86347700	1.37226700	C	2.47334200	-3.36361100	1.03747500
H	-0.68076400	2.58105600	-0.08074700	H	1.97004100	-4.32494100	1.07940400
C	-3.82052900	2.32820200	1.30370600	C	3.51505700	-3.07782800	1.96242600
H	-4.57515800	1.85424300	0.67141000	H	3.79463300	-3.81121000	2.71171700
H	-3.46282900	3.21442900	0.77475000	C	4.15748200	-1.88295300	1.88355100
H	-4.29401000	2.65610800	2.23611400	H	4.96345100	-1.63953500	2.57029300
C	-4.14510600	-0.74153600	1.94801400	C	3.79132400	-0.90048900	0.90807100
H	-4.65024000	-0.48093300	2.88444400	C	4.45496600	0.31970000	0.88895900
H	-4.01202800	-1.82541100	1.92235300	C	4.10234300	1.32070300	-0.01102000
H	-4.79423000	-0.46088100	1.11451900	C	4.79285500	2.57240800	-0.01622600
C	-1.17432300	-1.95933600	2.49705900	H	5.60572900	2.71196000	0.69097800
H	-0.32538800	-2.35031200	1.92952200	C	4.44227000	3.56341400	-0.88072500
H	-2.01573400	-2.64576800	2.38259500	H	4.97035600	4.51145600	-0.87787200
H	-0.89413600	-1.95146700	3.55623600	C	3.36907400	3.35368500	-1.78907200
C	0.88497800	0.41700400	2.18063600	H	3.08273100	4.14894100	-2.46985400
H	1.07459700	0.81584200	3.18427600	C	2.68791200	2.17201900	-1.81232800
H	1.47152600	1.00445400	1.47096000	H	1.86826800	2.07130300	-2.51063300
C	-0.85261300	-1.30834800	-1.09311400	C	3.02334500	1.09226700	-0.92605800
C	-0.72154200	-3.22626200	-2.28753700	N	-1.42728400	-2.51471200	-1.33604700
H	-1.03805700	-4.19724900	-2.63191900	N	0.24648500	-1.30277700	-1.89040300
C	0.33148700	-2.45843100	-2.64375100	Rh	-1.67207900	0.18994300	0.04002500
H	1.13645800	-2.63199800	-3.33895300	H	5.25975400	0.49878400	1.59775800
C	1.20797300	-0.21732000	-1.95371500	H	1.24752300	-0.61132100	2.14997000
H	0.61121800	0.69274900	-1.85607400	Cl	-3.49876100	0.25103000	-1.56258100
H	1.63655500	-0.23637200	-2.96176400	O	-0.79233400	1.86944000	-1.05148800
C	-2.66553700	-2.97898200	-0.72981500	H	-1.51182100	2.19153800	-1.61193300

Coordinates for Complex F



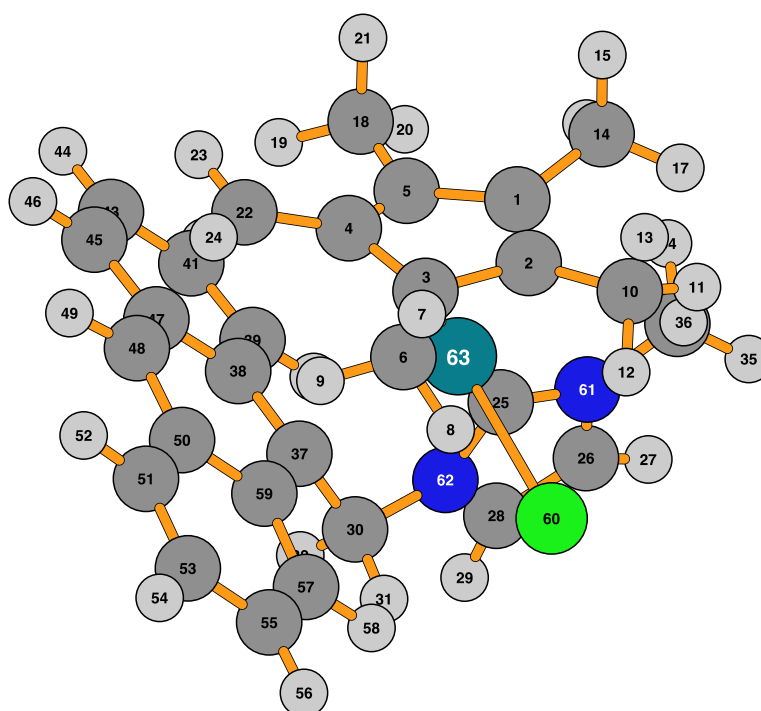
C	-1.65978300	-1.26668200	-2.11095500	H	-4.67169500	0.54123000	-0.66221300
C	-1.33966400	-2.64200700	-1.72466400	H	-5.19257500	-0.11779200	0.91241600
C	0.01454900	-2.68274100	-1.35830500	H	-3.97472800	-0.98538100	-0.05007000
C	0.66745200	-1.43279800	-1.80750400	C	1.13881600	1.25960900	1.22732600
C	-0.46912600	-0.49900000	-1.96188000	C	1.28763700	2.46853200	0.51269900
C	0.77029000	-3.86385700	-0.83969700	C	0.28921900	3.49977500	0.49952400
H	1.22364800	-4.43192700	-1.66078100	H	-0.65157300	3.34114200	1.00790300
H	0.12153100	-4.52960300	-0.26689600	C	0.47158700	4.66638600	-0.18798300
H	1.56977200	-3.52714900	-0.17426000	H	-0.31230800	5.41772500	-0.18558300
C	-2.30962500	-3.78077300	-1.70658400	C	1.66353400	4.89867200	-0.92850200
H	-3.32025800	-3.43690800	-1.47179000	H	1.78946900	5.82906900	-1.47241900
H	-2.02788100	-4.51859800	-0.95316200	C	2.63300100	3.94263200	-0.95568400
H	-2.33632900	-4.27674600	-2.68384000	H	3.54773000	4.09807100	-1.52120400
C	-2.92943200	-0.81255700	-2.75962500	C	2.48275100	2.71113500	-0.24384200
H	-2.86280100	-0.94573100	-3.84600200	C	3.49402200	1.75292900	-0.25422200
H	-3.11153700	0.24725000	-2.56486200	H	4.41102500	1.95254900	-0.80377100
H	-3.79460800	-1.37965200	-2.40753100	C	3.35205000	0.54400700	0.41865600
C	-0.30373700	0.93766800	-2.34945600	C	4.39410500	-0.43580500	0.37510000
H	0.53227500	1.38586000	-1.80845400	H	5.29892100	-0.19749400	-0.17716400
H	-1.19862500	1.52003700	-2.11560700	C	4.25155300	-1.63770700	0.99626900
H	-0.10177900	1.03226100	-3.42362200	H	5.04499700	-2.37728500	0.95424100
C	1.97597600	-1.18374000	-1.94265300	C	3.04362400	-1.93351800	1.68829400
H	2.33175200	-0.20420700	-2.24239200	H	2.91242700	-2.90792100	2.14831900
H	2.72145600	-1.93861800	-1.71906500	C	2.03503000	-1.01987300	1.76906000
C	-1.97058500	0.33364600	0.88609600	H	1.11535300	-1.32118200	2.25533100
C	-3.48432300	1.77605500	1.76129700	C	2.14613100	0.27219600	1.15316500
H	-4.45957900	2.20885800	1.91451400	Cl	-1.25816000	-2.45328900	1.99484400
C	-2.28326700	2.08733100	2.29070500	N	-3.27735300	0.70411400	0.90911000
H	-1.97440600	2.85004900	2.99097600	N	-1.36792900	1.20441800	1.73485900
C	0.00745800	1.10189200	2.22647500	Rh	-1.16444400	-1.26081800	-0.06619600
H	0.08194600	0.15334700	2.75372400	O	-0.08531100	4.21435200	3.57990200
H	0.10500000	1.90148400	2.96688200	H	0.64091000	4.10387200	4.19817900
C	-4.34775800	-0.00049500	0.23047900	H	0.33501900	4.39980000	2.73235100

Coordinates for Complex G



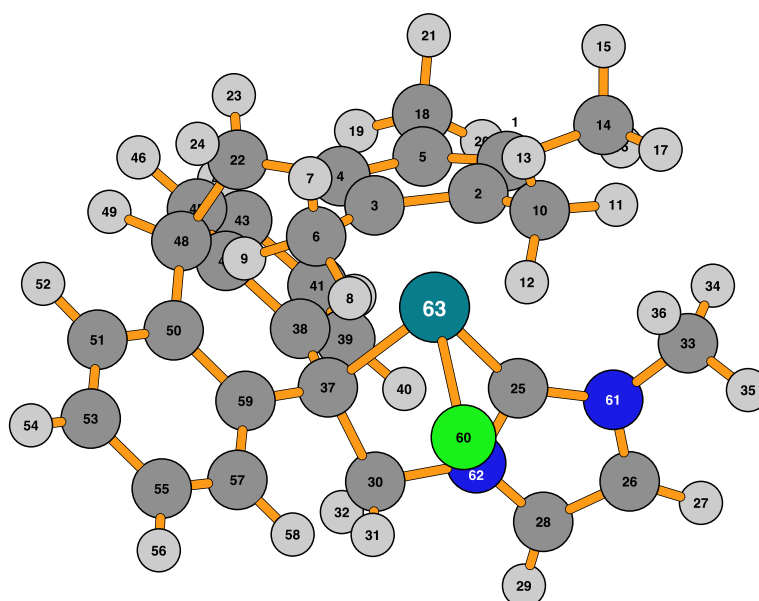
C	-1.61158500	-1.24397000	-2.07498700	C	-4.27666500	0.07592600	0.22481400
C	-1.34279000	-2.61516600	-1.63933500	H	-4.58417400	0.59240000	-0.68807600
C	0.01070300	-2.69380500	-1.27447200	H	-5.13145500	-0.01741200	0.89772000
C	0.70787800	-1.48892800	-1.77617100	H	-3.90324600	-0.91829800	-0.01997600
C	-0.39268700	-0.51681600	-1.95441800	C	1.18836100	1.36125700	1.20245800
C	0.72316700	-3.88283400	-0.71438300	C	1.33225000	2.55384400	0.46024900
H	1.14694100	-4.50113900	-1.51472400	C	0.37161200	3.61713700	0.48986300
H	0.05292800	-4.49841700	-0.11094000	H	-0.51272600	3.52565500	1.10497700
H	1.54058700	-3.55184400	-0.06809100	C	0.52830300	4.74361000	-0.26401100
C	-2.35299400	-3.71687200	-1.57854900	H	-0.22358300	5.52571300	-0.22373000
H	-3.35397100	-3.32738400	-1.37580300	C	1.66348100	4.90784100	-1.10462500
H	-2.10635000	-4.42509500	-0.78537200	H	1.76818100	5.80861300	-1.70070000
H	-2.38489700	-4.26008200	-2.53014800	C	2.61463800	3.93426400	-1.14809200
C	-2.86232300	-0.76380100	-2.74142800	H	3.49408600	4.04520600	-1.77646500
H	-2.79288100	-0.92375000	-3.82396300	C	2.48647200	2.74083000	-0.37148300
H	-3.01015300	0.30577900	-2.57233800	C	3.47803000	1.76200600	-0.39627200
H	-3.74790100	-1.29436900	-2.38351900	H	4.36841300	1.92275400	-0.99987400
C	-0.17440000	0.89901400	-2.38885900	C	3.35246600	0.58287200	0.33020300
H	0.68235700	1.33069000	-1.86757400	C	4.38222700	-0.40991200	0.28469300
H	-1.04370900	1.52359400	-2.16818400	H	5.26955200	-0.20068200	-0.30643200
H	0.02325800	0.95117600	-3.46675500	C	4.25006900	-1.58769700	0.95229500
C	2.02259900	-1.30185900	-1.94350500	H	5.03485200	-2.33644400	0.91031600
H	2.41358400	-0.35131000	-2.28852600	C	3.06227600	-1.84715100	1.69220800
H	2.73881700	-2.08016500	-1.70601800	H	2.93683300	-2.80410100	2.18906600
C	-1.90160500	0.43953500	0.88034900	C	2.06639400	-0.92002900	1.77566500
C	-3.43577700	1.86692400	1.74627800	H	1.16109300	-1.19500200	2.30279000
H	-4.41570800	2.28931900	1.89829300	C	2.17213800	0.35204100	1.11785500
C	-2.23836400	2.19165100	2.27456300	Cl	-1.24514400	-2.31072300	2.06823500
H	-1.96391700	2.95158200	2.98875600	N	-3.21356800	0.79663300	0.89929800
C	0.06919900	1.23337600	2.21702000	N	-1.30905800	1.32192900	1.72581800
H	0.14532900	0.29869800	2.76870700	Rh	-1.11041100	-1.18766200	-0.03120700
H	0.17477300	2.04230600	2.94735100				

Coordinates for Complex **Hr_s**



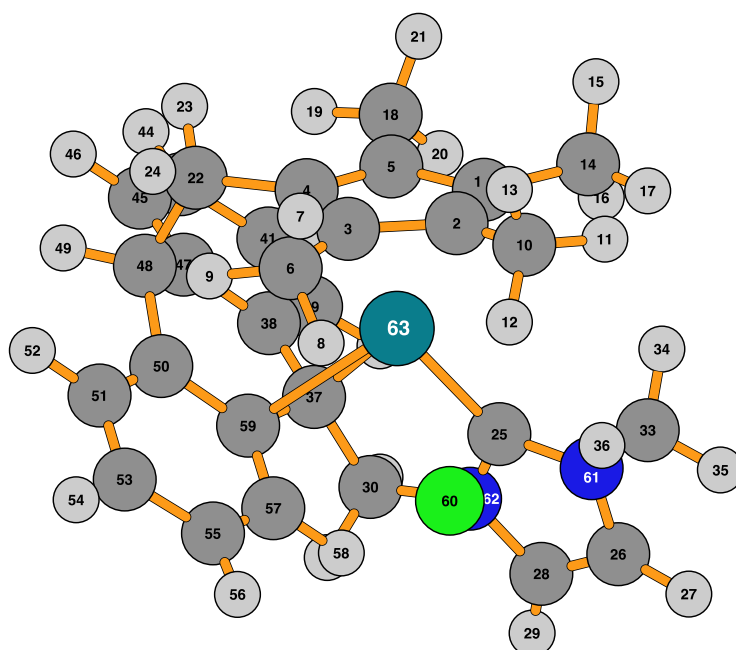
C	-1.52524500	-0.89693900	-2.09565600	C	-4.23834800	0.19487100	0.21379600
C	-0.99882700	-2.14146900	-1.60247600	H	-4.47373900	0.77846400	-0.67897200
C	0.40861900	-1.99524300	-1.44773800	H	-5.14763100	0.04750400	0.79868700
C	0.81351600	-0.75179500	-2.08900100	H	-3.83761400	-0.77749400	-0.07013700
C	-0.43154100	0.01993800	-2.21012700	C	0.86996100	0.88346200	1.17656500
C	1.32781300	-3.07040900	-0.95595700	C	1.10970300	1.99042300	0.27342700
H	1.43584500	-3.87269900	-1.69588800	C	0.28707800	3.15282100	0.24422600
H	0.93911000	-3.50337400	-0.02958200	H	-0.58100100	3.21557000	0.88753300
H	2.31809300	-2.66825200	-0.73389800	C	0.55515400	4.20606200	-0.59366100
C	-1.77026000	-3.39700600	-1.35018200	H	-0.09538600	5.07522100	-0.58510800
H	-2.82944900	-3.18880300	-1.18248200	C	1.66709600	4.17333400	-1.46343100
H	-1.39232500	-3.90281100	-0.45963800	H	1.87118500	5.01155900	-2.12157500
H	-1.68077200	-4.07441400	-2.20744300	C	2.48273600	3.07344000	-1.45990100
C	-2.88832300	-0.67279900	-2.67022700	H	3.34642400	3.02319700	-2.11809200
H	-2.86140900	-0.87857300	-3.74704700	C	2.23106100	1.97663300	-0.59517000
H	-3.20993900	0.36317700	-2.54359600	C	3.09650400	0.86051100	-0.58880800
H	-3.64074500	-1.32918900	-2.22883700	H	3.99866700	0.90550800	-1.19262900
C	-0.53093000	1.38100400	-2.82763200	C	3.02390500	-0.10131500	0.43277900
H	0.33680800	1.99350500	-2.57989800	C	4.05884700	-1.06865000	0.56820000
H	-1.41637700	1.91099100	-2.46724500	H	4.88742000	-1.03580500	-0.13474700
H	-0.59629300	1.30963700	-3.92101500	C	4.01973500	-2.00815100	1.55817500
C	2.07657200	-0.35727700	-2.43160600	H	4.81593900	-2.73832000	1.66116200
H	2.22224200	0.53207200	-3.03273600	C	2.91996000	-2.02366500	2.44993700
H	2.89431600	-1.06713500	-2.38860000	H	2.86969100	-2.77902500	3.22762300
C	-1.91225800	0.66945800	0.93931100	C	1.90713400	-1.11091200	2.33940700
C	-3.56483200	1.63782700	2.14200500	H	1.05941200	-1.20277000	3.00336900
H	-4.58047600	1.90322000	2.38697500	C	1.90828000	-0.10913000	1.32168800
C	-2.39763600	1.93669500	2.75401500	Cl	-1.15374500	-2.04879600	1.78264300
H	-2.18810600	2.50910000	3.64292900	N	-3.25137900	0.86194700	1.03739100
C	-0.00933600	1.19514300	2.37737000	N	-1.40644000	1.34351600	1.99842800
H	0.04401800	0.39976700	3.11911000	Rh	-0.71436700	-0.57240200	-0.11591100
H	0.31368500	2.13050000	2.85073000				

Coordinates for Complex I



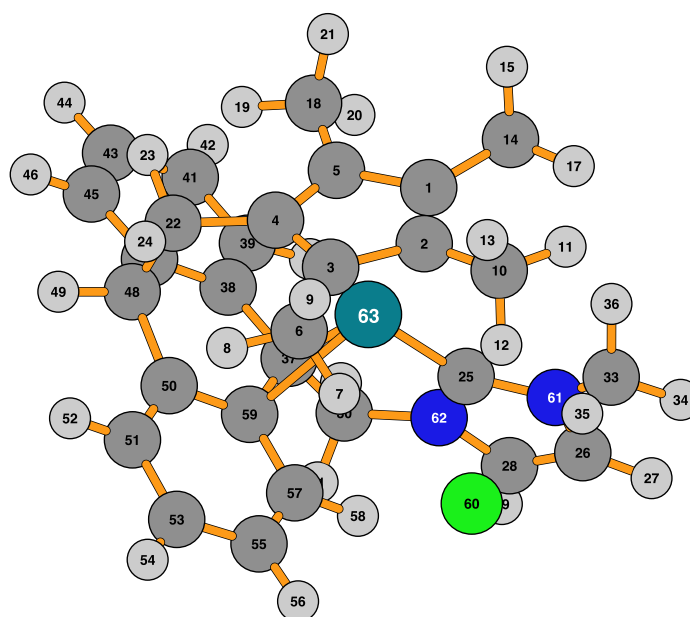
C	-1.56170500	-0.87139300	-2.17409100	C	-4.24267700	0.05077500	0.23290300
C	-1.10051200	-2.10402900	-1.66940000	H	-4.59958200	0.66308600	-0.59858100
C	0.33341400	-1.99237300	-1.45122300	H	-5.08761000	-0.23493300	0.86164600
C	0.74379900	-0.70480500	-1.87944800	H	-3.76490100	-0.85208400	-0.14595200
C	-0.44347100	0.04490000	-2.22193100	C	0.71861800	0.72232900	1.02252600
C	1.20327300	-3.10432700	-0.95257000	C	1.05933300	1.93008700	0.18139100
H	1.36430300	-3.85616500	-1.73414700	C	0.34655100	3.13879500	0.26386800
H	0.73186600	-3.59038500	-0.09413700	H	-0.50716300	3.22421200	0.92564900
H	2.17263600	-2.72863300	-0.61846000	C	0.69209900	4.24606700	-0.49974300
C	-1.88829100	-3.35222700	-1.42848500	H	0.11376100	5.16042400	-0.40610400
H	-2.96037700	-3.18198200	-1.55357900	C	1.77927000	4.19113600	-1.36743600
H	-1.72095100	-3.71100300	-0.40868100	H	2.06538100	5.05781700	-1.95461300
H	-1.58526200	-4.13854500	-2.12863200	C	2.49179500	3.00407800	-1.46761800
C	-2.91134200	-0.55902500	-2.74120400	H	3.33967500	2.93325100	-2.14536000
H	-2.86867300	-0.61804700	-3.83499000	C	2.13374900	1.88218200	-0.71943700
H	-3.22993600	0.45372900	-2.48299000	C	2.84661500	0.58294900	-0.93227700
H	-3.67761200	-1.25952500	-2.40343900	H	3.85539600	0.78983200	-1.30783400
C	-0.49945300	1.39993800	-2.85851400	C	2.95853400	-0.20153400	0.34089900
H	0.37246300	2.00205900	-2.60392400	C	4.06992900	-1.02164300	0.54042300
H	-1.38345900	1.95026100	-2.52668000	H	4.85903100	-1.02634200	-0.20858400
H	-0.54829700	1.30874100	-3.95091800	C	4.17602100	-1.82379800	1.66696200
C	2.15973400	-0.25146500	-2.06612300	H	5.04527600	-2.45694100	1.81384000
H	2.20359900	0.35188300	-2.97949200	C	3.14542700	-1.80009900	2.60252800
H	2.78177200	-1.13519100	-2.23828700	H	3.19487300	-2.42818600	3.48658500
C	-1.93042300	0.62095400	0.93481400	C	2.04215400	-0.98057600	2.41435900
C	-3.59562300	1.53953200	2.14167700	H	1.24597600	-1.03284700	3.14452000
H	-4.61623800	1.77730400	2.39416400	C	1.91773000	-0.15485200	1.28431400
C	-2.43033000	1.87853600	2.74011100	Cl	-1.02417200	-2.04967700	1.73261500
H	-2.23101200	2.46402500	3.62267600	N	-3.27254400	0.76372400	1.03819500
C	-0.01958100	1.14708700	2.29861000	N	-1.42989700	1.31538600	1.97747500
H	0.03798000	0.37736100	3.06591000	Rh	-0.65053900	-0.51341000	-0.11346400
H	0.37139700	2.08505800	2.71052100				

Coordinates for Complex JTs



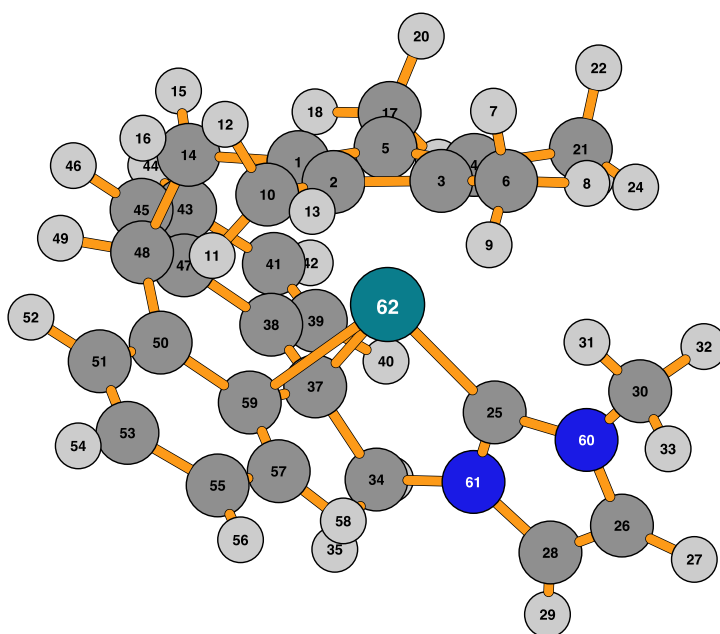
C	-1.46340700	-0.52425600	-2.07990700	C	-3.69814700	-1.33697200	0.97189700
C	-1.07869700	-1.84054400	-1.68189200	H	-3.85069300	-1.17850500	-0.09481000
C	0.34566600	-1.83660500	-1.56205700	H	-4.66833900	-1.43921200	1.45938400
C	0.86443300	-0.55590900	-1.99804700	H	-3.07325700	-2.22199100	1.15681400
C	-0.26109000	0.26222600	-2.31584000	C	0.61455000	1.30850500	0.78492300
C	1.11978300	-3.01291100	-1.06525600	C	1.20777600	2.33568900	-0.12128200
H	1.04075100	-3.83620700	-1.78427100	C	0.62190300	3.59772600	-0.30740100
H	0.69472100	-3.34779100	-0.10830100	H	-0.31133000	3.84298600	0.18854400
H	2.17331300	-2.77561000	-0.91603500	C	1.18420600	4.54950000	-1.14758900
C	-1.93682100	-3.04724700	-1.47437300	H	0.70002400	5.51404800	-1.26449000
H	-2.99786600	-2.80942300	-1.57699900	C	2.36257800	4.26784400	-1.83219300
H	-1.76353500	-3.46326700	-0.47351000	H	2.81997200	5.01079900	-2.47724000
H	-1.69334000	-3.80797600	-2.22490600	C	2.93523900	3.01058700	-1.68939800
C	-2.83369200	-0.04156800	-2.44235700	H	3.83886600	2.76176900	-2.24126700
H	-2.90376100	0.09132300	-3.52786200	C	2.36343600	2.03995300	-0.86666000
H	-3.05259800	0.91996400	-1.97187400	C	2.91787400	0.64189900	-0.89008600
H	-3.60436100	-0.75456800	-2.14672900	H	3.99549200	0.69231500	-1.08323300
C	-0.27030600	1.61869000	-2.94344700	C	2.67928800	-0.10393800	0.39209600
H	0.71603600	2.08238700	-2.93186300	C	3.50987700	-1.14385500	0.76543700
H	-0.95780900	2.29029200	-2.42361900	H	4.41847900	-1.32435800	0.19513800
H	-0.60239000	1.53518100	-3.98501300	C	3.17060500	-1.99777500	1.82125400
C	2.31524700	-0.17387300	-2.09738000	H	3.82309800	-2.82577300	2.07850100
H	2.47356200	0.41190600	-3.00887000	C	1.98030500	-1.80868800	2.49969400
H	2.91061400	-1.08576600	-2.20094100	H	1.64923700	-2.50554300	3.25967800
C	-1.80128300	0.25783100	1.15223400	C	1.16299300	-0.72354200	2.18384300
C	-3.42402900	0.47287900	2.68462600	H	0.24689800	-0.59918700	2.74876200
H	-4.36097200	0.24620500	3.16665200	C	1.50594800	0.16833700	1.14860700
C	-2.45370900	1.36039900	3.01066700	Cl	-1.06948300	-3.22974200	1.91106200
H	-2.37929900	2.06496600	3.82252000	N	-3.01566000	-0.18417700	1.54094800
C	-0.18442200	1.87685500	1.96596900	N	-1.47658800	1.21808700	2.04916700
H	0.35357300	1.70872200	2.90459000	Rh	-0.39417000	-0.25299300	-0.21106400
H	-0.34349000	2.95135800	1.87588600				

Coordinates for Complex K



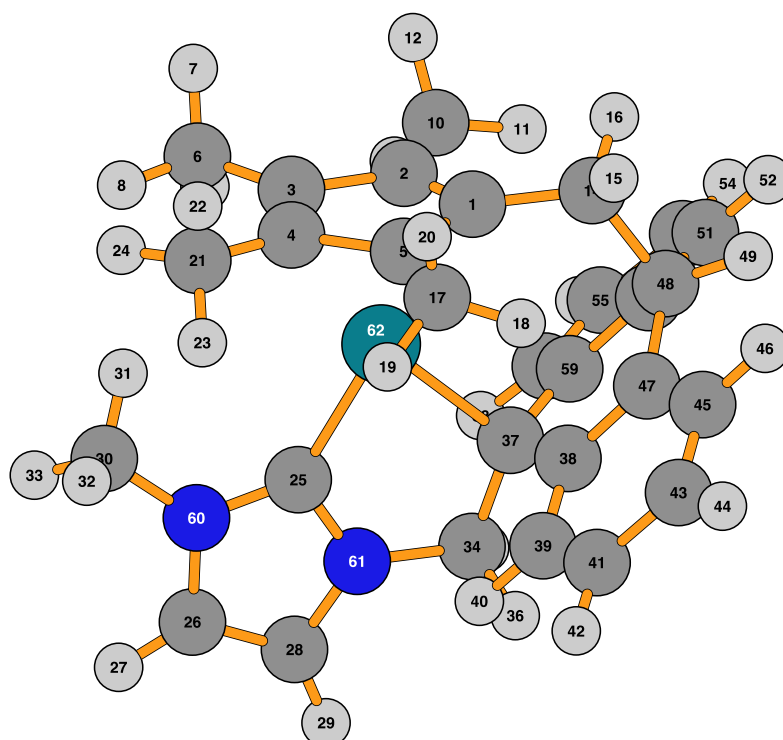
C	-1.44378900	-0.51601000	-2.01007800	C	-3.54685900	-1.24287900	1.18093000
C	-1.05206400	-1.82000800	-1.56883900	H	-4.49489000	-1.32699600	1.71339000
C	0.37338600	-1.82558100	-1.50758700	H	-2.90828000	-2.11503800	1.38253200
C	0.88266600	-0.56458700	-2.01349900	H	-3.74564500	-1.13821700	0.11522000
C	-0.24786500	0.24533500	-2.33270400	C	0.72566000	1.43754600	0.68644700
C	1.15754300	-2.98952900	-0.99762200	C	1.30425400	2.41542500	-0.28091500
H	0.76490300	-3.28986100	-0.01532900	C	0.72842300	3.67552500	-0.50639200
H	2.21734700	-2.75545900	-0.89509400	H	-0.18577200	3.95612700	0.00574300
H	1.04820400	-3.83622100	-1.68484000	C	1.27629900	4.58093800	-1.40536200
C	-1.90983000	-3.01111800	-1.28349100	H	0.80028600	5.54555500	-1.55139700
H	-2.97234100	-2.77143200	-1.36352200	C	2.42985600	4.25310600	-2.11106400
H	-1.70551900	-3.39006700	-0.27329500	H	2.87614100	4.95993900	-2.80274300
H	-1.69397200	-3.80254000	-2.01041900	C	2.99192300	2.99629300	-1.92789100
C	-2.82549200	-0.04147200	-2.33787400	H	3.87556900	2.71117700	-2.49433500
H	-2.95474400	-0.00028600	-3.42533800	C	2.43405800	2.07119100	-1.04541100
H	-3.00486000	0.96000200	-1.93980000	C	2.97380700	0.66694100	-1.02234200
H	-3.58787600	-0.71216400	-1.93968200	H	4.04670200	0.69735500	-1.24374800
C	-0.26874600	1.57413300	-3.01695400	C	2.75865700	-0.02309700	0.29502400
H	0.71925300	2.03356000	-3.04955700	C	3.57785500	-1.06247400	0.68742900
H	-0.94028200	2.27038200	-2.50881700	H	4.47123900	-1.27890100	0.10571100
H	-0.62752400	1.44844300	-4.04528400	C	3.24233300	-1.87945200	1.77572900
C	2.33175200	-0.19448600	-2.17630000	H	3.88561300	-2.71053400	2.04574300
H	2.46326200	0.35180300	-3.11609300	C	2.06713800	-1.65379800	2.46575100
H	2.92003600	-1.11291700	-2.26025800	H	1.73370600	-2.32458700	3.24762200
C	-1.66311300	0.37989900	1.19890300	C	1.26258900	-0.56148000	2.13275200
C	-3.22473900	0.65630200	2.78483800	H	0.36885200	-0.39479200	2.72165800
H	-4.13793200	0.44377500	3.31633700	C	1.60484400	0.29638300	1.06746100
C	-2.25596900	1.57288200	3.02222700	Cl	-0.92154500	-3.17158000	2.07460400
H	-2.15929100	2.32145100	3.79121000	N	-2.85271900	-0.05708400	1.66238100
C	-0.03842500	2.06078900	1.86172400	N	-1.31689900	1.39166800	2.02953300
H	0.53602600	1.95224300	2.78778300	Rh	-0.30458000	-0.17545500	-0.19775600
H	-0.21697800	3.12616200	1.71764300				

Coordinates for Complex L



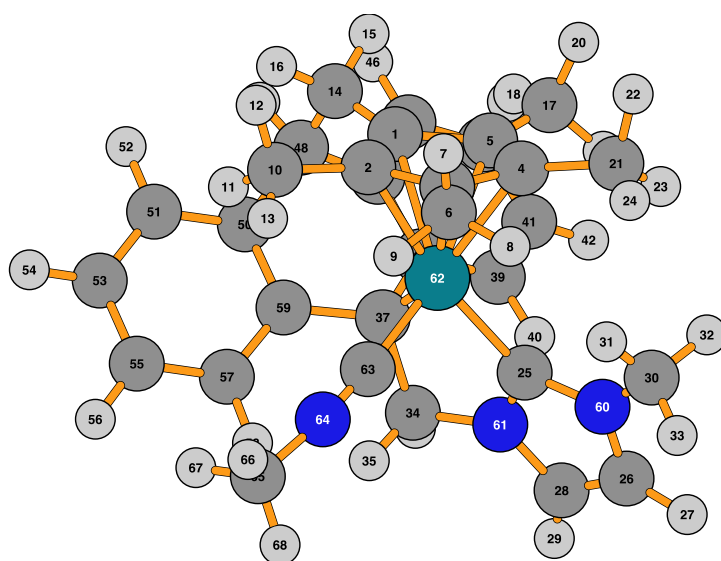
C	-0.83178100	1.46026000	-1.31112300	H	4.53069900	-1.06609600	-1.25633900
C	0.33504500	2.27833000	-1.04178500	H	5.09184100	-0.47011700	0.32524900
C	1.47254500	1.68439200	-1.65063200	C	0.03675800	-2.18658800	1.62959800
C	1.03153500	0.45014900	-2.25164900	H	-0.02776900	-2.09533500	2.71879700
C	-0.40584400	0.35423100	-2.10426000	H	-0.39283200	-3.15148500	1.36711600
C	2.81753100	2.33327500	-1.79677400	C	-0.70251600	-1.02492100	0.95305800
H	2.73771400	3.20902700	-2.44908500	C	-1.98262900	-1.39524100	0.27943800
H	3.54168000	1.65910000	-2.25803400	C	-2.21086600	-2.68196300	-0.23071800
H	3.22223700	2.67031300	-0.83894300	H	-1.43705900	-3.44020300	-0.17968800
C	0.32899200	3.58711500	-0.32107900	C	-3.41066600	-3.02056500	-0.84200700
H	-0.10416000	3.49985800	0.67835800	H	-3.55302600	-4.02590500	-1.22399600
H	-0.26921700	4.31519200	-0.87974300	C	-4.42521300	-2.07544500	-0.95720800
H	1.33908800	3.98640700	-0.21965600	H	-5.37313600	-2.33582800	-1.41525300
C	-2.23205100	1.78066800	-0.85907900	C	-4.20211500	-0.78703600	-0.48947500
H	-2.93571800	1.57545200	-1.67113800	H	-4.97630400	-0.03161500	-0.59808600
H	-2.29478300	2.85262800	-0.64970500	C	-2.99091000	-0.43208400	0.10411100
C	-1.25063300	-0.67604900	-2.78040900	C	-2.73584500	1.01616600	0.42408700
H	-2.29104700	-0.62660000	-2.45989500	H	-3.68200000	1.49286200	0.70046300
H	-0.89029700	-1.68736000	-2.57841800	C	-1.73937000	1.21162300	1.53279900
H	-1.21435000	-0.51529100	-3.86336600	C	-1.72547100	2.37001300	2.27760600
C	1.84388400	-0.46691100	-3.11039700	H	-2.53967600	3.08119300	2.16605600
H	1.73904300	-0.18035000	-4.16241000	C	-0.65258800	2.67631300	3.13363600
H	1.50865000	-1.50097200	-3.00826000	H	-0.66568200	3.59872100	3.70438600
H	2.90412900	-0.42479100	-2.85778000	C	0.41842000	1.81193100	3.22881700
C	1.92031500	-1.17921500	0.46863800	H	1.26047700	2.04452800	3.87111400
C	3.57314000	-2.59216400	1.06241400	C	0.40013900	0.59557900	2.52972100
H	4.58159100	-2.97201400	1.09712400	H	1.18470000	-0.12370700	2.73275900
C	2.43227600	-3.05672100	1.62148300	C	-0.69937700	0.24634300	1.70810800
H	2.24747500	-3.91900700	2.24132000	N	3.24416700	-1.44035800	0.36525600
C	4.21862500	-0.60801300	-0.31471400	N	1.43730100	-2.18000200	1.24010400
H	3.76156100	0.35945900	-0.50513800	Rh	0.59957300	0.24180100	-0.14281200

Coordinates for Complex **M_{Ts}**



C	-0.76776800	1.51084100	-1.31654300	H	3.70498900	-2.28433400	-2.05232400
C	0.41550700	2.17134100	-0.88694000	H	4.94987200	-1.67454000	-0.92998000
C	1.55221300	1.68236200	-1.68184500	C	0.26102000	-1.65905800	2.04987100
C	1.07810500	0.68947400	-2.54724900	H	0.54085700	-1.25979800	3.02427300
C	-0.34282300	0.51143300	-2.26322100	H	-0.35275700	-2.54456800	2.23360800
C	2.93260300	2.24625300	-1.57895900	C	-0.49111300	-0.61797300	1.19690800
H	2.94918100	3.26874400	-1.97051100	C	-1.65041900	-1.23069300	0.45178000
H	3.65553200	1.66087800	-2.14998600	C	-1.63858100	-2.57514800	0.04209600
H	3.26630800	2.28555600	-0.53877100	H	-0.76898300	-3.19600000	0.23751400
C	0.53079300	3.26952300	0.11548700	C	-2.71483600	-3.13660000	-0.63004700
H	-0.37917500	3.37888600	0.70479700	H	-2.67764100	-4.17929000	-0.92816300
H	0.73858400	4.21379800	-0.40006000	C	-3.84351900	-2.36794000	-0.90754800
H	1.35517700	3.07878900	0.80764500	H	-4.69814600	-2.80575100	-1.41173800
C	-2.17873500	1.79712300	-0.89065300	C	-3.85698800	-1.02982400	-0.53642100
H	-2.84244500	1.58064600	-1.73316700	H	-4.72363000	-0.41371700	-0.76311800
H	-2.26627400	2.86857000	-0.68765200	C	-2.76663800	-0.45003600	0.11441500
C	-1.21371800	-0.45739700	-2.98842700	C	-2.74092000	1.03003400	0.36403000
H	-2.15025700	-0.63700300	-2.46080000	H	-3.76885800	1.39133400	0.47376700
H	-0.70643200	-1.41627300	-3.11740000	C	-1.96114400	1.39128100	1.59523700
H	-1.43988100	-0.06099500	-3.98526300	C	-2.29826800	2.54159400	2.31157300
C	1.81312000	-0.05453000	-3.61665400	H	-3.19388300	3.09123800	2.03253000
H	1.44321200	0.24892500	-4.60136600	C	-1.50388100	2.99825900	3.35390900
H	1.66417600	-1.13384700	-3.52682400	H	-1.77937500	3.89113900	3.90444600
H	2.88495600	0.14801300	-3.59034100	C	-0.34111000	2.29958000	3.67184200
C	1.90521200	-1.40358500	0.26873500	H	0.30857200	2.65256200	4.46604800
C	3.36786300	-3.02187900	0.80426700	C	-0.01408000	1.14073600	2.98248500
H	4.25812100	-3.62304900	0.70923800	H	0.90795300	0.63197300	3.24671900
C	2.35987600	-3.07004500	1.71477800	C	-0.82984000	0.64015200	1.95326600
H	2.20847000	-3.71580200	2.56462500	N	3.07542100	-1.99543900	-0.06698600
C	3.89597300	-1.62103700	-1.20583700	N	1.48244500	-2.07319200	1.36574900
H	3.64709600	-0.59770600	-1.47990400	Rh	0.66511200	0.06899000	-0.43438000

Coordinates for Complex N



C	-0.55696800	1.45489800	-1.18847600	C	-3.77589200	-2.33895600	-0.88674700
C	0.57914100	2.24548500	-0.85087100	H	-4.64026500	-2.75322100	-1.39432700
C	1.70814100	1.76834400	-1.63025400	C	-3.75363000	-1.00308100	-0.51146800
C	1.26353400	0.66090000	-2.39236600	H	-4.60205300	-0.36127900	-0.73520900
C	-0.11773500	0.40611100	-2.07124700	C	-2.64930500	-0.45967500	0.14581100
C	3.05141800	2.42761600	-1.70562800	C	-2.59343100	1.01028600	0.42263000
H	3.02841800	3.25817600	-2.41901400	H	-3.61503700	1.39763400	0.49527300
H	3.82496900	1.72849900	-2.03118800	C	-1.88289400	1.30765200	1.71073300
H	3.35438100	2.83176000	-0.73704700	C	-2.26029100	2.42543700	2.45777300
C	0.56452300	3.47361100	0.00970300	H	-3.07626300	3.04668200	2.09689600
H	-0.12541000	3.35969900	0.84879900	C	-1.62477100	2.74404400	3.64844500
H	0.25541000	4.34559600	-0.57681500	H	-1.93378300	3.61016800	4.22347800
H	1.55588200	3.68465700	0.41678800	C	-0.60493600	1.91344600	4.10605400
C	-1.96576500	1.76969100	-0.79608300	H	-0.11701700	2.12025200	5.05391600
H	-2.60914000	1.57195000	-1.65914300	C	-0.22487700	0.80101800	3.36830600
H	-2.03432700	2.84145900	-0.58761900	H	0.57087000	0.18532900	3.77156100
C	-0.97077500	-0.58494700	-2.80232800	C	-0.83768500	0.47646900	2.14527300
H	-1.95189400	-0.36270100	-2.34211600	N	2.75652300	-2.45345900	-0.43904600
H	-0.50653800	-1.57391000	-2.81471400	N	1.29965200	-2.40290200	1.12728100
H	-1.11099900	-0.26453100	-3.84092900	Rh	1.03534700	0.18794400	-0.15144500
C	1.98857200	-0.02099600	-3.50918700	C	2.14394300	0.77475100	1.32371000
H	1.64391300	0.40110700	-4.45977900	N	2.78794600	1.22009800	2.18736900
H	1.77514000	-1.09139600	-3.53565000	C	3.39607000	1.81681100	3.32403900
H	3.06900000	0.12450000	-3.46188100	H	4.02401900	2.65093300	3.00701300
C	1.77855700	-1.68498400	0.09160400	H	2.61135000	2.18042000	3.99163500
C	2.86472900	-3.64891200	0.25570000	H	4.01098900	1.07821600	3.84073100
H	3.57551200	-4.40982500	-0.02369800				
C	1.94934300	-3.61278100	1.25186500				
H	1.70484300	-4.33186200	2.01667800				
C	3.64786700	-2.06609400	-1.51700700				
H	3.64650200	-0.97957800	-1.58573500				
H	3.32754200	-2.49759400	-2.46706100				
H	4.65795800	-2.40833500	-1.28698900				
C	0.34428400	-1.77840600	2.02882500				
H	0.91102200	-1.38453500	2.87218200				
H	-0.34300900	-2.53901300	2.41282300				
C	-0.40048000	-0.67237100	1.26739600				
C	-1.54671900	-1.25973100	0.47449600				
C	-1.57955500	-2.60554000	0.07296900				
H	-0.74443200	-3.26394200	0.28055100				
C	-2.67103200	-3.13640300	-0.60140500				
H	-2.66324400	-4.18203500	-0.89163100				

Reaction of **5a** with 1,3,5-triaza-7-phosphaadamantane (pta)

A mixture of **5a** (3 mg, 0.004 mmol, 1 eq.) and pta (0.7 mg, 0.004 mmol, 1 eq.) in DCM (10 mL) was stirred for 24 h at room temperature. ESI-mass (Figure S19) and $^{31}\text{P}\{^1\text{H}\}$ NMR spectra (Figure S20) of the reaction mixture were recorded.

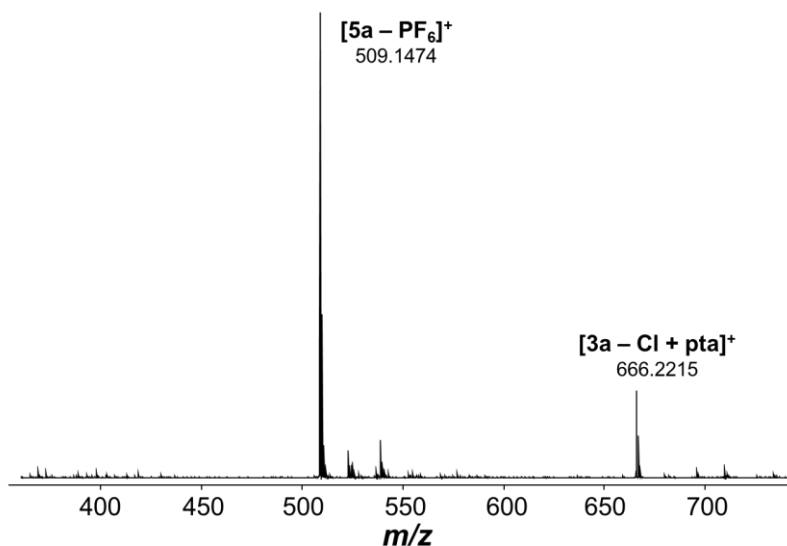


Figure S19. ESI-mass spectrum of the reaction mixture of **5a** and pta.

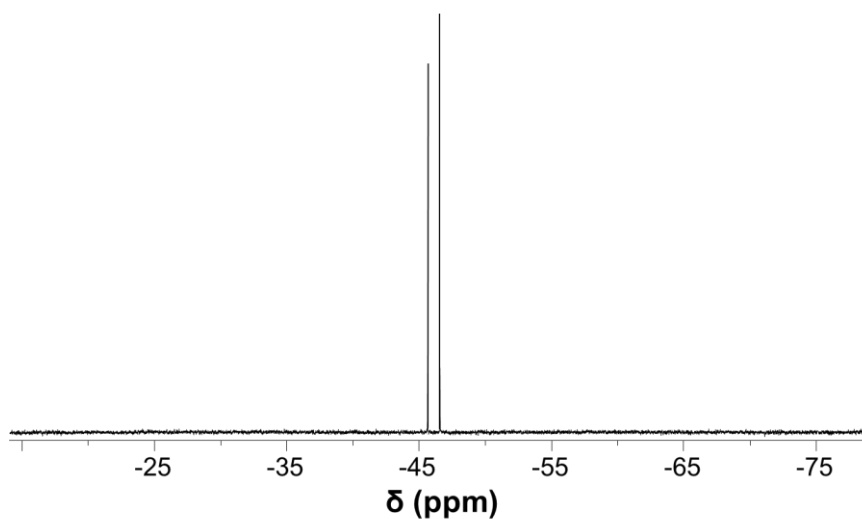


Figure S20. $^{31}\text{P}\{^1\text{H}\}$ NMR spectra of the reaction mixture of **5a** and pta.

Reaction of **5a** with *tert*-butylisocyanide (BIN)

A mixture of **5a** (5 mg, 0.007 mmol, 1 eq.) and 0.1 M BIN (0.07 ml, 0.007 mmol, 1 eq.) in DCM (10 mL) was stirred for 24 h at room temperature. An ESI-mass spectrum of the reaction mixture was recorded (Figure S22).

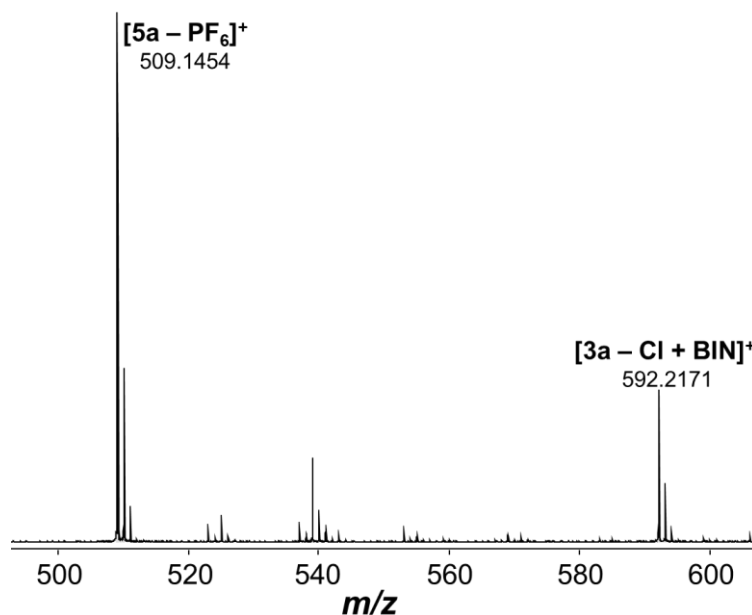


Figure S21. ESI-mass spectrum of the reaction mixture of **5a** and BIN.

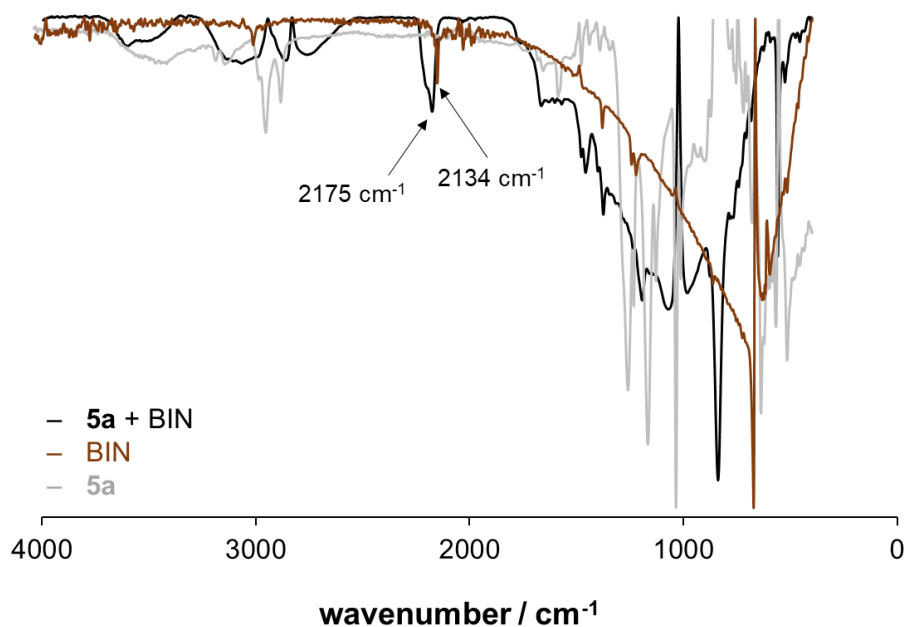


Figure S22. IR spectra of the reaction mixture of **5a** and BIN in comparison to those of the respective reagents.

^1H and $^{13}\text{C}\{^1\text{H}\}$ NMR spectra

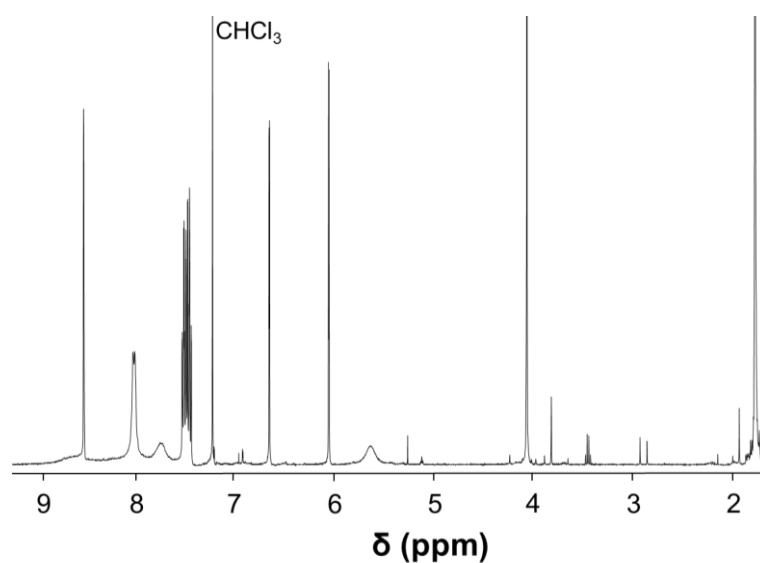


Figure S23. ^1H NMR spectrum of [dichlorido{1-(anthracen-9-ylmethyl)-3-methylimidazole-2-ylidene} $(\eta^5\text{-pentamethylcyclopentadienyl})$ rhodium(III)], **1a**.

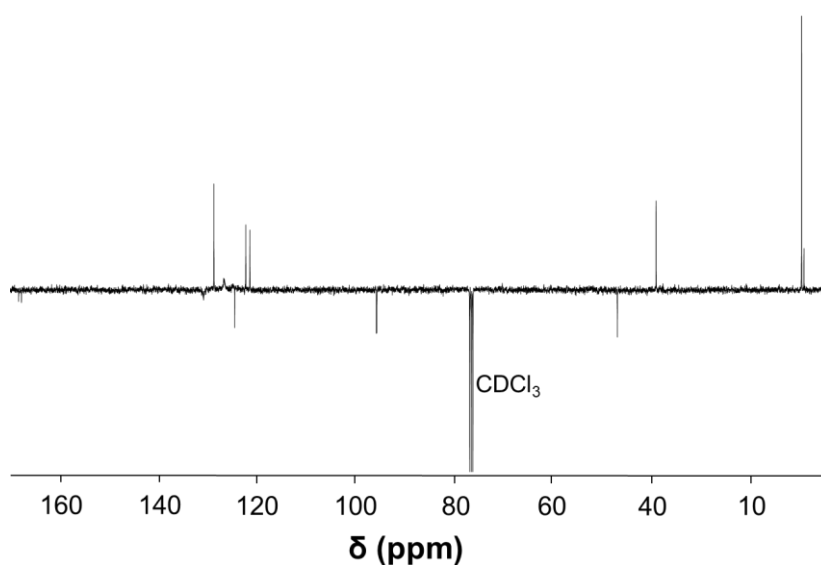


Figure S24. $^{13}\text{C}\{^1\text{H}\}$ NMR spectrum of [dichlorido{1-(anthracen-9-ylmethyl)-3-methylimidazole-2-ylidene} $(\eta^5\text{-pentamethylcyclopentadienyl})$ rhodium(III)], **1a**.

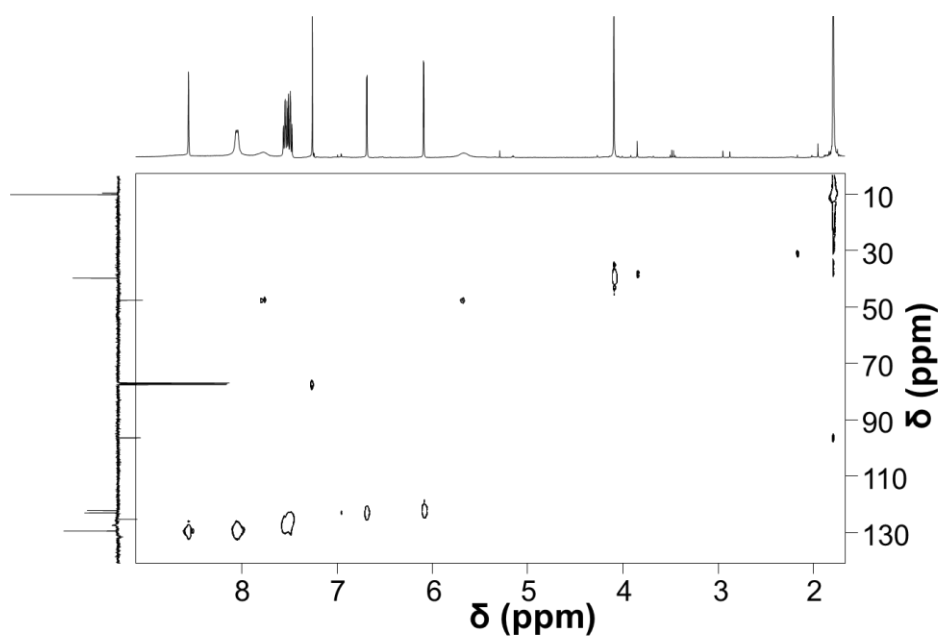


Figure S25. ^1H - ^{13}C HSQC NMR spectrum of [dichlorido{1-(anthracen-9-ylmethyl)-3-methylimidazole-2-ylidene} $(\eta^5\text{-pentamethylcyclopentadienyl})$ rhodium(III)], **1a**.

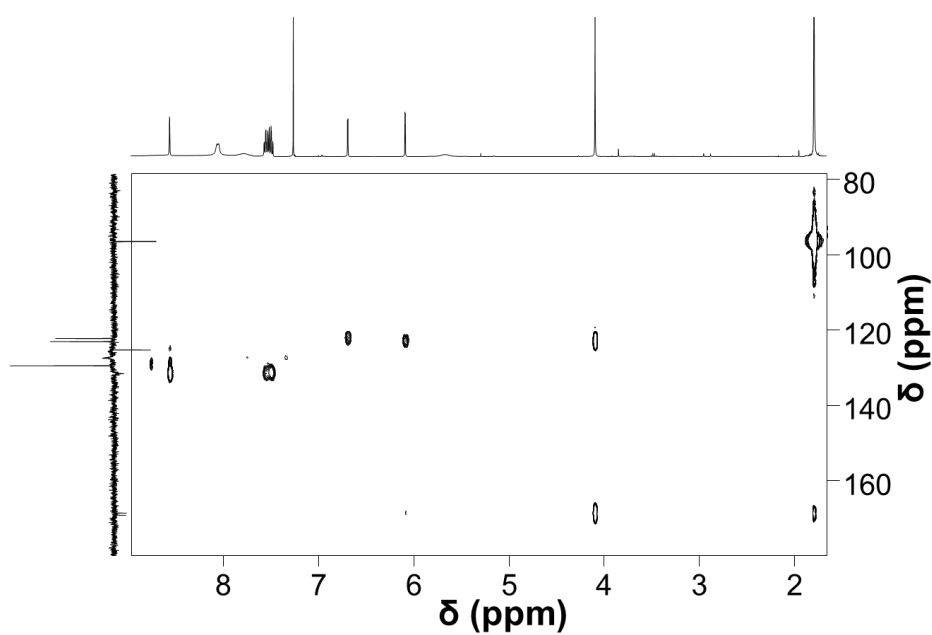


Figure S26. ^1H - ^{13}C HMBC NMR spectrum of [dichlorido{1-(anthracen-9-ylmethyl)-3-methylimidazole-2-ylidene} $(\eta^5\text{-pentamethylcyclopentadienyl})$ rhodium(III)], **1a**.

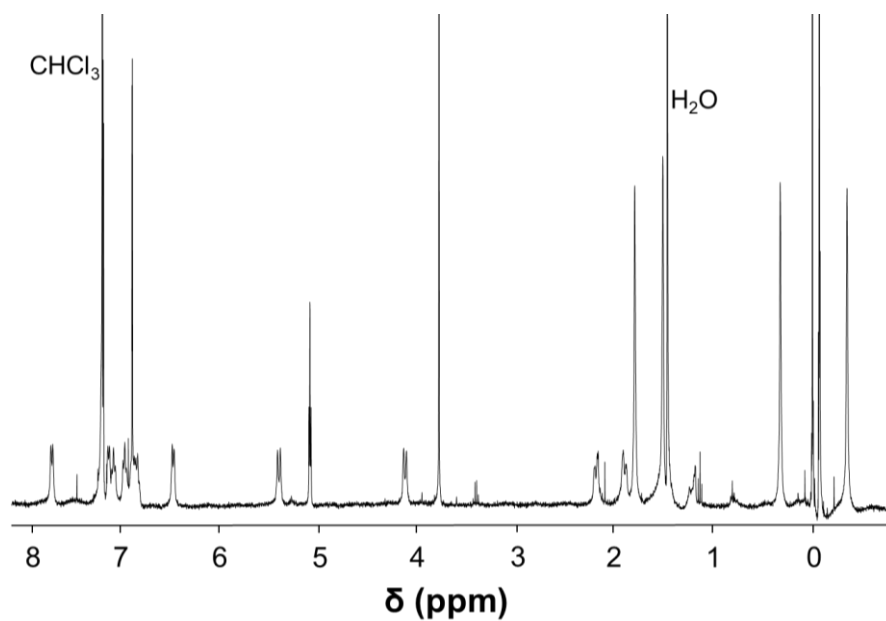


Figure S27. ^1H NMR spectrum of [chlorido{1-methyl-3-((10-[(η^5 -2,3,4,5-tetramethylcyclopentadienyl)methyl]-9,10-dihydroanthracene-9-yl- κ C)methyl)imidazole-2-ylidene}rhodium(III)], **3a**.

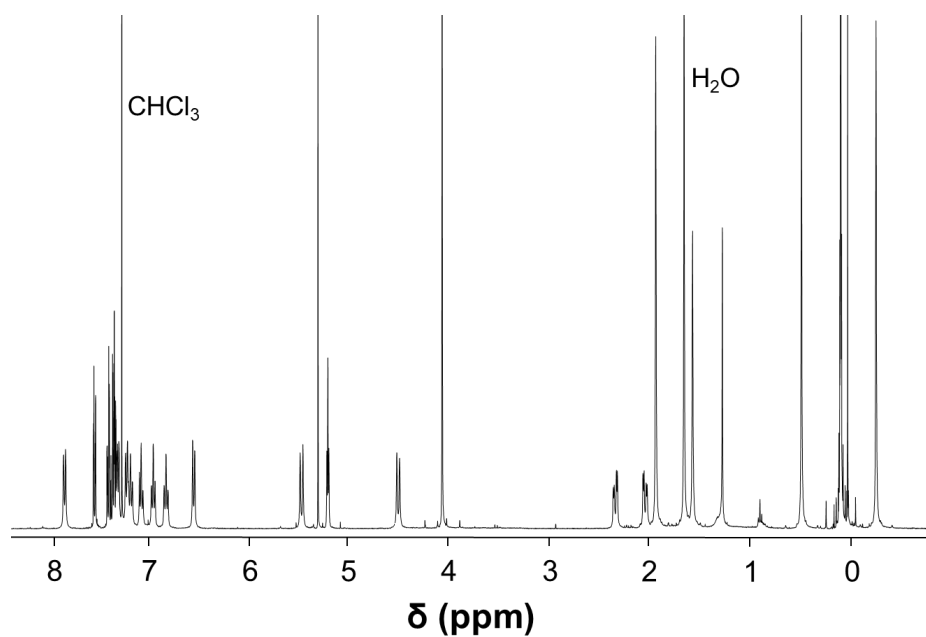


Figure S28. ^1H NMR spectrum of [chlorido{1-methyl-3-((10-[(η^5 -2,3,4,5-tetramethylcyclopentadienyl)methyl]-9,10-dihydroanthracene-9-yl- κ C)methyl)benzimidazole-2-ylidene}rhodium(III)], **4a**.

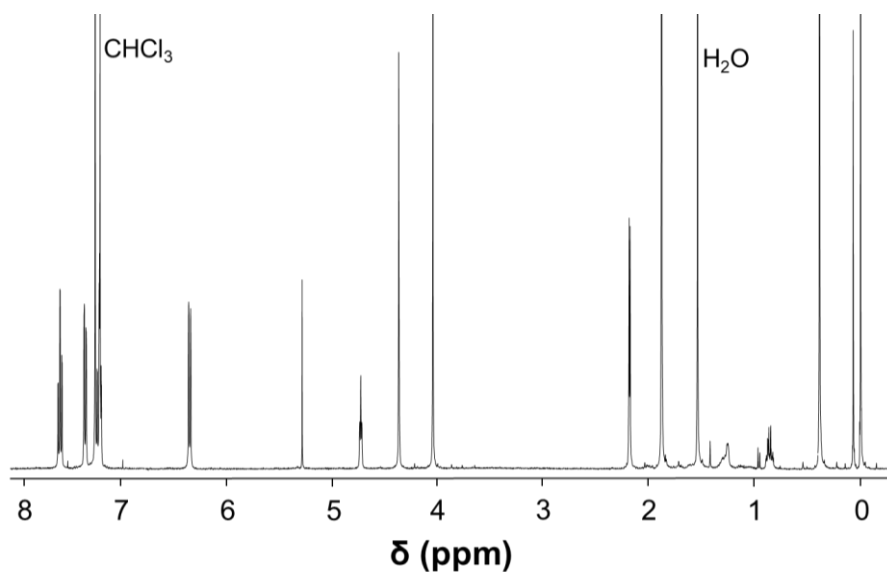


Figure S29. ^1H NMR spectrum of [{1-methyl-3-({10-[(η^5 -2,3,4,5-tetramethylcyclopentadienyl)methyl]-9,10-dihydroanthracene-9-yl- κC }methyl)imidazole-2-ylidene}rhodium(III)], **5a**.

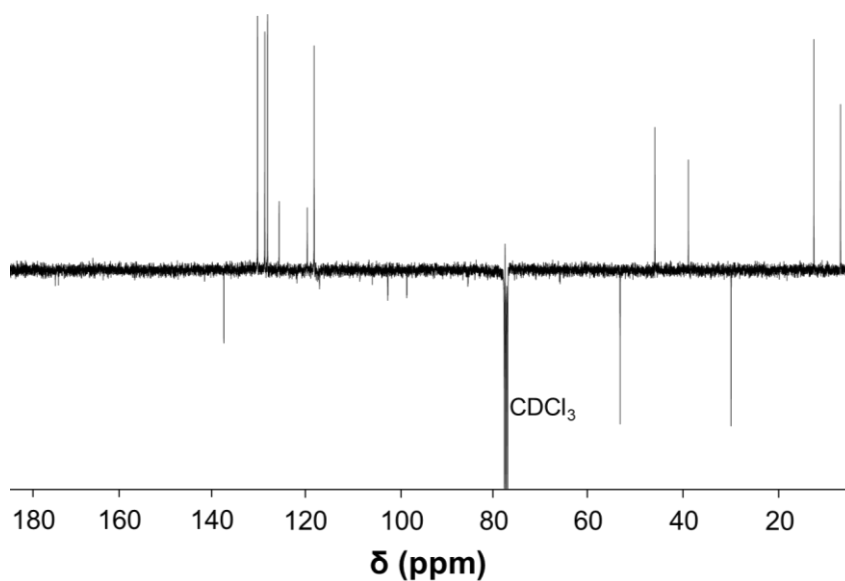


Figure S30. $^{13}\text{C}\{^1\text{H}\}$ NMR spectrum of [{1-methyl-3-({10-[(η^5 -2,3,4,5-tetramethylcyclopentadienyl)methyl]-9,10-dihydroanthracene-9-yl- κC }methyl)imidazole-2-ylidene}rhodium(III)], **5a**.

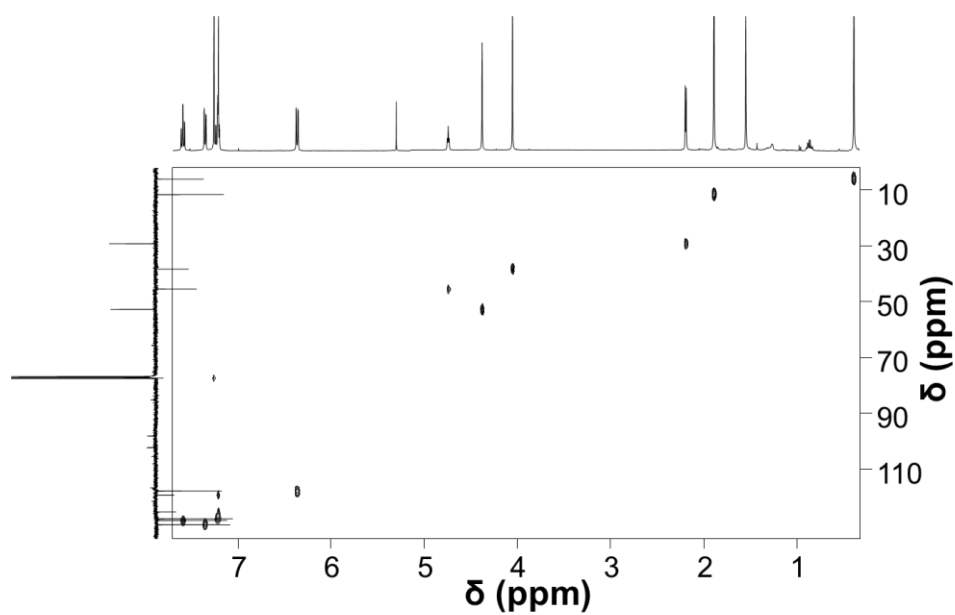


Figure S31. ^1H - ^{13}C HSQC NMR spectrum of [$\{1\text{-methyl-3-}(\{10\text{-}[(\eta^5\text{-2,3,4,5-tetramethylcyclopentadienyl)methyl]-9,10\text{-dihydroanthracene-9-yl-}\kappa\text{C}\}\text{methyl})\text{imidazole-2-ylidene}\}\text{rhodium(III)}$], **5a**.

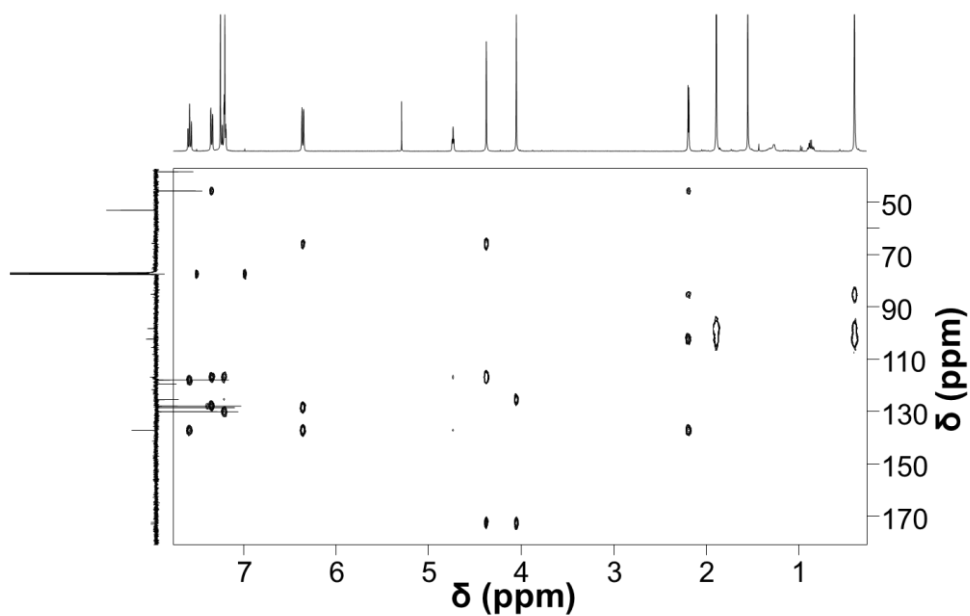


Figure S32. ^1H - ^{13}C HMBC NMR spectrum of [$\{1\text{-methyl-3-}(\{10\text{-}[(\eta^5\text{-2,3,4,5-tetramethylcyclopentadienyl)methyl]-9,10\text{-dihydroanthracene-9-yl-}\kappa\text{C}\}\text{methyl})\text{imidazole-2-ylidene}\}\text{rhodium(III)}$], **5a**.

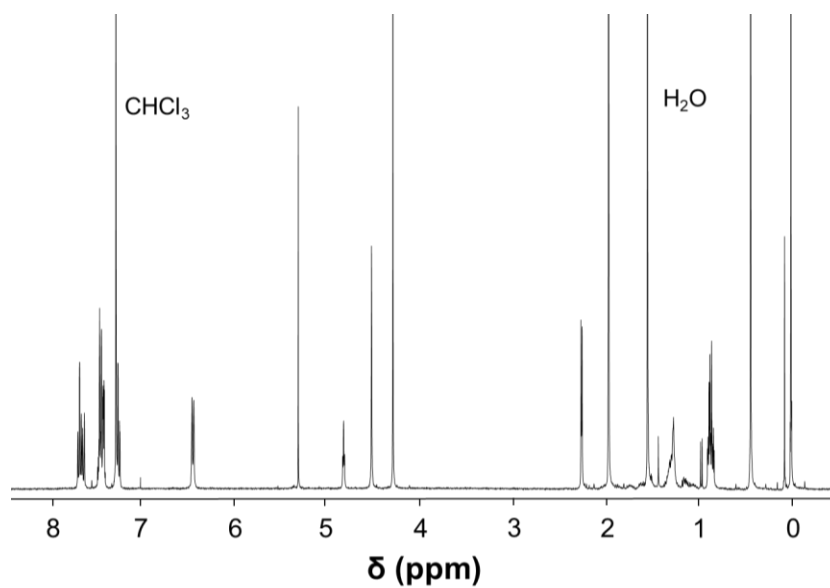


Figure S33. ^1H NMR spectrum of $[\{1\text{-methyl-3-}(\{10\text{-}[(\eta^5\text{-2,3,4,5-tetramethylcyclopentadienyl)methyl]\text{-9,10-dihydroanthracene-9-yl-}\kappa\text{C}\}\text{methyl})\text{benzimidazole-2-ylidene}\}\text{rhodium(III)}]$, **6a**.

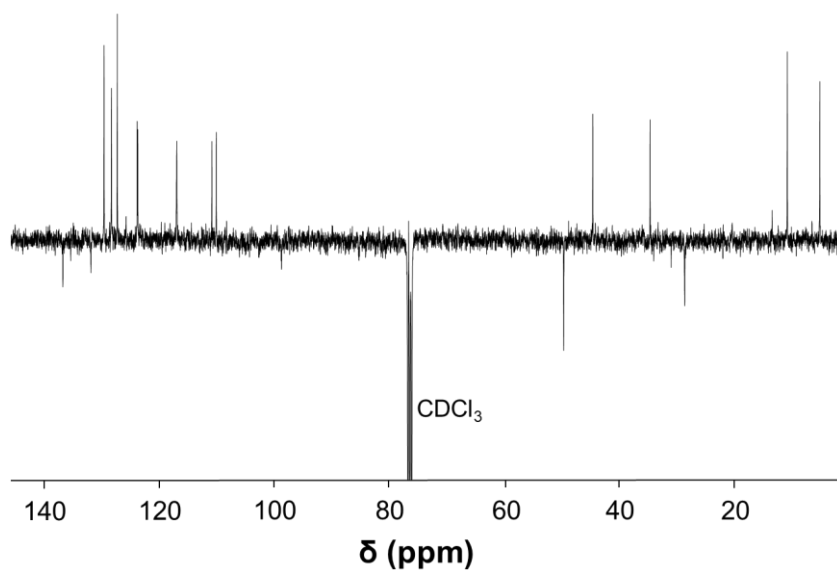


Figure S34. $^{13}\text{C}\{^1\text{H}\}$ NMR spectrum of $[\{1\text{-methyl-3-}(\{10\text{-}[(\eta^5\text{-2,3,4,5-tetramethylcyclopentadienyl)methyl]\text{-9,10-dihydroanthracene-9-yl-}\kappa\text{C}\}\text{methyl})\text{benzimidazole-2-ylidene}\}\text{rhodium(III)}]$, **6a**.

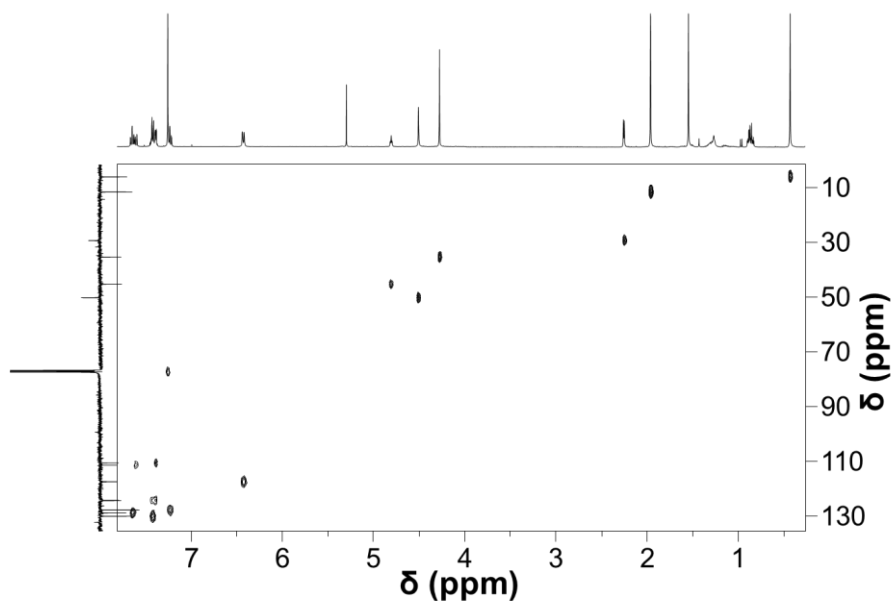


Figure S35. ^1H - ^{13}C HSQC NMR spectrum of [{1-methyl-3-((10-[(η^5 -2,3,4,5-tetramethylcyclopentadienyl)methyl]-9,10-dihydroanthracene-9-yl- κC)methyl)benzimidazole-2-ylidene}rhodium(III)], **6a**.

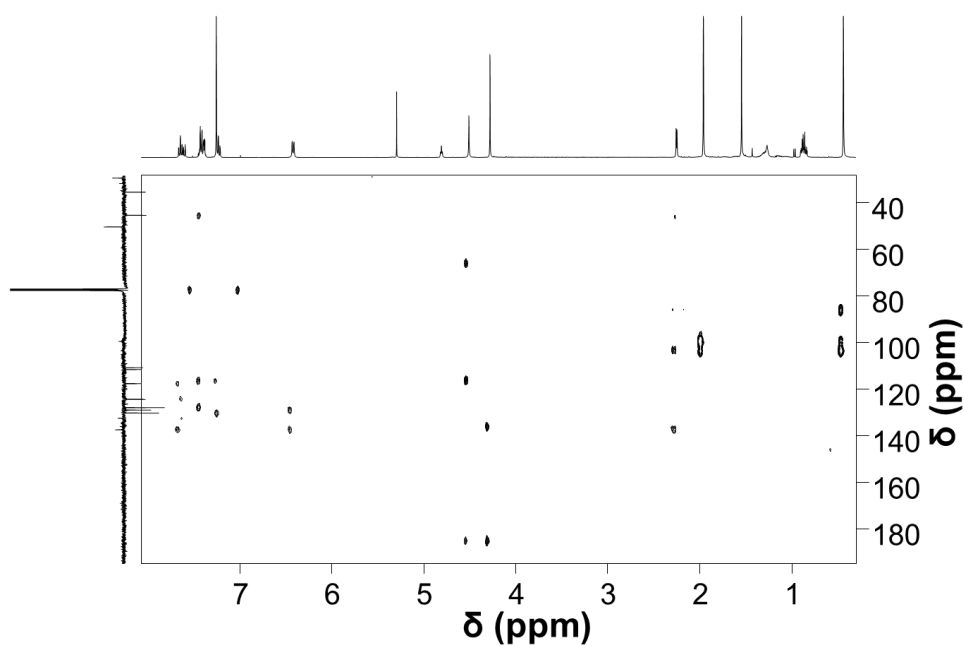


Figure S36. ^1H - ^{13}C HMBC NMR spectrum of [{1-methyl-3-((10-[(η^5 -2,3,4,5-tetramethylcyclopentadienyl)methyl]-9,10-dihydroanthracene-9-yl- κC)methyl)benzimidazole-2-ylidene}rhodium(III)], **6a**.

ESI-mass spectra

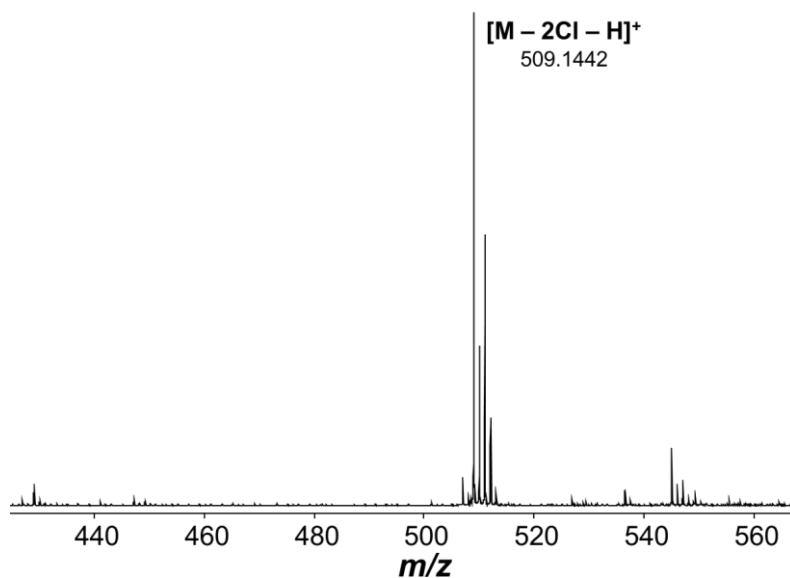


Figure S37. ESI-mass spectrum of [dichlorido{1-(anthracen-9-ylmethyl)-3-methylimidazole-2-ylidene} $\{\eta^5$ -pentamethylcyclopentadienyl}rhodium(III)], **1a**.

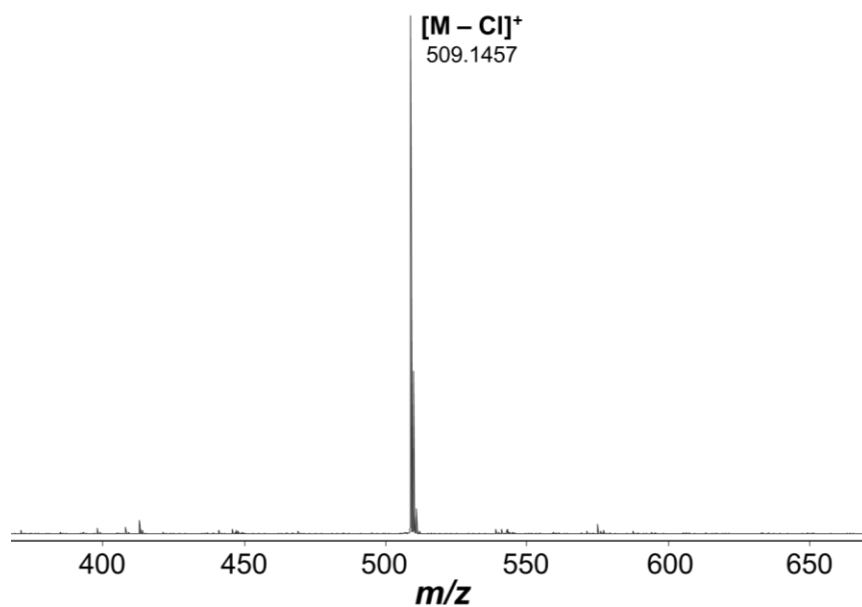


Figure S38. ESI-mass spectrum of [chlorido{1-methyl-3-({10-[(η^5 -2,3,4,5-tetramethylcyclopentadienyl)methyl]-9,10-dihydroanthracene-9-yl- κ C}methyl)imidazole-2-ylidene}rhodium(III)], **3a**.

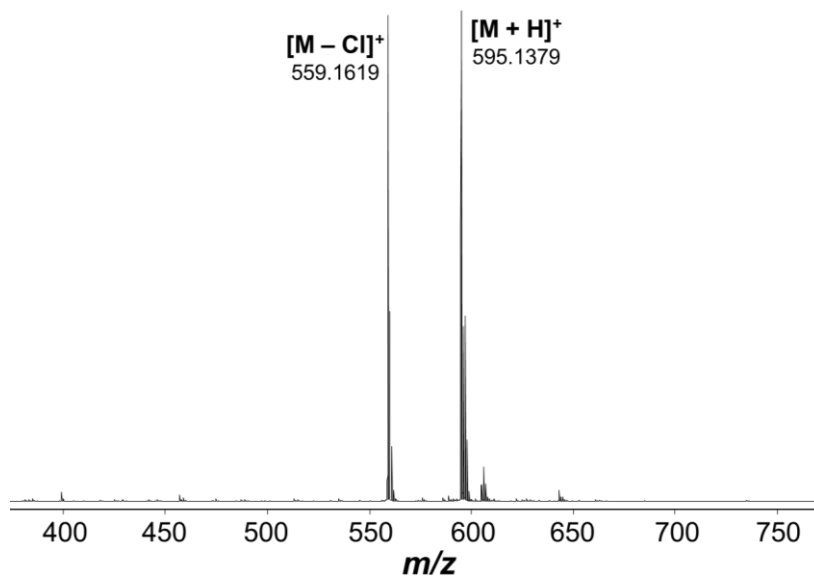


Figure S39. ESI-mass spectrum of [chlorido{1-methyl-3-({10-[(η^5 -2,3,4,5-tetramethylcyclopentadienyl)methyl]-9,10-dihydroanthracene-9-yl- κ C)methyl)benzimidazole-2-ylidene}rhodium(III)], **4a**.

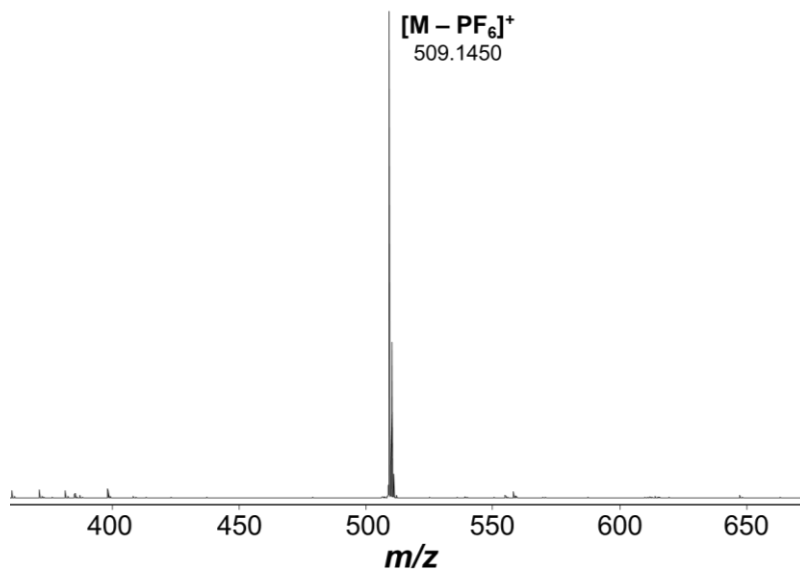


Figure S40. ESI-mass spectrum of [{1-methyl-3-({10-[(η^5 -2,3,4,5-tetramethylcyclopentadienyl)methyl]-9,10-dihydroanthracene-9-yl- κ C)methyl)imidazole-2-ylidene}rhodium(III)], **5a**.

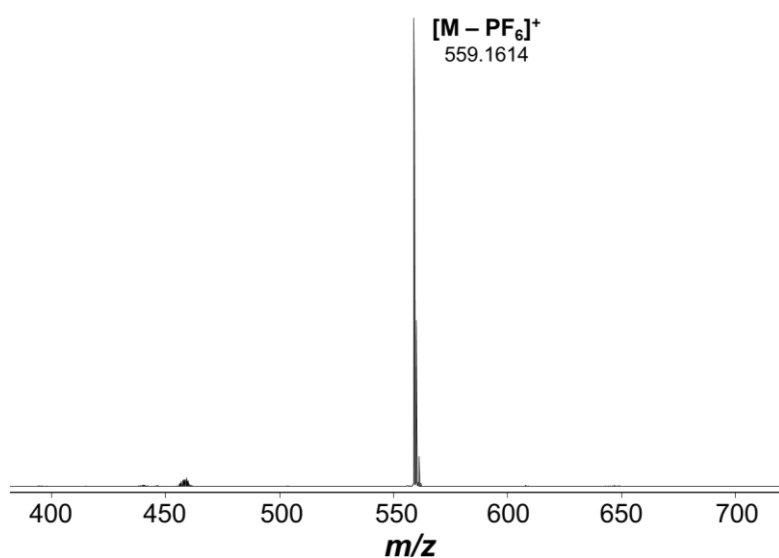


Figure S41. ESI-mass spectrum of $[\{1\text{-methyl-3-}(\{10\text{-}[(\eta^5\text{-}2,3,4,5\text{-tetramethylcyclopentadienyl)methyl]\text{-}9,10\text{-dihydroanthracene-}9\text{-yl-}\kappa\text{C}\}\text{methyl})\text{benzimidazole-}2\text{-ylidene}\}\text{rhodium(III)}], \mathbf{6a}$.

References

- (1) Kang, J. W.; Moseley, K.; Maitlis, P. M., Pentamethylcyclopentadienylrhodium and -iridium halides. I. Synthesis and properties. *J. Am. Chem. Soc.* **1969**, *91*, 5970-5977.
- (2) White, C.; Yates, A.; Maitlis, P. M.; Heinekey, D. M., (η^5 -Pentamethylcyclopentadienyl)Rhodium and -Iridium Compounds. In *Inorganic Syntheses*, John Wiley & Sons, Inc.: 2007; pp 228-234.
- (3) Truong, D.; Sullivan, M. P.; Tong, K. K. H.; Steel, T. R.; Prause, A.; Lovett, J. H.; Andersen, J. W.; Jamieson, S. M. F.; Harris, H. H.; Ott, I.; Weekley, C. M.; Hummitzsch, K.; Söhnle, T.; Hanif, M.; Metzler-Nolte, N.; Goldstone, D. C.; Hartinger, C. G., Potent Inhibition of Thioredoxin Reductase by the Rh Derivatives of Anticancer M(arene/Cp*)(NHC)Cl₂ Complexes. *Inorg. Chem.* **2020**, *59*, 3281-3289.
- (4) Sheldrick, G. M., A short history of SHELX. *Acta Crystallogr., Sect. A: Found. Crystallogr.* **2008**, *A64*, 112-122.
- (5) Dolomanov, O. V.; Bourhis, L. J.; Gildea, R. J.; Howard, J. A.; Puschmann, H., OLEX2: a complete structure solution, refinement and analysis program. *J. Appl. Crystallogr.* **2009**, *42*, 339-341.
- (6) Sheldrick, G., Crystal structure refinement with SHELXL. *Acta Crystallogr., Sect. C: Cryst. Struct. Commun.* **2015**, *71*, 3-8.
- (7) Blackburn, G. M.; Lockwood, G.; Solan, V., Intramolecular Fluorescence Quenching of Anthracene by Heterocyclic Ligands. *J. Chem. Soc. Perk. Trans. 2* **1976**, 1452-1456.
- (8) Becke, A. D., Density-functional thermochemistry. V. Systematic optimization of exchange-correlation functionals. *J. Chem. Phys.* **1997**, *107*, 8554-8560.
- (9) Chai, J.-D.; Head-Gordon, M., Long-range corrected hybrid density functionals with damped atom–atom dispersion corrections. *Phys. Chem. Chem. Phys.* **2008**, *10*, 6615-6620.
- (10) Śliwa, P.; Handzlik, J., Assessment of density functional methods for the study of olefin metathesis catalysed by ruthenium alkylidene complexes. *Chem. Phys. Lett.* **2010**, *493*, 273-278.
- (11) Kulkarni, A. D.; Truhlar, D. G., Performance of Density Functional Theory and Møller–Plesset Second-Order Perturbation Theory for Structural Parameters in Complexes of Ru. *J. Chem. Theory Comput.* **2011**, *7*, 2325-2332.

- (12) Minenkov, Y.; Singstad, Å.; Occhipinti, G.; Jensen, V. R., The accuracy of DFT-optimized geometries of functional transition metal compounds: a validation study of catalysts for olefin metathesis and other reactions in the homogeneous phase. *Dalton Trans.* **2012**, 41, 5526-5541.
- (13) Sperger, T.; Sanhueza, I. A.; Kalvet, I.; Schoenebeck, F., Computational Studies of Synthetically Relevant Homogeneous Organometallic Catalysis Involving Ni, Pd, Ir, and Rh: An Overview of Commonly Employed DFT Methods and Mechanistic Insights. *Chem. Rev.* **2015**, 115, 9532-9586.
- (14) Bursch, M.; Caldeweyher, E.; Hansen, A.; Neugebauer, H.; Ehlert, S.; Grimme, S., Understanding and Quantifying London Dispersion Effects in Organometallic Complexes. *Acc. Chem. Res.* **2019**, 52, 258-266.
- (15) Marenich, A. V.; Cramer, C. J.; Truhlar, D. G., Universal Solvation Model Based on Solute Electron Density and on a Continuum Model of the Solvent Defined by the Bulk Dielectric Constant and Atomic Surface Tensions. *J. Phys. Chem. B* **2009**, 113, 6378-6396.
- (16) Petersson, G. A.; Al-Laham, M. A., A complete basis set model chemistry. II. Open-shell systems and the total energies of the first-row atoms. *J. Chem. Phys.* **1991**, 94, 6081-6090.
- (17) Andrae, D.; Häußermann, U.; Dolg, M.; Stoll, H.; Preuß, H., Energy-adjusted ab initio pseudopotentials for the second and third row transition elements. *Theor. Chim. Acta* **1990**, 77, 123-141.
- (18) Marenich, A. V.; Jerome, S. V.; Cramer, C. J.; Truhlar, D. G., Charge Model 5: An Extension of Hirshfeld Population Analysis for the Accurate Description of Molecular Interactions in Gaseous and Condensed Phases. *J. Chem. Theory Comput.* **2012**, 8, 527-541.
- (19) Gorelsky, S. I.; Lever, A. B. P., Electronic structure and spectra of ruthenium diimine complexes by density functional theory and INDO/S. Comparison of the two methods. *J. Organomet. Chem.* **2001**, 635, 187-196.
- (20) Matta, C. F.; Boyd, R. J., An Introduction to the Quantum Theory of Atoms in Molecules. In *The Quantum Theory of Atoms in Molecules*, Matta, C. F.; Boyd, R. J., Eds. Wiley VCH: Weinheim, 2007; pp 1-34.
- (21) Contreras-García, J.; Johnson, E. R.; Keinan, S.; Chaudret, R.; Piquemal, J.-P.; Beratan, D. N.; Yang, W., NCIPLOT: A Program for Plotting Noncovalent Interaction Regions. *J. Chem. Theory Comput.* **2011**, 7, 625-632.

- (22) Lu, T.; Chen, F., Multiwfn: A multifunctional wavefunction analyzer. *J. Comput. Chem.* **2012**, *33*, 580-592.
- (23) de Silva, P.; Corminboeuf, C., Simultaneous Visualization of Covalent and Noncovalent Interactions Using Regions of Density Overlap. *J. Chem. Theory Comput.* **2014**, *10*, 3745-3756.
- (24) Lauher, J. W., Chem-Ray: A molecular graphics program featuring an umbra and penumbra shadowing routine. *J. Mol. Graphics* **1990**, *8*, 34-38.
- (25) Humphrey, W.; Dalke, A.; Schulten, K., VMD: Visual molecular dynamics. *J. Mol. Graphics* **1996**, *14*, 33-38.
- (26) AL-Saeedi, A.; Farooqui, M., (4+2) Cycloaddition Reactions of 9-Substituted Anthracene Compounds. *Orient. J. Chem.* **2013**, *29*, 1033-1039.
- (27) Fan, L.; Turner, M. L.; Hursthouse, M. B.; Malik, K. M. A.; Gusev, O. V.; Maitlis, P. M., Oxygen-induced methyl carbon-hydrogen activation in pentamethylcyclopentadienylruthenium complexes. *J. Am. Chem. Soc.* **1994**, *116*, 385-386.
- (28) Gemel, C.; Mereiter, K.; Schmid, R.; Kirchner, K., [Ru(η^5 -C₅Me₅)(Me₂NCH₂CH₂NMe₂)]⁺, a Stable 16-Electron Complex. Reaction with Dioxygen and Formation of a Monomeric Hydroxoruthenium Tetramethylfulvene Complex. *Organometallics* **1997**, *16*, 5601-5603.
- (29) Li, C.; Luo, L.; Nolan, S. P.; Marshall, W.; Fagan, P. J., Relative Binding Energies of Tertiary Phosphine Ligands to the Cp^{*}RuOCH₂CF₃ (Cp^{*} = η^5 -C₅Me₅) Moiety. *Organometallics* **1996**, *15*, 3456-3462.
- (30) Meredith, J. M.; Goldberg, K. I.; Kaminsky, W.; Heinekey, D. M., η^6 -Tetramethylfulvene and μ - η^3 : η^3 -Benzene Complexes of Iridium. *Organometallics* **2012**, *31*, 8459-8462.
- (31) Lohr, T. L.; Piers, W. E.; Parvez, M., Monomeric Platinum(II) Hydroxides Supported by Sterically Dominant α -Diimine Ligands. *Inorg. Chem.* **2012**, *51*, 4900-4902.
- (32) An alternative pathway was considered whereby the corresponding association intermediate with both chlorido ligands remained bonded to Rh as the OH⁻ nucleophile attacks the metal. This resulted in the expulsion of the neutral NHC ligand, which thus ruled out this sub-reaction pathway as a possibility.
- (33) Fukui, K., The path of chemical reactions - the IRC approach. *Acc. Chem. Res.* **1981**, *14*, 363-368.

- (34) As a precedent for this type of metal-assisted methyl deprotonation by OH^- , such a process has been previously suggested to occur during H/D exchange reactions involving Rh(III) phosphine complexes
- (35) Ciancaleoni, G.; Bolaño, S.; Bravo, J.; Peruzzini, M.; Gonsalvi, L.; Macchioni, A., Counterion-dependent deuteration of pentamethylcyclopentadiene in water-soluble cationic Rh(III) complexes assisted by PTA. *Dalton Trans.* **2010**, 39, 3366-3368.
- (36) Yatabe, T.; Kishima, T.; Nagano, H.; Matsumoto, T.; Yamasaki, M.; Yoon, K.-S.; Ogo, S., Structure and Reactivity of a Ru-based Peroxide Complex as a Reactive Intermediate of O_2 -Promoted Activation of a C–H Bond in a Cp^* Ligand. *Chem. Lett.* **2017**, 46, 74-76.
- (37) Kölle, U.; Kang, B.-S.; Thewalt, U., Reaktionen von $[\text{Cp}^*\text{RuOMe}]_2$ VI. Ligandenaustausch unter komplexierender Deprotonierung zu und Molekülstruktur von $(\eta^4\text{-1,5-Cyclooctadien})(\eta^6\text{-1,2,3,4-tetramethylfulven})\text{ruthenium}$. *J. Organomet. Chem.* **1990**, 386, 267-273.
- (38) Mayer, I., Bond order and valence indices: A personal account. *J. Comput. Chem.* **2007**, 28, 204-221.
- (39) Sparkes, H. A.; Chaplin, A. B.; Weller, A. S.; Howard, J. A. K., Bond catastrophes in rhodium complexes: experimental charge-density studies of $[\text{Rh}(\text{C}_7\text{H}_8)(\text{PtBu}_3)\text{Cl}]$ and $[\text{Rh}(\text{C}_7\text{H}_8)(\text{PCy}_3)\text{Cl}]$. *Acta Crystallogr., Sect. B: Struct. Sci.* **2010**, 66, 503-514.
- (40) Martínez-Martínez, A. J.; Tegner, B. E.; McKay, A. I.; Bukvic, A. J.; Rees, N. H.; Tizzard, G. J.; Coles, S. J.; Warren, M. R.; Macgregor, S. A.; Weller, A. S., Modulation of σ -Alkane Interactions in $[\text{Rh}(\text{L}_2)(\text{alkane})]^+$ Solid-State Molecular Organometallic (SMOM) Systems by Variation of the Chelating Phosphine and Alkane: Access to $\eta^2, \eta^2\text{-}\sigma\text{-Alkane Rh(I)}$, $\eta^1\text{-}\sigma\text{-Alkane Rh(III)}$ Complexes, and Alkane Encapsulation. *J. Am. Chem. Soc.* **2018**, 140, 14958-14970.
- (41) Bader, R. F. W., *Atoms in Molecules - A Quantum Theory*. Oxford University Press: Oxford, U.K., 1990; p 438.